# Investigating the role of oxidative stress in apoptosis induced by a sulphamoylated estradiol analogue in breast cell lines

by

Maphuti Tebogo Lebelo

11063654

Submitted in fulfilment of the requirements for the degree

Master of Science (Physiology)

Faculty of Health Sciences

University of Pretoria

2020

**Declaration**

I hereby declare that this dissertation is submitted in fulfilment of the Master of Science (Physiology) degree at University of Pretoria, and it is my own work which has not been submitted for any degree previously, in this or any other institution.

Signature | Date

**MT Lebelo** | **29 November 2019**

# Table of Contents

**Declaration** ..... i

**Summary** ..... v

**Acknowledgements** ..... vii

**Research outputs** ..... viii

**Publications** ..... viii

**Conferences** ..... viii

**List of abbreviations** ..... ix

**List of figures** ..... xii

**List of tables** ..... xiv

**Graphic representation of signaling pathways** ..... xv

**Chapter 1** ..... 1

**Introduction** ..... 1

**1.1 Cancer** ..... 1

**Literature review** ..... 1

1.1.1 Breast cancer ..... 1

1.1.2 Available treatment ..... 3

1.2 Overview of the cell cycle ..... 5

1.2.1 Cell cycle phases ..... 6

1.2.1.1 $G_1$ phase ..... 6

1.2.1.2 S-phase ..... 6

1.2.1.3 $G_2$/M ..... 7

1.2.2 Checkpoints ..... 7

1.2.2.1 $G_1$ checkpoint (restriction point) ..... 7

1.2.2.2 $G_2$ checkpoint (DNA checkpoint) ..... 8

1.2.2.3 M checkpoint (spindle checkpoint) ..... 8

1.3 Apoptosis ..... 8

1.4 2-Methoxyestradiol and sulphamoylated compounds ..... 11

1.5 Reactive oxygen species ..... 14

1.6 Relevance and aim of the study ..... 17

1.7 Objectives ..... 17

**Chapter 2** ..... 19

**Research procedure** ..... 19

**Methods and materials** ..... 19

**2.1 Materials** ..... 19

2.1.1 Cell lines ..... 19

**2.1.2 Reagents** ..... 19

**2.2 Methods** ..... 20

**2.2.1 Oxidative stress** ..... 20

2.2.1.1 Hydrogen peroxide generation using 2,7-dichlorofluoresceindiacetate (fluorescent microscopy) ..... 20

2.2.1.2 Superoxide generation using dihydroethidium (fluorescent microscopy) ..... 20

**2.2.2 Cell proliferation** ..... 21

2.2.2.1 Crystal violet staining (spectrophotometry) ..... 21

**2.2.3 Cell morphology** ..... 22

2.2.3.1 Light microscopy ..... 22

**2.2.4 Cell cycle progression and apoptosis induction** ..... 23

2.2.4.1 Propidium iodide staining (flow cytometry) ..... 23

**2.2.5 Mitochondrial potential** ..... 24

Mitochondrial membrane potential ..... 24

**2.2.6 Antioxidant activity** ..... 25

2.2.6.1 Superoxide dismutase activity (spectrophotometry) ..... 25

2.2.6.2 Catalase activity (spectrophotometry) ..... 26

**2.3 Statistics** ..... 26

**2.4 Logistics** ..... 27

**Ethical approval** ..... 27

**Chapter 3** ..... 28

**3.1 Results** ..... 28

**3.1.1 ROS production** ..... 28

**3.1.1.1 Fluorescent microscopy** ..... 28

**3.1.2 Cell proliferation** ..... 32

3.1.2.1 Cell growth inhibition by sulphamoylated vs. non-sulphamoylated compounds ..... 32

3.1.2.2 Cell growth inhibition in the presence or absence of ROS inhibitors ..... 34

**3.1.4 Cell morphology** ..... 44

3.1.4.1 Light microscopy ..... 44

**3.1.5 Cell cycle progression** ..... 51

**3.1.6 Mitochondrial membrane potential** ..... 57

**3.1.7 Antioxidant activity** ..... 61

3.1.7.1 Superoxide dismutase inhibition ..... 61

3.1.7.2 Catalase activity ..... 63

**Chapter 4** ..... 65

**4.1 Discussion** ..... 65

**Chapter 5** ..... 72

**5.1 Conclusion** ..... 72

**References** ..... 73

**Appendix A: Ethical approval certificate** ..... 89

**Summary**

2-Methoxyestradiol (2ME), a 17β-estradiol metabolite, exerts anticancer properties however, the compound was found to possess low bioavailability. This resulted in the *in silico*-design of 2ME analogues with a sulphamoyl moiety which made them more potent than the parent compound. Sulphamoylated 2ME analogues are suspected to induce the antitumourigenic effects through the induction of reactive oxygen species. However, the exact role of oxidative stress in the activity exerted by these compounds remains elusive.

In the current study, 2-ethyl-13-methyl-17-oxo-7,8,9,11,12,13,14,15,16,17-decahydro-6-cyclopenta[*a*]phenanthrane-3 sulphamate (ESE-one) was chosen as a sulphamoylated estradiol analogue representative to investigate the role of reactive oxygen species (ROS) in the effects exerted by these sulphamoylated compounds on cell proliferation, morphology, cell cycle progression, antioxidant activity and mitochondrial membrane potential in estrogen receptor positive breast epithelial adenocarcinoma (MCF-7) cells and estrogen receptor negative breast epithelial adenocarcinoma (MDA-MB-231) cells.

Fluorescent microscopy data revealed that sulphamoylated estradiol analogues induced more ROS production compared to their non-sulphamoylated counterparts in both MCF-7- and MDA-MB-231 cells. Crystal violet staining demonstrated a significant growth inhibition in cells exposed to sulphamoylated estradiol analogues compared to cells exposed to the non-sulphamoylated compounds. ESE-one exposure resulted in a ROS-dependent growth inhibition which was repressed by tiron (superoxide inhibitor), trolox (peroxyl inhibitor) and DMTU (hydrogen peroxide inhibitor). ESE-one exposure to MCF-7- and MDA-MB-231 cells resulted in an accumulation of cells in $G_2$/M phase after 24 hours and sub-$G_1$ phase after 48 hours. The effect induced after 24 hours exposure was inhibited by tiron and trolox, and that induced after 48 hours exposure was inhibited by tiron, trolox and DMTU. Proliferation data was confirmed by morphology studies.

Tiron, trolox and DMTU significantly decreased the number of rounded cells, shrunken cells and apoptotic bodies in MCF-7 and MDA-MB-231 cells induced by ESE-one exposure; cell density was recuperated indicating the rescue effects of ROS inhibitors. Antioxidant activity data demonstrated that ESE-one induced cell rounding and antiproliferative effects via ROS evident in the reduced catalase protein concentration in MCF-7 cells which was opposed by tiron and DMTU and in MDA-MB-231 cells, inhibited by tiron and trolox. Reduction in mitochondrial membrane potential was inhibited by tiron in MCF-7 cells and DMTU in MDA-MB-231 cells.

This *in vitro* study suggests that ESE-one induces growth inhibition, cell rounding, cell cycle arrest, catalase inhibition and depolarization of the mitochondrial membrane by production of superoxide anion, peroxyl radical and hydrogen peroxide which culminates in apoptosis. This study contributes to targeted therapy based on ROS-dependent cell death pathways in tumourigenic breast cells.

**Key words**: ESE-one, sulphamoylated, non-sulphamoylated, ROS, tiron, trolox, DMTU, antiproliferation, apoptosis, antioxidant

**Acknowledgements**

- Dr MH Visagie (supervisor) for designing and facilitating my study, for trusting me to carry out the study under her guidance, for equipping me with the technical skills, for her support, motivation and channelling me in the right direction throughout the study.
- Prof AM Joubert (Head of Department and co-supervisor) for granting me the opportunity to conduct my study in the department, to use the facilities and equipment in the department and for financial support through the National Research Foundation.
- Cancer Association of South Africa, Struwig Germeshuysen Trust, Research Committee of the University of Pretoria (RESCOM), The Medical Research Council and First Rand Foundation for financially supporting my study.
- A special thank you to Dr TV Mqoco for financial support through the National Research Foundation.
- Flow Cytometer (Department of Immunology and Department of Pharmacology), University of Pretoria, Pretoria, South Africa.
- Ms Mabena and Mr Ramphisa for sterilizing the glassware and for lab maintenance.
- A very special thank you to my parents, my siblings and my partner for their continuous support throughout this journey and for always believing in me.
- My family, friends and colleagues for supporting me and sharing insight.
- All this would not have been possible had it not been for the Almighty God who created this opportunity and carried me through this academic journey.

## Research outputs

### Publications

- Lebelo MT, Joubert AM, Visagie MH. Warburg effect and its role in tumourigenesis. Archives of Pharmacal Research. 2019; 42(10):833-847.
- Soldatkina MA, Klochko VV, Zagorodnya SD, Rademan S, Visagie MH, Lebelo MT, Gwangwa MV,Joubert AM, Lall N, Reva ON. Promising anticancer activity of batumin: a natural polyene antibiotic produced by Pseudomona batumici. Future Medicinal Chemistry. 2018; 10(18):2187-2199.
- Reva ON, Rademan S, Visagie MH, Lebelo MT, Gwangwa MV, Klochk VV, Joubert AM, Lall N. Comparison of structures and cytotoxicity of mupirocin and batumin against melanoma and several other cancer cell lines. Future Medicinal Chemistry. 2019; 11(7):677-691.

### Conferences

- Lebelo MT, Joubert AM, Mqoco TV, Visagie MH. Role of oxidative stress in apoptosis induced by a sulphamoylated estradiol analogue in breast cell lines. Faculty Day, University of Pretoria, 2018.
- Lebelo MT, Joubert AM, Mqoco TV, Visagie MH. Influence of an estradiol antimitotic compound and subsequent glutamine deprivation in breast tumourigenic and non-tumourigenic cells. PSSA conference, University of Pretoria, 2017.

**List of abbreviations**

| | |
|---|---|
| 2-ESE-diol | 2-Ethyl-13-methyl-7,8,9,11,12,13,14,15,16,17-decahydro-6-cyclopenta[a]phenanthrane-3,17-diol |
| 2ME | 2-Methoxyestradiol |
| AKT | Protein kinase B |
| APC | Anaphase promoting complex |
| APAF-1 | Apoptosis protease-activating factor 1 |
| ATM | Ataxia telangiectasia mutated |
| ASK | Apoptosis signal-regulating kinase |
| ATR | ATM and Rad-related |
| BAD | Bcl-2 associated death promotor homologue |
| BAK | B-cell homologue antagonist/killer |
| BAX | B-cell lymphoma associated X |
| BCL-2 | B-cell lymphoma 2 |
| BCL-XL | B-cell lymphoma extra large |
| BH3 | B-cell lymphoma 3 homologue |
| BID | BH3 interacting domain death agonist |
| BIK | Bcl-2 interacting killer |
| BMF | Bcl-2 modifying factor |
| BRCA1 | Breast cancer gene 1 |
| BRCA2 | Breast cancer gene 2 |
| BUD | Budding uninhibited by benomyl |
| CA | Carbonic anhydrase |
| Carboxy-PTIO | 2-(4-Carboxyphenyl)-4,4,5,5-tetramethylimidazoline-1-oxyl-3-oxide |
| CCCP | Carbonyl cyanide 3-chlorophenylhydrazone |
| CD8+ | Cluster of differentiation 8+ |

| | |
|---|---|
| CDC6 | Cell division cycle |
| CDK | Cyclin dependent kinase |
| CDT1 | Chromatin licensing and DNA replication factor 1 |
| c-Myc | Cellular myelocytomatosis |
| $CO_2$ | Carbon dioxide |
| CTLA4 | Cytotoxic T-lymphocyte associated antigen 4 |
| DCFDA | 2,7-Dichlorofluoresceindiacetate |
| DHE | Dihydroethidine |
| DIABLO | Direct IAP-binding protein with low pI |
| DISC | Death inducing signaling complex |
| DMEM | Dulbecco's minimum essential medium eagle |
| DMTU | N,N'-dimethylthiourea |
| DNA | Deoxyribonucleic acid |
| DR4 | Death receptor 4 |
| DR5 | Death receptor 5 |
| EE-15-ol | 2-Ethyl-17estra-1,3,5(10)16-tetraene |
| EE-one | 2-Ethylestrone |
| EMBS | (8R,13S,14S,17S)-2-ethyl-13-methyl-7,8,9,11,12,13,14,15,16,17-decahydro-6H-cyclopenta[a]phenanthrane-3,17-diyl bis(sulphamate) |
| ER | Estrogen receptor |
| ESE-15-ol | 2-Ethyl-estra-17-methylbenzenesulfenohydrazide |
| ESE-ol | 2-Ethyl-17-hydroxy-13-methyl-7,8,9,11,12,13,14,15,16,17-decahydro-6-cyclopenta[a]phenanthren-3-yl sulphamate |
| ESE-one | 2-Ethyl-13-methyl-17-oxo-7,8,9,11,12,13,14,15,16,17-decahydro-6-cyclopenta[a]phenanthrane-3 sulphamate |
| FADD | Fas-associated death domain |
| FasL | Fas ligand |

| | |
|---|---|
| FCS | Fetal calf serum |
| FOXO | Forkhead box |
| G0 | Gap 0 phase |
| G1 | Gap 1 phase |
| G2 | Gap 2 phase |
| HER2 | Human epidermal growth factor receptor 2 |
| HRK | Protein harakiri |
| IAP | Inhibitor of apoptosis protein |
| JNK | c-Jun-terminal kinase |
| M | Mitotic |
| MAD2 | Mitotic arrest deficient 2 |
| MAPK | Mitogen activated protein kinase |
| MCM2-7 | Mini-chromosome maintenance 2-7 |
| NAC | N-acetyl cystein |
| NADPH | Nicotinamide adenine dinucleotide phosphate |
| NF-κB | Nuclear factor kappa-light-chain enhancer of activated B-cells |
| ORC | Origin recognition complex |
| PBS | Phosphate buffer solution |
| PD-1 | Programmed cell death protein 1 |
| PI | Propidium iodide |
| PR | Progesterone receptor |
| pRB | Retinoblastoma protein |
| PUMA | p53 upregulated modulator of apoptosis |
| ROS | Reactive oxygen species |
| SMAC | Second mitochondria-derived activator of caspase |
| SOD | Superoxide dismutase |

| | |
|---|---|
| S-phase | Synthesis phase |
| tBID | Truncated Bid |
| TNF | Tumour necrotic factor |
| TRAIL | Tumour necrosis factor related apoptosis-inducing ligand |
| WAF-1 | Wildtype p53-activated fragment 1 |

**List of figures**

Figure 1.1: Process of apoptosis. 9

Figure 1.2: Extrinsic- and intrinsic apoptosis pathways. 11

Figure 1.3: Production of ROS from an oxygen molecule. 15

Figure 1.4: Conversion of superoxide and hydrogen peroxide by antioxidants. 15

Figure 3.1: Fluorescent micrographs of MCF-7 and MDA-MB-231 cells exposed to sulphamoylated and non-sulphamoylated compounds. 30

Figure 3.2: MCF-7 and MDA-MB-231 graphs demonstrating the mean fluorescent intensity. 31

Figure 3.3: Graph of MCF-7 and MDA-MB231 cells exposed to sulphamoylated and non-sulphamoylated compounds. 34

Figure 3.4: Cell growth inhibition graphs of MCF-7 and MDA-MB-231 cells exposed to ESE-one in combination with tiron (superoxide anion inhibitor). 36

Figure 3.5: Cell growth inhibition graph of MCF-7 and MDA-MB-231 cells exposed to ESE-one in combination with DMTU (hydrogen peroxide inhibitor). 37

Figure 3.6: Cell growth inhibition graphs of MCF-7 and MDA-MB-231 cells exposed to ESE-one in combination with trolox (peroxyl radical inhibitor). 39

Figure 3.7: Cell growth inhibition graphs of MCF-7 and MDA-MB-231 cells exposed to ESE-one in combination with mannitol (hydroxyl radical inhibitor). 40

Figure 3.8: Cell growth inhibition graphs of MCF-7 and MDA-MB-231 cells exposed to ESE-one in combination with sodium azide (oxygen singlet inhibitor). 41

Figure 3.9: Cell growth inhibition graphs of MCF-7 and MDA-MB-231 cells exposed to ESE-one in combination with carboxy-PTIO (nitric oxide inhibitor). 43

Figure 3.10: Light micrographs of MCF-7 and MDA-MB-231 cells propagated in growth medium, vehicle treated and ESE-one exposed. 46

Figure 3.11: Light micrographs of MCF-7 and MDA-MB-231 cells exposed to tiron alone, and tiron in combination with ESE-one. 47

Figure 3.12: Light micrographs of MCF-7 and MDA-MB-231 cells exposed to DMTU alone, and DMTU in combination with ESE-one. 48

Figure 3.13: Light micrographs of MCF-7 and MDA-MB-231 cells exposed to trolox alone, and trolox in combination with ESE-one. 49

Figure 3.14: Cell cycle progression graphs of MCF-7 and MDA-MB-231 cells exposed to ESE-one in the presence or absence of ROS inhibitors (tiron, trolox and DMTU) for 24 hours. 52

Figure 3.15: Cell cycle progression graphs of MCF-7 and MDA-MB-231 cells exposed to ESE-one in the presence or absence of ROS inhibitors (tiron, trolox and DMTU) for 48 hours. 55

Figure 3.16: SOD inhibition graphs of MCF-7 (A) and MDA-MB-231 (B) cells exposed to ESE-one in the presence or absence of ROS inhibitors (tiron, trolox and DMTU). 58

Figure 3.17: Catalase activity graphs of MCF-7 and MDA-MB-231 cells exposed to ESE-one in the presence or absence of ROS inhibitors (tiron, trolox and DMTU). 59

Figure 3.18: Mitochondrial membrane graphs of MDA-MB-231 cells exposed to ESE-one in the presence or absence of ROS inhibitors (tiron, trolox and DMTU). 62

Figure 3.19: Mitochondrial potential graphs of MCF-7 and MDA-MB-231 cells exposed to ESE-one in the presence and absence of ROS inhibitors (tiron, trolox and DMTU). 64

Figure 4.1: Proposed mechanism utilized by ESE-one to induce cell death 71

**List of tables**

Table 1.1: Classification of breast cancer 3

Table 1.2: *In silico*-designed sulphamoylated- and non-sulphamoylated compounds 13

Table 2.1: ROS scavengers and concentration ranges that were used 22

Table 3.1: Sulphamoylated compounds and their non-sulphamoylated counterparts 29

Table 3.2: Sulphamoylated compounds and their non-sulphamoylated counterparts 33

Table 3.3: Percentage of MCF-7 cells in different morphological states as determined by means of light microscopy. 50

Table 3.4: Percentage of MDA-MB-231 cells in different morphological states as determined by means of light microscopy. 50

Table 3.5: Percentage MCF-7 cells occupying each cell cycle phase as determined by means of flow cytometry using PI after 24 hours exposure. 53

Table 3.6: Percentage MDA-MB-231 cells occupying each cell cycle phase as determined by means of flow cytometry using PI after 24 hours exposure. 53

Table 3.7: Percentage MCF-7 cells occupying each cell cycle phase as determined by means of flow cytometry using PI after 48 hours exposure. 56

Table 3.8: Percentage MDA-MB-231 cells occupying each cell cycle phase as determined by means of flow cytometry using PI after 48 hours exposure. 56

Table 3.9: Percentage of MCF-7 cells polarity of the mitochondrial membrane as determined by means of flow cytometry. 60

Table 3.10: Percentage of MCF-7 cells polarity of the mitochondrial membrane as determined by means of flow cytometry. 60

**Graphic representation of signaling pathways**

All graphic signaling pathways were created by MT Lebelo using Microsoft Publisher 2013 (Microsoft Corporation, United States). Structures were created by Dr MH Visagie using ACD/ChemSketch version 1101 released on 2007/10/19 (Advanced Chemistry Development, Inc., ACD/Labs, Toronto, Canada). Permission was granted by Dr MH Visagie to use chemical structures in this dissertation.

# Chapter 1

## Introduction

### 1.1 Cancer

Cancer is a global health threat and is one of the leading causes of premature deaths globally. The International Agency for Research in Cancer reported an estimated 18.1 million new cancer cases in 2018 globally with 9.6 million cancer-related deaths (1). An estimated 10 million cancer mortality is expected by 2020 (2). Breast- and lung cancer are reported to be the most commonly diagnosed types of cancer (11.6% each) and are also the leading causes of cancer-related mortality; followed by prostate (7.1%)- and colorectal cancer (6.1%) (3). In addition, breast cancer is the most prevalent cancer diagnosed in women worldwide and is the leading cause of cancer-related mortality in women, also accounting for 30% of overall female cancer cases (4, 5). Approximately 8% of all deaths in South Africa in 2014 were due to cancer, with cervical cancer being the leading cause of cancer deaths in women followed by breast cancer (6).

**Literature review**

1.1.1 Breast cancer

Breast cancer is the most commonly diagnosed type of cancer and the second leading cause of cancer-related mortality in African women (7). Africa accounted for 5.8% and 7.3% of the new cancer cases and cancer-related mortalities in 2018. Approximately 11.6% of the new cancer cases expected in 2018 were breast cancer, also accounting for 6.6% cancer-related deaths. Southern African women have the highest incidence rate in all African districts due to urbanization and economic development (7). In addition, the risk of developing breast cancer increases with age irrespective of family history (8).

Different classifications of breast cancer include histological, morphological and molecular/intrinsic classification subtypes of this disease (9, 10). Cancer is either luminal or basal, invasive or non-invasive, and also express various receptors (estrogen, progesterone or human epidermal growth factor 2 (HER2)) (11-13). Ductal carcinoma *in situ* is a non-invasive tumour which is frequently observed and develops within normal (untransformed) breast ducts. Furthermore, this type of

cancer can develop into an invasive type if left untreated (2). Invasive ductal carcinoma originates from the ductal tissue of the mammary glands and infiltrates other breast tissue outside the duct (2, 14). Invasive lobular breast cancer originates from the breast lobules and is mostly found in elderly women of above the age of 60 years (2). This breast cancer can also spread into other breast tissue. Metastatic/stage IV breast cancer occurs when the cancer cells have spread from the organ of origin to other parts of the body making it challenging to eradicate the whole tumour including the remnants (15-17). This type of cancer is capable of returning more aggressively years after the removal of the primary tumour possibly due to the disseminated tumour cells entering a senescence/dormant state (18). The disseminated tumour cells may remain in a senescent state for years, thus evading treatment subjected to tumourigenic cells. Thereafter, dormant tumour cells enter the active cell cycle (rapidly proliferating) and become more aggressive and difficult to treat (19, 20).

Molecular classification of breast cancer includes luminal A, luminal B, HER2-enriched, triple negative (sometimes used interchangeably with basal-like breast cancer) and normal-like breast cancer (similar to luminal A) (21-23). Luminal A carcinoma is estrogen receptor (ER)- and progesterone receptor (PR) positive, HER2 negative (not overexpressed) and express low levels of protein ki67 (proliferation marker) (2). Ki67 is a nuclear protein associated with cell proliferation and is present in all four active cell cycle phases, it is also used as a proliferation marker in tumour cells (24). Luminal B carcinoma is ER and/or PR positive, HER2 positive/negative (can be either), and has high levels of protein ki67. HER2-enriched carcinoma has low expressions of luminal and basal masses, is ER and PR negative, and bares overexpression of HER2. Triple negative breast cancer does not express any of the three receptors (estrogen, progesterone nor HER2) (2, 25-27). Normal-like breast cancer is the non-invasive breast cancer which is ER- and/or PR positive, HER2 negative and express low levels of protein ki67 (table 1.1) (2).

Table 1.1: Classification of breast cancer

| Breast cancer subtype | Receptors | Ki67 protein |
|---|---|---|
| Luminal A | ER and/or PR positive, HER2 negative | Low (2, 25, 28) |
| Luminal B | ER and/or PR positive, HER2 positive/negative | High (2, 25, 28) |
| HER2-enriched | ER and PR negative, HER2 positive | High (29) |
| Triple negative | ER, PR and HER2 negative | High (28, 29) |
| Normal-like | ER and/or PR positive, HER2 negative | Low (2) |

There are various risk factors for breast cancer including early menarche, having first childbirth at age above 30, late menopause, oral contraceptives, hormone therapy, having close relatives diagnosed with breast cancer, living a sedentary lifestyle and living on a Western diet (30-32). Moreover, the longer one is exposed to estrogen in their lifetime, the higher the risk of developing breast cancer (33). This is due to most types of cancer being dependent on estrogen for tumour growth (34). Thus, the more estrogen present in the body, the higher the likelihood of tumour growth (35, 36).

Furthermore, the risk associated with breast cancer is elevated if there is a genetic mutation present including the breast cancer gene mutations (BRCA1 or BRCA2) or a mutation of the tumour suppressor p53 (37). BRCA gene is a tumour suppressor which repairs damaged deoxyribonucleic acid (DNA) (38). Mutations in this gene are associated with the inability to repair damaged DNA and thus increases the risk of breast cancer (39).

### 1.1.2 Available treatment

There are different stages of breast cancer thus warranting for differential treatment strategies. The four main treatment methods include surgery, radiation, chemotherapy and immunotherapy (40-43). Surgery is mainly used for primary tumours where the tumourigenic cells/tissue is removed (44). This method is not feasible when the cancer has metastasised referring to the disseminated cancer

cells spreading from the primary site to other organs including the brain, liver or lungs (45). Radiation therapy involves the use of high energy X-rays to target actively proliferating cells (46, 47). This is used at different stages of breast cancer and is highly effective at targeting any cancer cells that remain after surgery, and subsequently reduces the chances of recurrence (47). Chemotherapy involves the administration of drugs orally or intravenously to treat or control breast cancer. Chemotherapy is the main treatment method for triple negative breast cancer and breast cancer that has metastasised to other organs together with targeted therapy (48). This treatment method can be given before surgery (neoadjuvant) or after surgery (adjuvant) depending on the extent of the cancer. Neoadjuvant chemotherapy is used in order to shrink the size of the tumour so that all of it can be removed, reducing the chances of leaving any cancerous cells or tissue behind whereas adjuvant chemotherapy is used to target the remaining cancer cells after surgery and also to limit the chances of recurrence (49). Chemotherapy agents include platinum-based (interfere with DNA replication), alkylating agent (damage DNA), mitotic inhibitors (inhibit cell division) and anti-metabolites (inhibit DNA production) (50, 51). Immunotherapy involves the use of the immune cells (usually T-cells) to target highly proliferative cells. Tumourigenic cells exhibit different antigens compared to non-tumourigenic cells and thus can be identified by the immune system allowing for antigen-ligand interaction (52). Various studies have reported that targeting T-cell checkpoint molecules (programmed cell death protein 1 (PD-1) and cytotoxic T-lymphocyte-associated antigen 4 (CTLA-4)) can improve anti-tumour immunity and survival (52, 53). Antibodies that interfere with T-cell checkpoint molecules have demonstrated a positive effect on various cancers including lung, melanoma, bladder, head and neck, and renal cancer (53). It was reported that stimulated cluster of differentiation 8+ (CD8+) T-cells in triple negative breast cancer penetrate the tumour and attack intracellularly however, combination therapy with immune vaccine, chemotherapy and trastuzumab has demonstrated promising results in different types of breast cancer (42, 54). There are various clinical trials underway for the use of immunotherapy in breast cancer treatment (42, 54, 55). Tamoxifen has been used for over two decades to treat breast cancer and also used on women that have a high risk of breast cancer (family history or BRCA mutation) however, it only works on ER positive types of cancer and usually used in

premenopausal women (56, 57). Tamoxifen is also used as a neoadjuvant drug to help shrink the tumour size to make it easier to remove (58). In postmenopausal women, aromatase inhibitors (eg. letrozole) are used and is particularly effective at lowering the estrogen levels (56). Trastuzumab is usually used in HER2-enriched types of cancer and for metastatic cancer, various drugs are used including pertubumab, lapatinib, everolimus and trastuzumab among others (54, 59).

Most cancer treatments operate by targeting or interrupting the cell cycle machinery. By so doing, cell cycle progression is halted, and cells fail to proceed to the next phase of the cycle (60, 61). Drugs targeting cell cycle proteins have shown promising results in clinical trials as tumourigenic cells depend on the overexpression of cell cycle proteins for survival and progression through the cell cycle (62, 63).

## 1.2 Overview of the cell cycle

The cell cycle entails the process whereby DNA duplicates, divides, and new cells are produced. The cycle encompasses a series of 5 steps namely; gap 0/quiescence phase ($G_0$) where cells are not active, gap 1 phase ($G_1$) where the cell is active and prepares for replication of genetic material, synthesis phase (S-phase) where the DNA is replicated and the cell readies for division, gap 2 phase ($G_2$) where the genetic material increases and the cell prepares itself for division, and the 5$^{th}$ step is the mitotic phase (M) where the cell divides its cytoplasm and genetic material into two cells in a series of four mitosis phases (prophase, anaphase, metaphase, telophase). $G_1$, S-phase and $G_2$ all fall under the interphase segment of cell cycle before the commencement of the actual cell division in mitosis (64-67).

The events of the cell cycle take place under strict control of various checkpoints composed of protein kinases. Cyclin-dependent kinases (CDK), catalytic proteins, pair up with cyclins (regulatory subunits), to form a complex (together with various proteins) that tightly regulates cell cycle progression (68, 69). Cyclin D-CDK2/4 complex assist with the rise in of DNA content in $G_1$ phase before the cell can go through a checkpoint regulated by cyclin E-CDK2 (63, 70). Once the cell gets to the S-phase, it undergoes DNA replication mediated by cyclin A–CDK2 complex. This then allows the cell to go through $G_2$ phase for further accumulation of DNA in

preparation for cell division and this process is regulated by cyclin A–CDK 1 complex. Progression of cells to the M-phase is regulated by cyclin B–CDK1 by making sure that the DNA integrity is intact thus allowing for the cell to divide into two identical daughter cells with equal- and identical genetic material (71, 72).

### 1.2.1 Cell cycle phases

#### 1.2.1.1 $G_1$ phase

The $G_1$ phase is where the cell fate is determined on whether to proceed to the next phase or not based on the various cell growth regulators and mitogens, and acquires all the necessary components required for it to proceed to the S-phase (73, 74). The cell has to ensure it is the right size, possesses adequate organelles (centrosomes, centrioles, mitochondria) and all the required enzymes, and should have all the necessary growth signals. Should it fail one of these required factors the cell will not continue to the S-phase but rather continue to be in the $G_1$ phase until it has received all the necessary components to proceed or the cell will instead enter the $G_0$ phase (75, 76). As the cell approaches the late $G_1$ phase, it encounters the restriction point (R-point) which is guarded by retinoblastoma protein (pRB). If the cell has all properties required for it to proceed, pRB is phosphorylated allowing for the cell to enter late $G_1$. The cyclin D–CDK4/6 complex plays an essential role in the $G_1$ phase by facilitating pRB phosphorylation allowing for the progression of the cell to the next phase. Transcription factor E2F is bound to pRB in $G_1$ phase and upon phosphorylation of pRB, E2F is released resulting in the transcription of genes that allow for the transition from the $G_1$ phase to the S-phase (76, 77).

#### 1.2.1.2 S-phase

The S-phase is a crucial stage of the cell cycle and thus it necessitates strict regulation to ensure good quality DNA copies. Origin recognition complexes (ORC), which consists of six subunits, bind to replication sites on the chromosomes and recruits pre-replication complexes. Pre-replication complexes are usually inactive in the M- and $G_1$ phases and are activated in S-phase to instigate DNA replication (78, 79). Pre-replication complexes include cell division cycle 6 (CDC-6) which is important for the initiation of DNA replication, chromatin licensing and DNA replicating factor1 (cdt1) which ensures that DNA only replicates once per cycle, and

mini-chromosome maintenance 2-7 (MCM2-7) protein complex which unwinds the DNA helix (80-82).

1.2.1.3 $G_2$/M

Once the DNA has finished replicating and all necessary requirements are met, the cell proceeds to the $G_2$ phase where it grows in preparation for cytoplasm and chromatin splitting/division. The $G_2$ phase is regulated by cyclin A–CDK1 which is phosphorylated thus allowing for the cell to proceed to the M phase. In the M phase, cyclin B–CDK 1 is activated and regulates the division of one cell into two identical daughter cells (83). Mitosis is comprised of four successive phases; prophase, metaphase, anaphase and telophase. In this cell cycle phase, chromosomes condense (prophase), and the nuclear envelope becomes visible, followed by the alignment of chromosomes on the equatorial plate (metaphase). The chromosomes are then pulled to the opposite pole (anaphase) and the cell membrane forms furrows to separate the two newly formed daughter cells (telophase) (67).

1.2.2 Checkpoints

Cell cycle progression is regulated at three important sites known as cell cycle checkpoints. $G_1$ checkpoint (restriction point) regulates the progression of cells from the $G_1$ phase to the S-phase, $G_2$ checkpoint regulates the progression of cells from the $G_2$ phase to the M phase and the M checkpoint (spindle checkpoint) regulates the progression of cell division from mitosis to anaphase (84).

1.2.2.1 $G_1$ checkpoint (restriction point)

The $G_1$ checkpoint (also known as the restriction point) is found towards the end of $G_1$ phase and this is the point where the fate of cell is decided, whether it will enter the S-phase for DNA replication or to stay in $G_1$ phase until required components are in place. The key regulator of the $G_1$ checkpoint is p53 tumour repressor gene which upon DNA damage activates cyclin/CDK inhibitors to stop the progression of the cell from the $G_1$ phase to the S-phase. The tumour suppressor, p53, is activated by various protein kinases including ataxia-telangiectasia mutated (ATM) and ATM- and Rad3-related (ATR) kinases due to DNA damage and upon activation, p53 targets CDK inhibitors (p21/WAF1) which subsequently results in cell cycle arrest. The cell

remains in the $G_1$ phase until the DNA is repaired from then it can proceed to S-phase for DNA replication or it exits the cell cycle to the $G_0$ phase where it becomes inactive and awaits further instructions. Should the DNA not be able to be repaired, the cell then undergoes apoptosis (programmed cell death) (84, 85).

#### 1.2.2.2 $G_2$ checkpoint (DNA checkpoint)

The cell proceeds to the S-phase if it meets all requirements including DNA integrity (no DNA damage), CDK activation and energy reserves (66, 86, 87). In the S-phase, the DNA is replicated and subsequently the cell proceeds to the $G_2$ phase where it prepares for cell division (mitosis) (88). For the cell to pass the $G_2$ checkpoint, the DNA replication must be satisfactory with no DNA damage present, possess appropriate protein reserves and a good cell size. Should there be any DNA damage; the cell will be arrested in the $G_2$/M phase. Cyclin B-CDK1 is kept inactive to prevent the progression of cells from $G_2$ to M phase (84, 87, 89).

#### 1.2.2.3 M checkpoint (spindle checkpoint)

The M checkpoint is situated towards the end of metaphase and ensures that the cell does not proceed do anaphase until all the kinetochores are attached to the mitotic spindles from opposite poles in order to allow equal separation of chromatids in anaphase (90, 91). The M checkpoint plays a regulatory role by inhibiting anaphase-promoting complex (APC) until all kinetochores are attached to spindle microtubules (92). Budding uninhibited by benomyl (Bud) and mitotic arrest deficient (Mad) proteins are activated to regulate the checkpoint. Mad2 binds to kinetochores thus preventing the activation of anaphase-promoting complex (which facilitates transition of cells from metaphase to anaphase) resulting in a metaphase block (67, 93, 94).

## 1.3 Apoptosis

Apoptosis, also referred to as programmed cell death, is a type of cell death mechanism used by the organism to regulate tissue size, shape and also to maintain systemic homeostasis (95). Furthermore, the body utilizes this process to get rid of damaged cells. Apoptosis is characterised by several morphological hallmarks including shrinkage of cells from other surrounding cells, blebbing of the plasma membrane, cytoplasm- and nuclear condensation, margination of condensed

chromatin, nuclear fragmentation and cell destruction resulting in apoptotic bodies (figure 1.1) (73, 96). In addition, phosphatidylserine, a phospholipid located on the inner side of the plasma membrane bilayer, is externalized and exposed on the outside of the plasma membrane of the apoptotic bodies which can be a signal for macrophages to engulf the dead cell. This flip in the cell membrane causes the externalization of the phosphatidylserine, allowing for various cellular proteins like Annexin V to bind to the exposed phosphatidylserine which is indicative of apoptosis (73, 96-98).

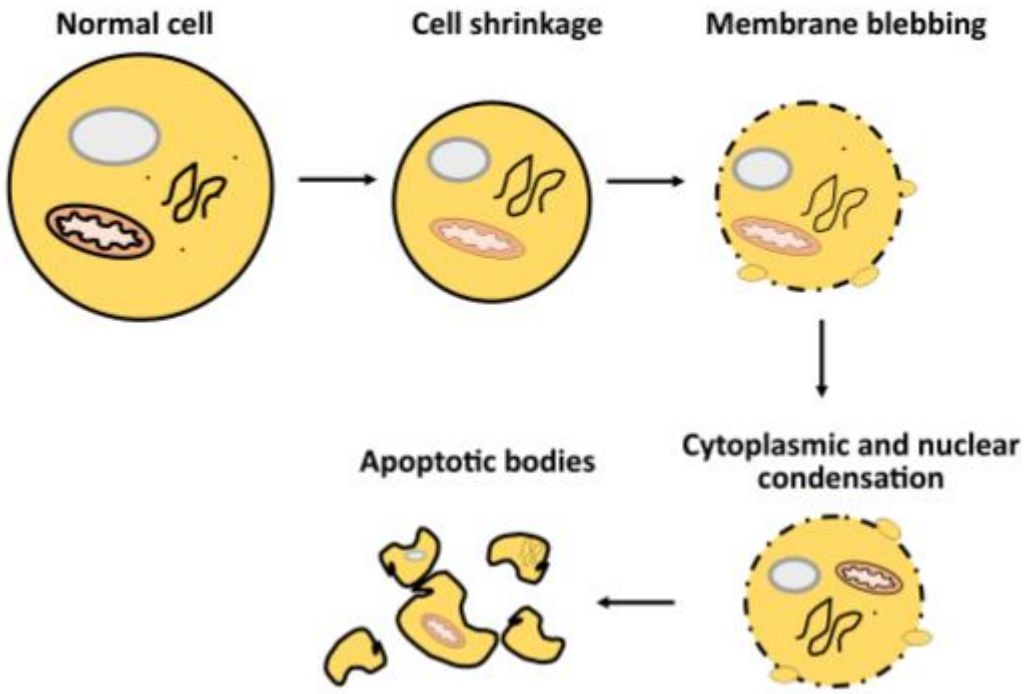


Figure 1.1: Process of apoptosis. Apoptosis is characterised by morphological changes that occurs during apoptosis including cell shrinkage, membrane blebbing, DNA fragmentation, cytoplasm and nuclear condensation, and appearance of apoptotic bodies (diagram created by MT Lebelo using Microsoft Publisher 2013 (Microsoft Corporation, Washington, United Sates of America)).

Apoptosis can take place via the extrinsic (death receptor pathway), the intrinsic (mitochondrial) or the endoplasmic reticulum pathway which are caspase-dependent (figure 1.2) (99, 100). Alternatively, apoptosis can also take place via the caspase-

independent pathway where caspases are not involved and instead effectors such as apoptosis inducing factor (AIF) induce apoptotic cell death (101). The extrinsic pathway initiates extracellularly and is triggered by the interaction between pro-apoptotic death receptors (DR) including DR4 or DR5 and ligands of the tumour necrotic factor (TNF) family such as apoptosis stimulating fragment ligand (FasL) and tumour necrosis factor related apoptosis-inducing ligand (TRAIL) on the cell membrane (102, 103). A Fas receptor adaptor molecule, Fas-associated protein with death domain (FADD) recruits inactive initiator caspases (procaspase 8 and procaspase 10) forming a death inducing signaling complex (DISC) which causes cleavage of inactive caspases to active caspases (caspase 8 and caspase 10) which further results in the activation of the executioner caspases (caspase 3, 6 and 7) and ultimately apoptosis induction (104, 105). The intrinsic apoptosis pathway is activated by cellular stressors including elevated reactive oxygen species (ROS) and DNA damage among others, and initiates intracellularly (106). This activates pro-apoptotic proteins of the B-cell lymphoma 3 homologue (BH3) family which activates B-cell lymphoma associated X (BAX)/B-cell 2 homologue antagonist killer (BAK) oligomerization directly or indirectly by binding to pro-apoptotic B-cell lymphoma-2 (Bcl-2) proteins (107). Bcl-2 proteins exist in two groups of pro-apoptotic (Bcl-2 associated death promotor homologue (Bad), BH3 interacting domain death agonist (Bid), Bim, Bcl-2 modifying factor (Bmf), protein harakiri (Hrk), Noxa, Bcl-2 interacting killer (Bik), p53 upregulated modulator of apoptosis (Puma)) and anti-apoptotic (Bcl-2, Bcl-$X_L$) factors which play a vital role in intrinsic apoptosis (107, 108). The activation of initiator caspase 8 causes the inactive Bid to be converted to truncated Bid (tBid) which is the active form and this then activates Bax/Bak on the mitochondrial membrane (109). Activation of Bax/Bak oligomer results in mitochondrial membrane permeabilization and subsequent release of cytochrome *c* and second mitochondria-derived activator of caspase/direct inhibitor of apoptosis binding protein with low pI (Smac/DIABLO) (110, 111). Cytochrome *c* binds to apoptosis protease-activating factor 1 (Apaf-1) forming a proteasome which activates procaspase 9 to active caspase 9, resulting in the activation of executioner caspases (caspase 3,6,7) leading to apoptotic cell death (figure 1.2) (112). Smac/DIABLO release from the mitochondria results in the inhibition of the inhibitor of apoptosis protein (IAP) and subsequent activation of executioner caspases resulting in

apoptosis (103). Mitochondrial membrane potential is important for the integrity of the mitochondrial and ATP production thus excessive changes, like a drop in mitochondrial membrane potential, can result in cell death (113). Permeability of the mitochondrial membrane may result in membrane depolarization and release of cytochrome *c* into the cytoplasm, ultimately leading to apoptosis (113-115).

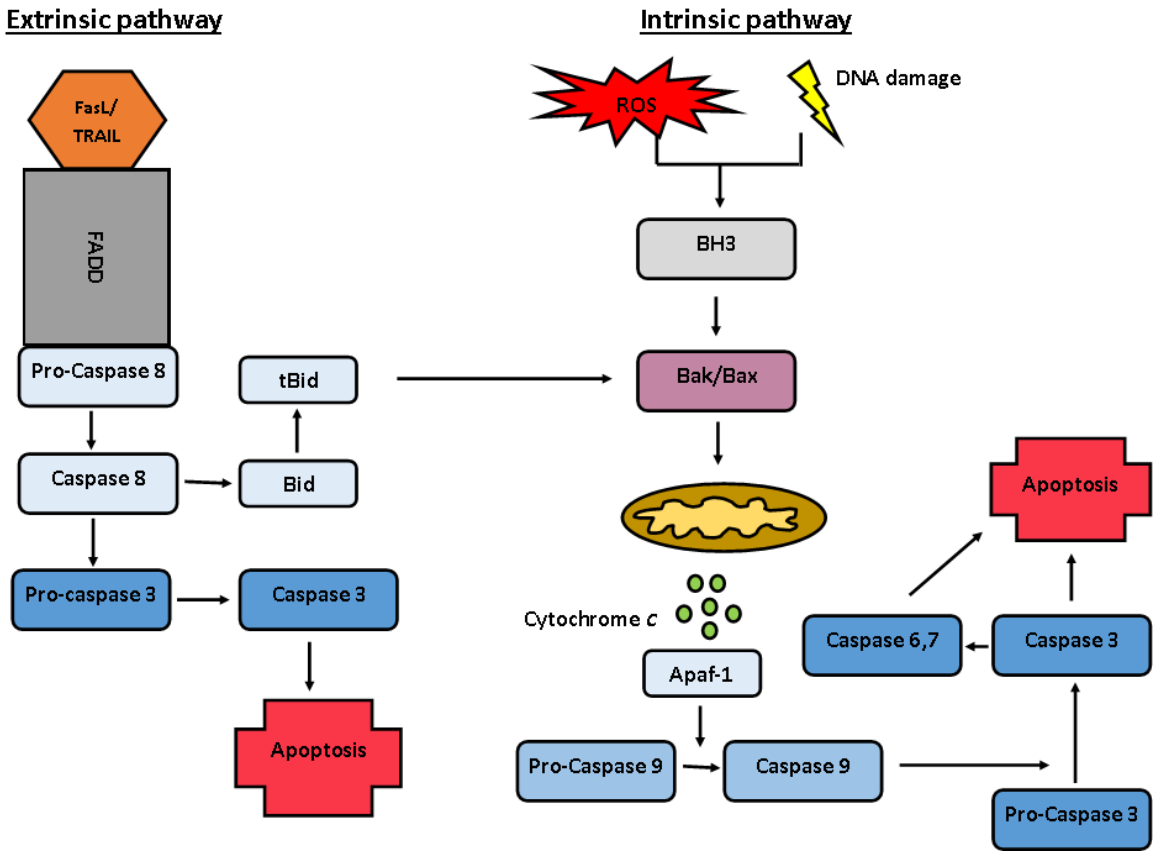


Figure 1.2: Extrinsic- and intrinsic apoptosis pathways. The extrinsic apoptotic pathway involves death receptor ligands FasL and TRAIL which activates caspase 8. Caspase 8 activates caspase 3 that ultimately leads to apoptosis, and Bid which activate the Bak/Bax complex resulting in mitochondrial depolarization and cytochrome *c* release. The intrinsic pathway involves the activation of BH3 protein family by DNA damage and oxidative stress which activates the Bak/Bax complex causing cytochrome *c* release from the mitochondria. Caspase 9 is then activated, which activates caspase 3 resulting in apoptosis induction.

## 1.4 2-Methoxyestradiol and sulphamoylated compounds

2-Methoxyestradiol (2ME), a 17-β estradiol metabolite, exhibits anticancer-, antiangiogenic- and antitumour activity (116). Furthermore, 2ME is destructive to the tubulin structure of cells regardless of the ER estrogen receptor status and induces apoptosis. Despite the desired effects that 2ME has on tumourigenic cells, it has low

bioavailability and is easily degraded. This lead to the *in silico*-design of several sulphamoylated- and non-sulphamoylated estradiol compounds with improved bioavailability (117) (Table 1.2). Estradiol- and 2ME derivatives with a sulphamate moiety revealed improved bioavailability when compared to 2ME since the sulphamoylation allows for bypassing the liver without undergoing first pass metabolism (118). In addition, sulphamoylated compounds are believed to reversibly bind to carbonic anhydrase II (CA II). CAs are a group of zinc containing isozymes that facilitate the interconversion between $CO_2$ and $HCO_3^-$ (119). There are several CA isoforms identified in humans, with the cytosolic ones trapping acid intracellularly whereas the cellular membrane ones are responsible for extracellular acidification. CAIX was reported to be associated with solid tumours and regulation of tumour pH (120).

Table 1.2: *In silico*-designed sulphamoylated- and non-sulphamoylated compounds. Structures were created by Dr MH Visagie using ACD/ChemSketch version 1101 released on 2007/10/19 (Advanced Chemistry Development, Inc., ACD/Labs, Toronto, Canada).

| Non-sulphamoylated compound | Sulphamoylated compound |
|---|---|
| 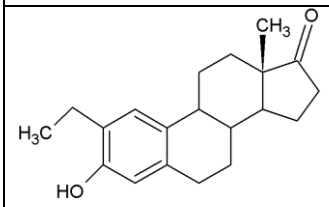 2-Ethylestrone (EE-one) also known as C5). | 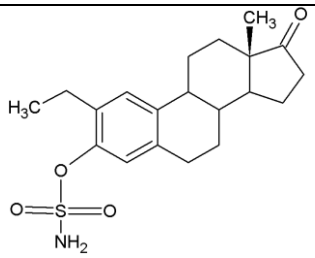 2-Ethyl-13-methyl-17-oxo-7,8,9,11,12,13,14,15,16,17-decahydro-6-cyclopenta[*a*]phenanthrane-3 sulphamate (ESE-one) also known as C15. |
| 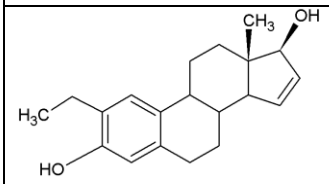 2-Ethyl-17estra-1,3,5(10)16-tetraene (EE-15-ol) also known as C11. | 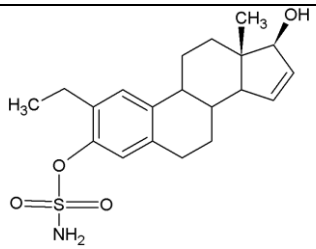 2-Ethyl-estra-17-methylbenzenesulfenohydrazide (ESE-15-ol) also known as C10. |
| 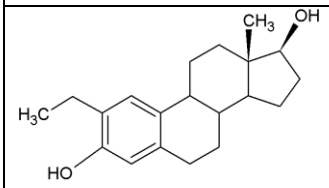 2-Ethyl-13-methyl-7,8,9,11,12,13,14,15,16,17-decahydro-6-cyclopenta[*a*]phenanthrane-3,17-diol (2-E-diol) also known as C13. | 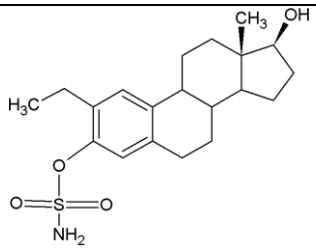 2-Ethyl-17-hydroxy-13-methyl-7,8,9,11,12,13,14,15,16,17-decahydro-6-cyclopenta[*a*]phenanthren-3-yl sulphamate (ESE-ol) also known as C16. |

Several estradiol sulphamoylated analogues including 2-methoxyestradiol-bis-sulphamate, (8*R*,13*S*,14*S*,17*S*)-2-ethyl-13-methyl-7,8,9,11,12,13,14,15,16,17-decahydro-6H-cyclopenta[a]phenanthrane-3,17-diyl bis(sulphamate) (EMBS) (also known as C14), ESE-15-ol and ESE-ol have demonstrated antiproliferative-, antimitotic- and apoptotic activity in tumourigenic cell lines including breast tumourigenic cell lines (MCF-7, MDA-MB-231) and an oesophageal tumourigenic cell line (SNO) (117, 121-125). Furthermore, EMBS, increases ROS production in the MDA-MB-231 cell line which is associated with a decrease in cell proliferation, mitochondrial membrane damage, cell cycle arrest, decrease in metabolic activity and apoptosis induction. Furthermore, the addition of N-acetyl cysteine (NAC) abrogated antiproliferative activity, cell cycle arrest and cell death suggesting that ROS production is essential for the ability of EMBS to induce cell death. However, the specific ROS-dependent signaling cascade induced by EMBS including the relevant involved ROS remains unknown (126).

These sulphamoylated estradiol compounds exert antiproliferative-, antimitotic- and cell death inducing activity that correlates with ROS induction. However, the exact mode of action still remains elusive (117, 121-125). Identification of the aberrant ROS modulated by the estradiol sulphamoylated antimitotic compounds in cancer cell lines and the mechanism of action utilised by the sulphamoylated antimitotic compounds will identify a novel oxidative-stress dependent signaling used by antimitotic compounds to induce apoptosis in breast cell lines.

## 1.5 Reactive oxygen species

ROS are oxygen species possessing an unpaired electron which are highly reactive (figure 1.3 and figure 1.4) (127). ROS include, among others, singlet oxygen, superoxide radical, perhydroxyl radical, hydrogen peroxide and hydroxyl radical, and play a major role in apoptosis induction and cell signaling (128). Mitochondrial generation of superoxide and subsequent hydrogen peroxide are the major contributors for ROS production in an actively proliferating cell (129). Superoxide, which is made by receiving an electron from nicotinamide adenine dinucleotide phosphate (NADPH), is converted to hydrogen peroxide via superoxide dismutase

(SOD) in the cytosol, and catalase converts hydrogen peroxide to water. ROS are generated via the mitochondria as a typical cell maintenance mechanism whereby a balance is maintained between ROS production and ROS elimination (130).

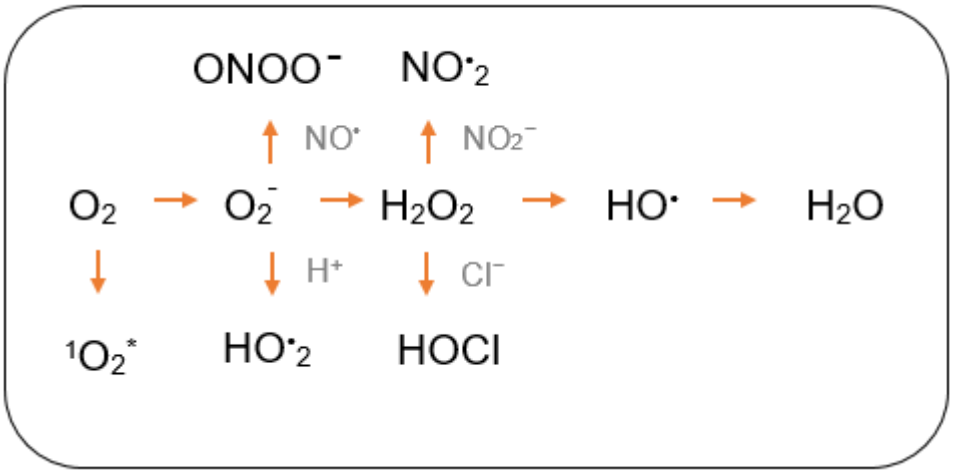


Figure 1.3: Production of ROS from an oxygen molecule (diagram created by M.T Lebelo in Microsoft Word 2013 (Microsoft Corporation, Washington, United Sates of America)).

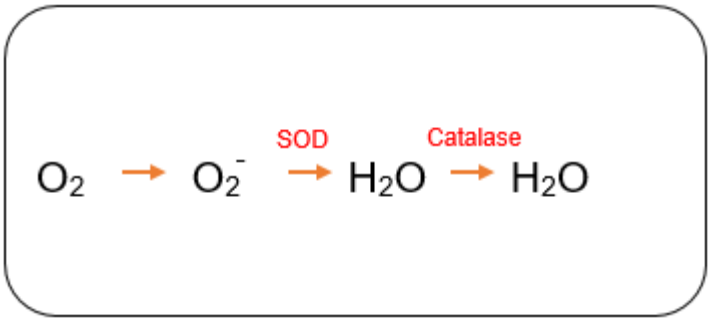


Figure 1.4: Conversion of superoxide and hydrogen peroxide by antioxidants. SOD converts superoxide to hydrogen peroxide and thereafter, hydrogen peroxide is converted to water by catalase (diagram created by M.T Lebelo in Microsoft Word 2013 (Microsoft Corporation, Washington, United Sates of America)).

ROS are produced during metabolic processes and are maintained at an acceptable level by the antioxidant production including SOD, catalase and glutathione (131). Literature has shown that proliferation of breast-, liver- and lung cancer cells including MCF-7- and MDA-MB-231, is dependent on ROS. The ROS-dependent proliferation mechanism was confirmed when a ROS scavenger (NAC) supressed proliferation. A moderate increase in ROS results in increased cell proliferation

however, the introduction of antioxidants have an opposing effect indicating that ROS has a positive cell growth effect in various tumourigenic cells which can be inhibited by a ROS scavenger (132-134). Overexpression of SOD inhibited breast cancer metastasis in mouse xenographs demonstrating the importance of antioxidants in limiting metastasis in tumourigenic cells (132). Furthermore, ROS exert proliferative effects in breast cancer cells by recruiting cells into the S phase of the cell cycle, thus enhancing cellular myelocytomatosis (c-Myc) expression and increases transcription factors including nuclear factor kappa-light-chain enhancer of activated B cells NF-κB (NF-κB) activity involved in cell transformation, survival, angiogenesis, proliferation and metastasis (135). Thus, ROS have been reported to contribute to cancer initiation and progression while on the other hand, excessive ROS production has been linked to cell death, indicating that ROS are a double-edged sword (136, 137).

Excessive ROS quantities resulting from increased ROS production or a decrease in antioxidants results in inhibition of tumour growth and apoptosis induction (135). Pisano *et al*. (2019) demonstrated that ROS-induced cell death by vanadium is inhibited by a ROS scavenger (NAC), in a A375 melanoma cell line which suggested ROS-dependent cell death (138). ROS mediate pro-death signaling via apoptosis signal-regulating kinase 1 (ASK) activation of mitogen activated protein kinase (MAPK) and c-Jun-terminal kinase (JNK) which results in the induction of apoptosis. ASK-1 activates p38 and JNK resulting in the transcription of FasL thus initiating the extrinsic apoptosis pathway. FasL-FAD complex activate caspase-3 (initiator) and bid (upregulating BAX) ultimately resulting in apoptosis. JNK and MAPK stimulate the upregulation of pro-apoptotic signals and downregulation of anti-apoptotic signals. ROS-mediated JNK/MAPK downregulates cyclin, CDK inhibition therefore resulting in cell cycle arrest (132).

ROS are mainly produced by the mitochondria thus aberrant mitochondrial function is frequently associated with inconsistent ROS quantities. Furthermore, mitochondria are also the main target of ROS resulting in various pathologies (139). An elevation in ROS leads to an aberrant change in the mitochondrial membrane potential resulting in membrane depolarization. A loss/decrease of mitochondrial membrane

potential has been associated with apoptosis. Permeabilization of the mitochondrial membrane by various factors (including ROS) results in transmembrane depolarization and the release of apoptosis-promoting factors including cytochrome *c* which ultimately results in apoptosis via the mitochondrial pathway (intrinsic) (140-142).

In the current study, tumourigenic breast cell lines were exposed to an oxidative stress-inducing compound culminating in antiproliferative activities and cell death induction whereby various ROS inhibitors were used in an attempt to identify the ROS that is crucial for these effects induced by sulphamoylated *in silico*-designed compounds. Identification of the ROS modulated by the estradiol sulphamoylated antimitotic compounds and the mechanism of action utilised by the sulphamoylated antimitotic compounds will identify a novel oxidative-stress dependent signaling pathway used by antimitotic compounds to induce apoptosis in breast cell lines.

## 1.6 Relevance and aim of the study

This study is considered an *in vitro* study since it was conducted on commercially available cancer cell lines and the findings thereof cannot be extrapolated to an *in vivo* environment. The scientific findings in this study will contribute to understanding the oxidative stress-dependent mechanism of action utilised by ESE-one and other sulphamoylated estradiol analogues in the induction of apoptosis. The aim of the study was to evaluate the mode of action utilised by oxidative stress in the induction of apoptosis by ESE-one in breast tumourigenic cell lines.

## 1.7 Objectives

The objectives of the study were:

1. to compare the ROS production induced by ESE-one to other sulphamoylated compounds and their non-sulphamoylated estradiol counterpart compounds. This was done by utilizing DCFDA and DHE (fluorescent microscopy).
2. to quantify the hydrogen peroxide and superoxide production induced by ESE-one by utilizing 2,7-dichlorofluoresceindiacetate (DCFDA) and dihydroethidine (DHE) (fluorescent microscopy).

3. to identify which ROS are required for antiproliferative activity exerted by ESE-one in breast cancer cell lines. This was done by demonstrating the effects of ESE-one on cell growth in the presence or absence of various scavengers by means of crystal violet staining (spectrophotometry).

4. to determine if the cell rounding effects induced by ESE-one is dependent on the production of ROS. This was done by means of light microscopy after cells have been exposed to ESE-one in the presence or absence of the scavengers (identified in Objection 1).

5. to determine if the antimitotic- and cell death inducing activity induced by ESE-one is dependent on ROS production. This was accomplished by establishing the influence of ESE-one on the cell cycle progression and cell death induction in the presence or absence of various scavengers (identified in Objective 1) by means of propidium iodide (PI) staining (flow cytometry).

6. To determine if the effect of ESE-one on the mitochondrial membrane potential and possible activation of the intrinsic (mitochondrial) apoptosis pathway is dependent on ROS production. This was accomplished by establishing the influence of ESE-one on the mitochondrial membrane potential in the presence or absence of various scavengers (identified in Objective 1) by means of Mitoprobe JC-1 assay kit (flow cytometry).

7. to determine the influence ESE-one on the innate antioxidant system by demonstrating the effects of ESE-one on catalase- and superoxide dismutase activity by means of spectrophotometry.

# Chapter 2

## Research procedure

## Methods and materials

### 2.1 Materials

2.1.1 Cell lines

MDA-MB-231 is a triple negative tumourigenic breast cell line, indicating that MDA-MB-231 cells do not express ER, PR and HER. The MDA-MB-231 cell line was derived from an adenocarcinoma metastatic site (143). The MDA-MB-231 cell line was obtained from the American Type Culture Collection (Manassas, Virginia, United States of America) (126). The MCF-7 cell line is an adenocarcinoma ER positive, PR positive and HER2 negative breast epithelial cell line. The MCF-7 cell line is able to process estradiol by the cytoplasmic estrogen receptors ERs and is also able to form domes (116). The MCF-7 cell line was obtained from the American Type Culture Collection (Manassas, Virginia, United States of America). The MDA-MB-231- and the MCF-7 cell lines were cultured in 25 $cm^2$ tissue flask in Dulbecco's Minimum Essential Medium Eagle (DMEM) with 10% heat-inactivated fetal calf serum (FCS) (56°C, 30 min), 100 U/ ml penicillin G, 100 mg/ml streptomycin and fungizone (250 mg/l) at 37°C and 5% $CO_2$.

### 2.1.2 Reagents

All reagents were obtained from (Sigma Chemical Co) (St. Louis, Missouri, United States of America) unless otherwise specified. The PI, DHE, DCFDA and ROS inhibitors were manufactured and obtained from Sigma Chemical Co. (St. Louis Missouri, United States of America). Crystal violet dye was manufactured and provided by Merck & Co., Inc. (Kenilworth, New Jersey, United States of America). The SOD activity assay kit and human catalase activity kit simplestep was purchased from Abcam plc. (Cambridge, England, United Kingdom). Mitoprobe JC-1 assay kit was purchased from Thermo Fisher Scientific (Waltham, Massachusetts, Unites States of America).

## 2.2 Methods

### 2.2.1 Oxidative stress

2.2.1.1 Hydrogen peroxide generation using 2,7-dichlorofluoresceindiacetate (fluorescent microscopy)

The effects of the sulphamoylated- and non-sulphamoylated estradiol compounds on hydrogen peroxide production were quantified as an indicator of oxidative stress. DCFDA was used to measure hydrogen peroxide production. DCFDA, a non-fluorescent probe is oxidised to its fluorescent derivative DCF, by hydrogen peroxide (144, 145).

MCF-7- and MDA-MB-231 cells were seeded in 24-well plates at a density of 20 000 cells per well and incubated for 24 hours at 37°C and 5% $CO_2$ to allow for attachment. Cells were exposed to various sulphamoylated compounds (0.5 µM) (ESE-15-ol, ESE-one and ESE-ol) and non-sulphamoylated compounds (0.5 µM) (EE-one, EE-15-ol and 2-E-diol) for 24 hours at 37°C and 5% $CO_2$. Upon termination, 1% hydrogen peroxide was added to the positive control well for 5 minutes at room temperature. Thereafter, cells were washed with phosphate buffer solution (PBS). Cells were incubated with 20 µM DCFDA for 25 minutes at 37°C and 5% $CO_2$. Samples were washed with PBS and 0.5 µl PBS was subsequently added to each well. Zeiss Axiovert CFL40 microscope, Zeiss Axiovert MRm monochrome camera (Zeiss, Oberkochen, Germany) and Zeiss filter 9 was employed to capture images of the DCFDA-stained (green) cells. Fluorescence images were analyzed using Image J software developed by the National Institutes of Health (Bethesda, Maryland, United States of America). The fluorescent intensity of at least 100 cells was evaluated per condition in each experiment.

2.2.1.2 Superoxide generation using dihydroethidium (fluorescent microscopy)

The effects of the sulphamoylated- and non-sulphamoylated estradiol compounds on superoxide production were quantified as an indicator of oxidative stress. DHE was used to measure superoxide production. Superoxide oxidizes DHE to form a fluorescent red 2-hydroethidine cation (146).

MCF-7- and MDA-MB-231 cells were seeded in 24-well plates at a density of 20 000 cells per well and incubated for 24 hours at 37°C and 5% $CO_2$ to allow for attachment. Cells were then exposed to a various sulphamoylated compounds (0.5 µM) (ESE-15-ol, ESE-one and ESE-ol) and non-sulphamoylated compounds (0.5 µM) (EE-one, EE-15-ol and 2-E-diol) for 24 hours at 37°C and 5% $CO_2$. Upon termination, cells were washed with PBS. Cells were incubated with 10 µM DHE for 45 minutes at 37°C and 5% $CO_2$. Samples were washed with PBS and 0.5 µl PBS was subsequently added to each well. Zeiss Axiovert CFL40 microscope, Zeiss Axiovert MRm monochrome camera (Zeiss, Oberkochen, Germany) and Zeiss filter 15 was employed to capture images of DHE-stained (red) cells. Fluorescence images were analyzed using Image J software developed by the National Institutes of Health (Bethesda, Maryland, United States of America). The fluorescent intensity of at least 100 cells was evaluated per condition in each experiment.

### 2.2.2 Cell proliferation

2.2.2.1 Crystal violet staining (spectrophotometry)

Crystal violet staining was used to determine the influence of ESE-one on cell proliferation in the presence and absence of various ROS inhibitors. In addition, crystal violet staining was also done to determine if there is a significant differential effect exerted by sulphamoylated compounds when compared to their non-sulphamoylated compound counterparts. The crystal violet technique involves staining of the nuclei and cellular DNA with a triphenylmethane cation dye that binds to proliferating cells. This method is frequently used for proliferation studies to acquire the number of cells cultured in a monolayer. Spectrophotometry was used together with crystal violet staining to obtain the absorbance of the solubilized dye at a wavelength of 570 nm (147).

MCF-7- and MDA-MB-231 cells were seeded in 96-well plates at 4000 cells per well and incubated at 37°C and 5% $CO_2$ for 24 hours to allow for the attachment of cells to the plate. Cells were then exposed to 0.5 µM ESE-one since previous studies conducted in our laboratory with several sulphamoylated compounds demonstrated optimal antiproliferative activity at this dose in several tumourigenic cell lines (121).

In addition, cells were also exposed to additional sulphamoylated compounds (0.5 µM) for comparison with their non-sulphamoylated compound (0.5 µM) counterparts. Cells were exposed to ESE-one in the absence or presence of ROS scavengers (mannitol, trolox, tiron, 2-(4-carboxyphenyl)-4,4,5,5-tetramethylimidazoline-1-oxyl-3-oxide (Carboxy-PTIO), sodium azide and N,N'-dimethylthiourea (DMTU)) (Table 2.1) and incubated for 24 hours at 37°C and 5% $CO_2$. Upon termination, cells were fixed with 1% gluteraldehyde (100 µl) at room temperature for 15 minutes. Gluteraldehyde was then replaced with 0.1% crystal violet (100 µl) at room temperature for 30 minutes. Plates were left to dry overnight. Thereafter, 0.2% triton X-100 (200 µl) was added to the plates and incubated overnight to solubilize the crystal violet. Absorbances were read by means of an EPOCH Microplate Reader (Biotek Instruments, Inc. (Winooski, Vermont, United States of America)) at a wavelength of 570 nm. Data was then analyzed using Microsoft Excel 2010 (Microsoft Corporation, Washington, United Sates of America).

Table 2.1: ROS scavengers and concentration ranges that were used.

| Reactive oxygen species | Scavenger | Concentration |
|---|---|---|
| Hydrogen peroxide | N,N-dimethylthiourea (DMTU) | 1-10 mM (148) |
| Hydroxyl radical | Mannitol | 20-100 mM (148) |
| Nitric oxide | 2-(4-Carboxyphenyl)-4,4,5,5-tetramethylimidazoline-1-oxyl-3-oxide (Carboxy-PTIO) | 10-100 µM (148, 149) |
| Peroxyl radical | Trolox | 10-100 µM (150, 151) |
| Singlet oxygen | Sodium azide | 1-10 mM (148, 152) |
| Superoxide anion | Tiron | 1-10 mM (153, 154) |

### 2.2.3 Cell morphology

2.2.3.1 Light microscopy

Light microscopy was employed to investigate if the cell rounding effects induced by ESE-one are dependent on ROS formation. MCF-7- and MDA-MB-231 cells were seeded in 24-well plates at a density of 20 000 cells per well and incubated at 37°C

and 5% $CO_2$ for 24 hours to allow for the attachment of cells to the plate. After 24 hours, cells were exposed to 0.5 µM ESE-one in the presence and absence of ROS scavengers for 24 hours at 37°C and 5% $CO_2$. Thereafter, an Olympus CKX53 inverted microscope (Olympus Corporation, Tokyo, Japan) was used to capture images in order to compare the morphology of cells exposed to ESE-one in presence and absence of ROS scavengers. Light microscopy images were analysed using Image J software developed by the National Institutes of Health (Bethesda, Maryland, United States of America). At least 1000 cells were counted per condition in each experiment.

### 2.2.4 Cell cycle progression and apoptosis induction

2.2.4.1 Propidium iodide staining (flow cytometry)

The effects of ESE-one on cell cycle progression in the presence and absence of ROS scavengers were investigated by means of ethanol fixation, PI and flow cytometry. PI is a dye that stains the DNA of a cell and thus enables the quantification of DNA correlating with stages of the cell cycle during cell division (155).

Cells (MCF-7 and MDA-MB-231) were seeded at a density of 500 000 cells per T25 $cm^2$ tissue culture flask and incubated at 37°C and 5% $CO_2$ for 24 hours to allow for cell attachment. Subsequently, cells were exposed to 0.5 µM ESE-one in the presence or absence of ROS scavengers for 24- and 48 hours at 37°C and 5% $CO_2$. Upon termination, cells were trypsinized and resuspended in 1 ml growth medium. Samples were then centrifuged for 5 minutes at 300 x *g*. Supernatant was removed and pellet was resuspended in ice-cold PBS containing 0.1% FCS. Thereafter, 4 ml of 70% ice-cold ethanol was added in a drop-wise manner whilst vortexing and samples were kept at 4°C for at least 24 hours. Cells were then centrifuged at 300 x *g* for 5 minutes and the supernatant was removed. Cells were resuspended in 1 ml PBS containing PI (40 µg/ml), ribonuclease A (100 µg/ml) and triton X-100 (0.1%) and incubated at 37°C for 45 min. PI fluorescence was measured with the Gallios flow cytometer (Beckman Coulter, Inc. (Indianapilis, United States of America). Data from cell debris (particles smaller than apoptotic bodies) and clumps of 2 or more cells was removed from further analysis. Cell cycle distributions was calculated with

Kaluza analysis software version 2.0 software from Beckman Coulter Life Sciences (Indianapolis, United States) by assigning relative DNA content per cell to sub-$G_1$, $G_1$, S and $G_2$/M fractions.

### 2.2.5 Mitochondrial potential

Mitochondrial membrane potential

The influence of ESE-one on the cells' mitochondrial potential was investigated using MitoProbe™ JC-1 Assay Kit employing flow cytometry. JC-1 dye was added to samples being investigated and it fluoresces green if the mitochondrial potential is depolarized and fluoresces red when the mitochondrial membrane potential is polarized. Depolarization of the mitochondrial membrane is indicative of apoptosis via the mitochondrial pathway. The green fluorescence was measured at 525 nm excitation whereas the red one was at 575 nm excitation for JC-1 dye (156-158).

Cells (MCF-7 and MDA-MB-231) were seeded at a density of 500 000 cells per 25 $cm^2$ tissue flask and incubated at 37°C and 5% $CO_2$ for 24 hours to allow for attachment. Subsequently, cells were exposed to 0.5 µM ESE-one in the presence or absence of ROS scavengers for 24 hours at 37°C and 5% $CO_2$. Thereafter, cells were trypsinized and resuspended in 1 ml warm PBS. Subsequently, samples were centrifuged at 300 x *g* for 5 minutes and the supernatant was discarded afterwards. Carbonyl cyanide 3-chlorophenylhydrazone (CCCP) (50 µM) was added to the positive control sample and incubated for 5 minutes at 37°C and 5% $CO_2$ thereafter, centrifuged and the supernatant discarded. The samples were resuspended in warm PBS (1 ml) and subsequently JC-1 dye solution (2 µM) was added to each sample. Samples were then incubated for 15 minutes at 37°C and 5% $CO_2$. After the incubation period, cells were centrifuged at 300 x *g* for 5 minutes and the supernatant was discarded. Cells were then resuspended in warm PBS (1 ml) and centrifuged at 300 x *g* for 5 minutes and the supernatant was discarded. PBS (0.5 ml) was added to each sample and samples were processed using the Gallios flow cytometer (Beckman Coulter, Inc. (Indianapilis, United States of America) at an excitation wavelength of 488 nm. Mitochondrial membrane potential data was analysed using Kaluza analysis software version 2.0 software from Beckman Coulter

Life Sciences (Indianapolis, United States) by quantifying the mitochondrial depolarization.

### 2.2.6 Antioxidant activity

2.2.6.1 Superoxide dismutase activity (spectrophotometry)

The influence of ESE-one on the cells' antioxidant systems was investigated by quantifying SOD. SOD is an antioxidant enzyme involved in the defence system against ROS. SOD catalyses the reaction of superoxide radical anion to hydrogen peroxide (159). Quantification of SOD was an indication regarding the influence of ESE-one on the cells' innate antioxidant defence systems.

Cells (MCF-7 and MDA-MB-231) were seeded at a density of 2 000 000 cells per 75 $cm^2$ tissue culture flask and incubated at 37°C and 5% $CO_2$ for 24 hours to allow for attachment. Subsequently, cells were exposed to 0.5 µM ESE-one with or without the ROS scavengers for 24 hours at 37°C and 5% $CO_2$. Cells were trypsinized and samples were placed in ice-cold 0.1 M Tris/HCl (pH 7.4) containing 0.5% triton X-100, 5 mM β-mercaptoethanol and 0.1 mg/ml phenylmethylsulfonyl fluoride. Cells were centrifuged at 14 000 x *g* for 5 minutes at 4°C. The supernatant was transferred to new eppendorfs and kept on ice. Supernatant (10 µl) was then transferred to the 96-well plate (row 1 and row 3) and double distilled water (10 µl) was added to row 2 and row 4. A further WST working solution (100 µl) was added to all the wells and SOD enzyme solution (10 µl) was only added to row 1 and 2. SOD dilution buffer (10 µl) was added to row 3 and row 4 thereafter, incubated for 1 hour on the plate shaker at 400 rpm (covered in foil). After the incubation period, the plate was read on the spectrophotometer, with the absorbance measured at 450 nm using an EPOCH Microplate Reader (Biotek Instruments, Inc. (Winooski, Vermont, United States of America). The data was then analysed using Microsoft Excel 2010 (Microsoft Corporation, Washington, United Sates of America).

2.2.6.2 Catalase activity (spectrophotometry)

The influence of ESE-one on the cells' innate antioxidant systems was investigated by quantifying catalase. Hydrogen peroxide is catalysed to water and oxygen by catalase and thus protecting the cell from oxidative stress (160).

Cells (MCF-7 and MDA-MB-231) were seeded at a density of 2 000 000 cells per 75 $cm^2$ tissue culture flask and incubated at 37°C and 5% $CO_2$ for 24 hours to allow for attachment. Subsequently, cells were exposed to 0.5 µM ESE-one in the presence or absence of ROS scavengers for 24 hours at 37°C and 5% $CO_2$. Cells were then scraped off the surface of the flask and suspended in PBS. After centrifuging, the supernatant was discarded and ice-cold cell extraction buffer (100 µl) was added to each sample and left on ice for 20 minutes. Thereafter, cells were centrifuged at 14000 *x g* for 15 minutes and the supernatant (50 µl) was transferred to a 96-well plate. A further antibody cocktail (50 µl) was added to the wells (providing a final volume of 100 µl) and incubated on the plate shaker for 90 minutes at 400 rpm. Wells were then washed thrice with wash buffer (250 µl) and TMB substrate (100 µl) was added to the wells and incubated for a further 15 minutes on the plate shaker at 400 rpm. After the incubation time, stop solution was added to the wells and read on the spectrophotometry. The absorbance was measured at 450 nm using an EPOCH Microplate Reader (Biotek Instruments, Inc. (Winooski, Vermont, United States of America). The data was analysed using Microsoft Excel 2010 (Microsoft Corporation, Washington, United Sates of America).

## 2.3 Statistics

Quantitative data was obtained from spectrophotometry (cell proliferation and antioxidant activity), fluorescent microscopy (ROS production), light microscopy (morphology) and flow cytometry (cell cycle progression and mitochondrial membrane potential). Qualitative data was obtained from light microscopy- and fluorescent microscopy. Three independent experiments were conducted where the average and the standard deviation were calculated. Averages are illustrated by bar charts and standard deviations are shown with errors bars. A $P$-value $< 0.05$ calculated by means of the Student $t$-test was used for statistical significance and is indicated by an asterisk (*). Flow cytometry analysis involves at least 10 000 events

and was repeated three times. Fluorescent- and light microscopy images were analyzed using Image J software developed by the National Institutes of Health (Bethesda, Maryland, United States of America). The fluorescent intensity of at least 100 cells was evaluated per condition in each experiment and at least 100 cells were counted in the light microscopy images per condition in each experiment.

### 2.4 Logistics

All the required equipment is available and all relevant techniques and protocols have been standardized in the Department of Physiology (University of Pretoria, South Africa). Dr M.H. Visagie and Professor A.M. Joubert were consulted on all the required techniques. The cell culture laboratory of the Department of Physiology at the University of Pretoria was used to conduct the research project. The Zeiss Axiovert CFL40 microscope, Zeiss Axiovert MRm monochrome camera (Zeiss, Oberkochen, Germany), EPOCH Microplate Reader (Biotek Instruments, Inc. (Winooski, Vermont, United States of America)) and Olympus CKX53 inverted microscope (Olympus Corporation, Tokyo, Japan) are available at the Department of Physiology, University of Pretoria, South Africa and were employed in the study. The Gallios flow cytometer (Beckman Coulter, Inc. (Indianapolis, California, United States)) utilised in this study is available from the Department of Immunology, University of Pretoria, South Africa and the FC500 flow cytometer (Beckman Coulter, Inc. (Indianapolis, California, United States)) is available from the Department of Pharmacology, University of Pretoria, South Africa.

### Ethical approval

The protocol was submitted to the Ethics Committee of the Faculty of Health Sciences and ethical approval was obtained (Ethics number 14/2018).

## Chapter 3

## 3.1 Results

### 3.1.1 ROS production

#### 3.1.1.1 Fluorescent microscopy

Fluorescent microscopy studies were conducted to evaluate the ROS (superoxide anion and hydrogen peroxide) production induced by sulphamoylated compounds utilizing DCFDA and DHE (figure 3.1 and figure 3.2). ESE-15-ol exposure induced hydrogen peroxide production with a mean florescent intensity of 146 and 149; and a mean fluorescent intensity of 30 and 56 for superoxide anion production in MCF-7- and MDA-MB-231 cells respectively (figure 3.1 F and H) whereas EE-15-ol exposure demonstrated a mean fluorescent intensity of 40 and 48 for hydrogen peroxide, and a mean fluorescent intensity of 33 and 35 for superoxide anion production in MCF-7- and MDA-MB-231 cells respectively (figure 3.1 E and G). ESE-one exposure resulted in a mean fluorescent intensity of 187 and 178 for hydrogen peroxide production, and a mean fluorescent intensity of 41 and 59 for superoxide anion production in MCF-7- and MDA-MB-231 cells respectively (figure 3.1 J and L) whereas EE-one exposure resulted in a mean fluorescent intensity of 27 and 33 for hydrogen peroxide production and a mean fluorescent intensity of 31 and 41 for superoxide anion production in MCF-7- and MDA-MB-231 cells respectively (figure 3.1 I and K). ESE-ol exposure resulted in a mean fluorescent intensity of 156 and 153 for hydrogen peroxide production, and a mean fluorescent intensity of 31 and 45 for superoxide anion production in MCF-7- and MDA-MB-231 cells respectively (figure 3.1 N and P) whereas 2E-diol exposure demonstrated a mean fluorescent intensity of 35 and 28 for hydrogen peroxide, and a mean fluorescent intensity of 11 and 37 for superoxide anion production in MCF-7- and MDA-MB-231 cells respectively (figure 3.1 M and O). Fluorescence microscopy data demonstrated that sulphamoylated compounds induced ROS production in both MCF-7- (figure 3.2 A) and MDA-MB-231 cells (figure 3.2 B) compared to the non-sulphamoylated compounds. Furthermore, sulphamoylated compounds induced more hydrogen peroxide production in MCF-7 cells compared to MDA-MB-231 cells and more superoxide anion production in MDA-MB-231 cells compared to MCF-7 cells. Thus, exposure to all the sulphamoylated compounds resulted in induction of superoxide anion and hydrogen peroxide compared to the vehicle-treated cells. Exposure to the

non-sulphamoylated compounds however, induced less superoxide anion and hydrogen peroxide suggesting that ROS induction is more prominently induced by sulphamoylated compounds.

Table 3.1 Sulphamoylated compounds and their non-sulphamoylated counterparts.

| Non-sulphamoylated | Sulphamoylated |
|---|---|
| EE-15-ol | ESE-15-ol |
| EE-one | ESE-one |
| 2E-diol | ESE-ol |

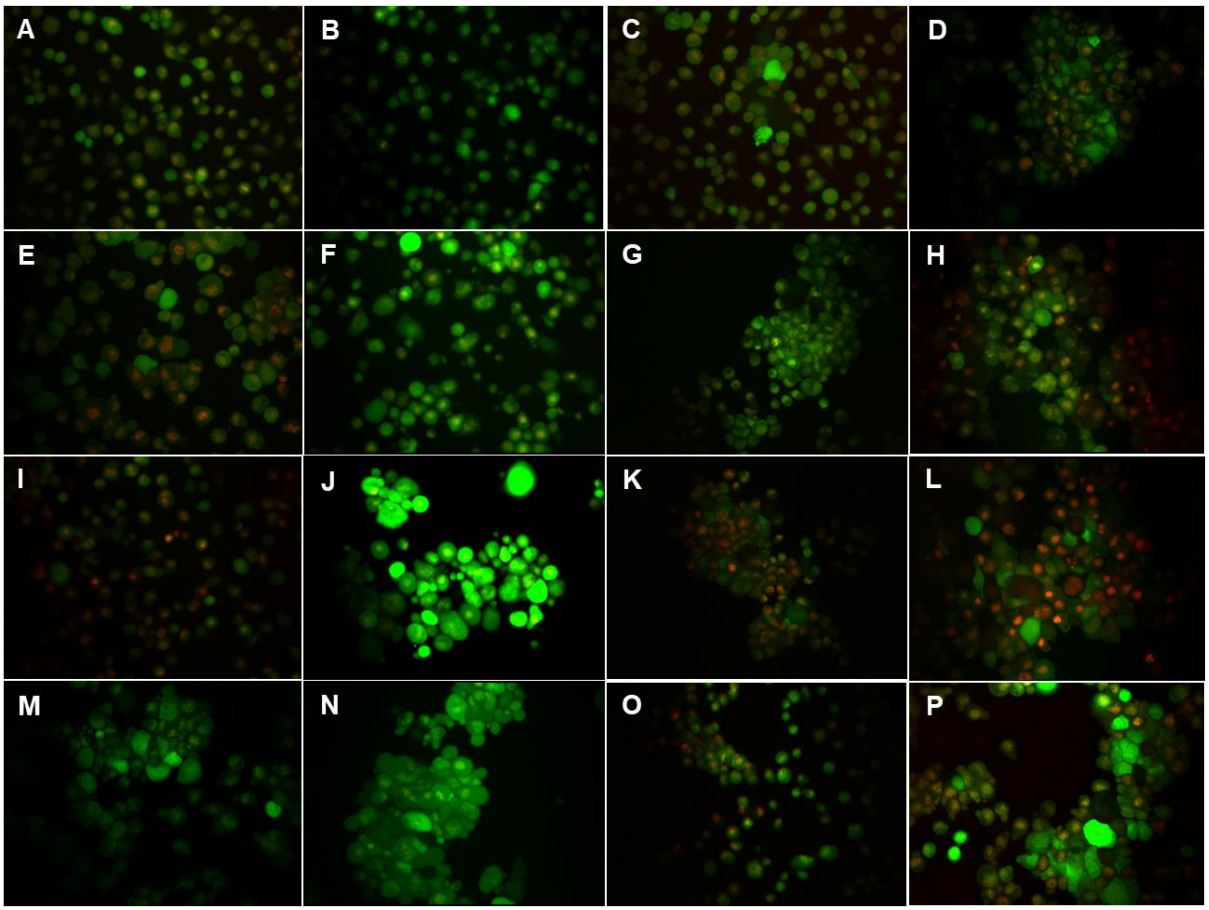


Figure 3.1: Fluorescent micrographs of MCF-7 and MDA-MB-231 cells exposed to sulphamoylated and non-sulphamoylated compounds. Sulphamoylated compounds induced ROS production in both MCF-7 and MDA-MB-231 cells compared to their non-sulphamoylated counterparts. A: MCF-7 cells propagated in growth medium, B: Vehicle treated MCF-7 cells, C: MDA-MB-231 cells propagated in growth medium, D: Vehicle treated MDA-MB-231 cells, E: EE-15-ol (non-sulphamoylated) treated MCF-7 cells, F: ESE-15-ol (sulphamoylated) treated MCF-7 cells, G: EE-15-ol (non-sulphamoylated) treated MDA-MB-231 cells, H: ESE-15-ol (sulphamoylated) treated MDA-MB-231 cells, I: EE-one (non-sulphamoylated) treated MCF-7 cells, J: ESE-one (sulphamoylated) treated MCF-7 cells, K: EE-one (non-sulphamoylated) treated MDA-MB-231 cells, L: ESE-one (sulphamoylated) treated MDA-MB-231 cells, M: 2E-diol (non-sulphamoylated) treated MCF-7 cells, N: ESE-ol (sulphamoylated) treated MCF-7 cells, O: 2E-diol (non-sulphamoylated) treated MDA-MB-231 cells, P: ESE-ol (sulphamoylated) treated MDA-MB-231 cells (20X magnification).

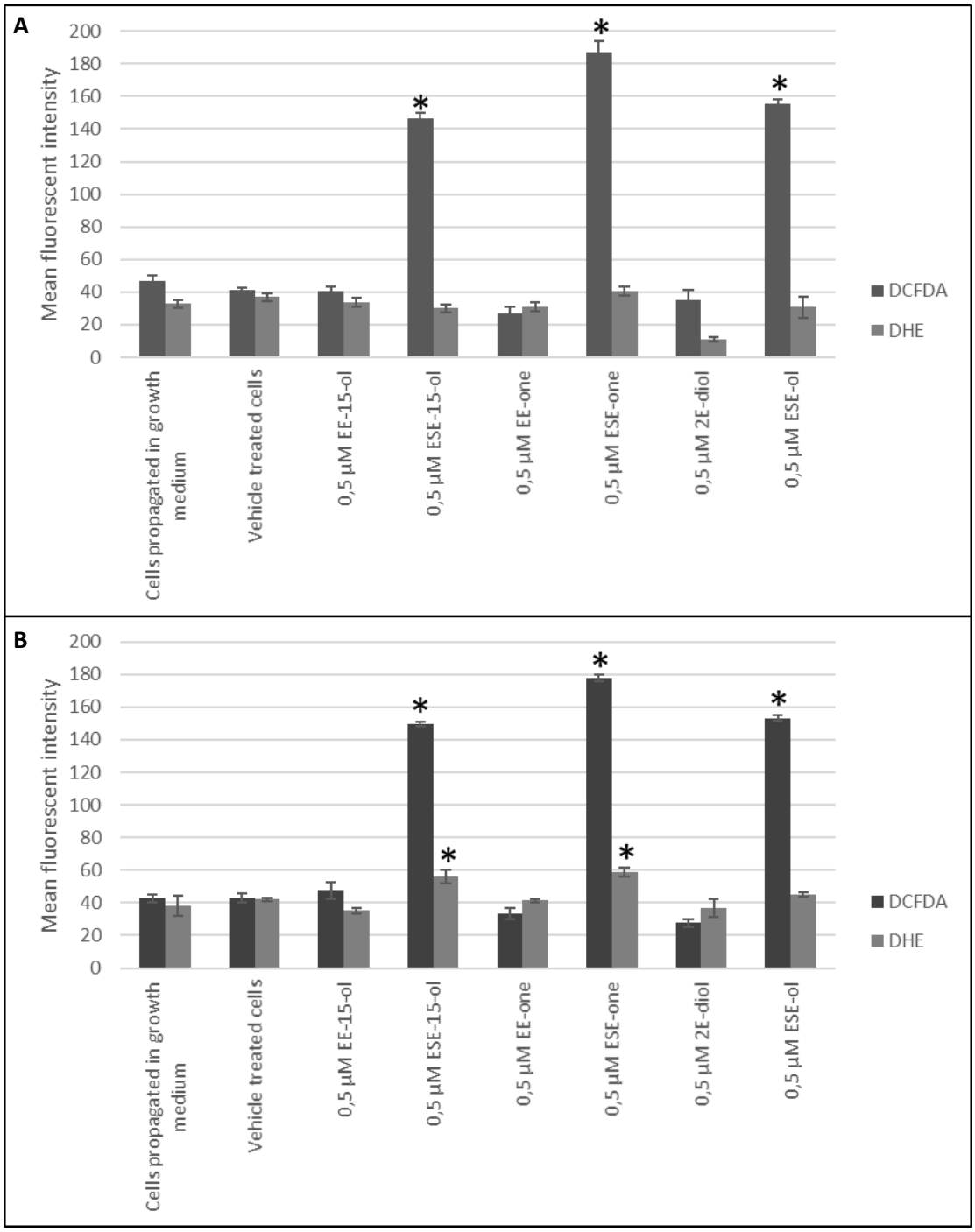


Figure 3.2: MCF-7 and MDA-MB-231 graphs demonstrating the mean fluorescent intensity. Sulphamoylated compounds induced superoxide anion and hydrogen peroxide production in both MCF-7 and MDA-MB-231 cells compared to the non-sulphamoylated compounds. A: MCF-7 cells, B: MDA-MB-231 cells. Asterisk (*) represents p-value ($P<0.05$) compared to vehicle-treated cells.

### 3.1.2 Cell proliferation

Crystal violet and spectrophotometry were used for proliferation studies. Crystal violet is a triphenylmethane dye which is used to stains the DNA of cells in monolayer to determine cell number. The stain is solubilized, and absorbance read on the spectrophotometry to quantify the amount of dye taken up by the viable cells (161). Thus, crystal violet allows for the quantification of live and dead cells based on the intensity of the crystal violet dye where the absorbance is read at 750 nm.

3.1.2.1 Cell growth inhibition by sulphamoylated vs. non-sulphamoylated compounds

MCF-7- and MDA-MB-231 cell lines were exposed to 3 types of sulphamoylated compounds (ESE-15-ol, ESE-one and ESE-ol) and their non-sulphamoylated (EE-15-ol, EE-one and 2-E-diol) counterparts in order to determine the effect of sulphamoylated compounds on tumourigenic cell lines in comparison to non-sulphamoylated compounds. Cells were exposed to sulphamoylated and non-sulphamoylated compounds for 24 hours at a concentration of 0.5 µM. Cells exposed to EE-15-ol exhibited 95% cell growth in the MCF-7 cell line (figure 3.3 A) and 106% cell growth in the MDA-MB-231 cell line (figure 3.3 B) compared to those exposed to its sulphamoylated counterpart (ESE-15-ol) which resulted in only 67% cell growth in the MCF-7 cell line and 64% cell growth in the MDA-MB-231 cell line. EE-one exposure resulted in 102% and 114% cell growth in MCF-7- and MDA-MB-231 cell lines, respectively, whereas ESE-one exposure demonstrated 57% cell growth in the MCF-7 cell line and 71% growth in the MDA-MB-231 cell line. 2-E-diol exposure resulted in 119% and 130% cell growth in MCF-7 and MDA-MB-231 cell lines compared to 52% and 72% growth, respectively (figure 3.3 A and B). Crystal violet studies demonstrated that the compounds owning a sulphamate moiety indeed have a significant inhibitory effect on actively proliferating cells as they exhibited more prominent cell growth inhibition compared to their non-sulphamoylated counterparts which had the opposite effect by inducing cell growth.

ESE-one was chosen as a representative for the sulphamoylated compounds and was thus used in subsequent experiments.

Table 3.2 Sulphamoylated compounds and their non-sulphamoylated counterparts.

| Non-sulphamoylated | Sulphamoylated |
|---|---|
| EE-15-ol | ESE-15-ol |
| EE-one | ESE-one |
| 2E-diol | ESE-ol |

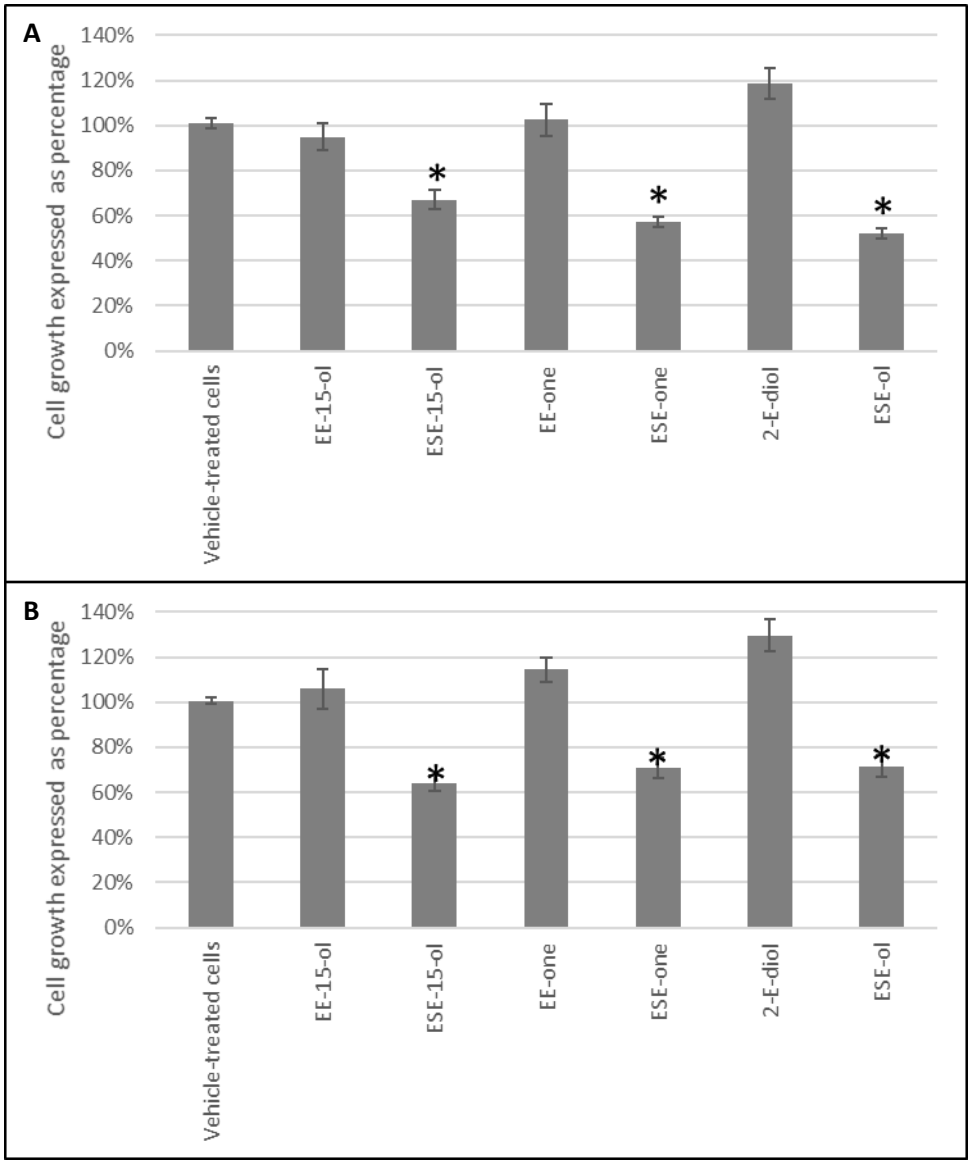


Figure 3.3: Graph of MCF-7 and MDA-MB231 cells exposed to sulphamoylated and non-sulphamoylated compounds. Non-sulphamoylated compounds exerted no significant inhibiting effect on cell growth in MCF-7 cell inhibition whereas sulphamoylated compounds demonstrated at least 28% cell inhibition in both cell lines. Non-sulphamoylated compounds had an opposite effect and caused cell growth demonstrated by EE-one and 2-E-diol. A: MCF-7, B: MDA-MB231. Asterisk (*) represents p-value ($P<0.05$) compared to cells exposed to non-sulphamoylated compounds.

### 3.1.2.2 Cell growth inhibition in the presence or absence of ROS inhibitors

Since fluorescent microscopy demonstrated that all three sulphamoylated compounds including ESE-one induced similar significant increased ROS quantities all subsequent studies were conducted using 0.5 µM ESE-one as a representative of

the sulphamoylated compounds in order to investigate the role of ROS in the activity exerted by these compounds. Cell growth studies were done using 0.5 µM ESE-one in the presence or absence of ROS inhibitors. These inhibitors include mannitol which inhibits hydroxyl radical, sodium azide which inhibits oxygen singlet, carboxy-PTIO which inhibits nitric oxide, tiron which inhibits superoxide anion, DMTU which inhibits hydrogen peroxide and trolox which inhibits perhydroxyl radical.

Tiron, an inhibitor of superoxide anion, was used to determine if the growth inhibitory effect of ESE-one is dependent on superoxide. Co-exposure to tiron resulted in a significant restoration of cell growth to 82% (1 mM), 97% (2 mM), 104% (3 mM), 130% (4 mM) and 121% (5 mM) respectively compared to cells exposed to ESE-one only which demonstrated 66% cell growth in MCF-7 cells (figure 3.4 A). Tiron exposure significantly increased cell growth at just 1 mM and completely obliterated ESE-one's growth inhibitory effect at 3 mM concentration in MCF-7 cells. Furthermore, tiron exposure in MDA-MB-231 cells restored cell growth to 82% (1 mM), 84% (2 mM), 82% (3 mM), 91% (4 mM) and 99% (5 mM) respectively compared to ESE-one only exposure which resulted in 69% cell growth (figure 3.4 B). Furthermore, tiron also demonstrates a significant opposing effect to the antiproliferative effect exerted by ESE-one in MDA-MB-231 cells. This suggests that the superoxide anion production is induced by ESE-one exposure culminating in decreased cell growth. A concentration of 5 mM was chosen to continue for subsequent experiments since it was the only concentration which completely obliterated the antiproliferative effects of ESE-one in both MCF-7- and MDA-MB-231 cell lines.

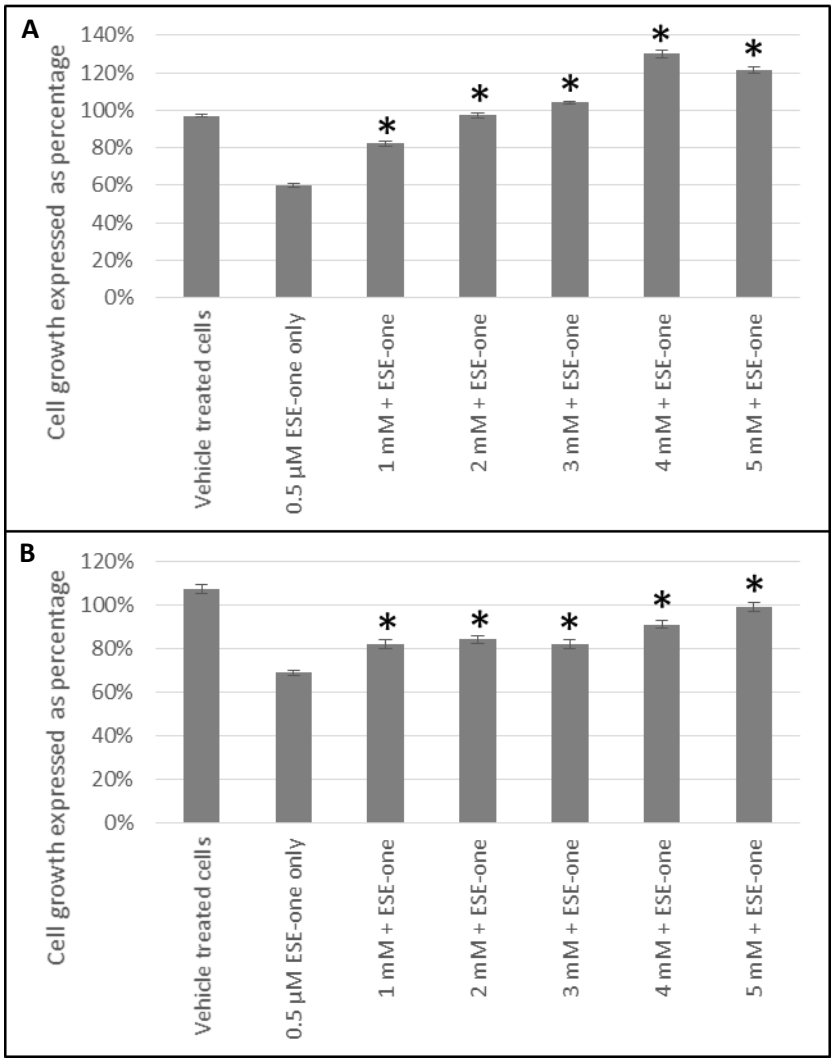


Figure 3.4: Cell growth inhibition graphs of MCF-7- and MDA-MB-231 cell lines exposed to ESE-one in the presence or absence of tiron (superoxide anion inhibitor). Tiron exposure to MCF-7 and MDA-MB-231 cells significantly opposed the antiproliferative effect of ESE-one. The growth inhibitory effect of ESE-one was completely demolished at 3 mM in MCF-7 cells and 5 mM in MDA-MB-231 cells. A: MCF-7, B: MDA-MB231. Asterisk (*) represents p-value ($P$<0.05) compared to ESE-one treated cells.

DMTU, an inhibitor of hydrogen peroxide, was used to evaluate if antiproliferative activity induced by ESE-one in MCF-7 and MDA-MB-231 cell lines is dependent on the production of hydrogen peroxide. Co-exposure to DMTU restored cell growth to 93% (2 mM), 104% (4 mM), 101% (6 mM), 102% (8 mM) and 96% (10 mM) compared to 60% cell growth induced by ESE-one exposure in MCF-7 cells (figure 3.5 A). These results demonstrate that DMTU inhibits the antiproliferative effect

exerted by ESE-one from a concentration of 2 mM, suggesting that hydrogen peroxide plays an essential role in the antiproliferative effect induced by ESE-one. DMTU exposure to MDA-MB-231 cells restored cell growth to 64% (2 mM), 80% (4 mM), 79% (6 mM), 87% (8 mM) and 84% (10 mM) cell growth respectively compared to 69% cell growth induced by ESE-one (figure 3.5 B). DMTU exposure significantly increases cell growth in MDA-MB-231 exposed cells at 8 mM. However, cell growth was only partially restored by DMTU in the MDA-MB-231 cell line.

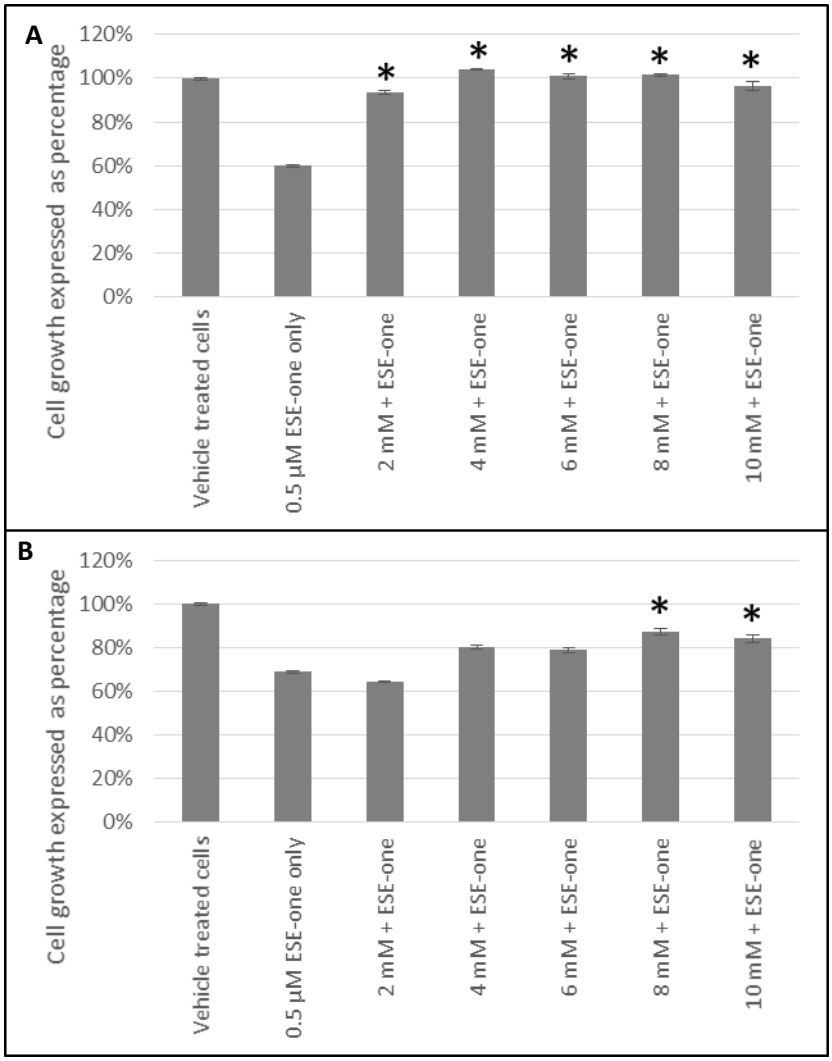


Figure 3.5: Cell growth inhibition graphs of MCF-7- and MDA-MB-231 cells exposed to ESE-one in combination with DMTU (hydrogen peroxide inhibitor). DMTU exposure to MCF-7 and MDA-MB-231 cells significantly opposed the antiproliferative effect of ESE-one in both cell lines. The antiproliferative effect of ESE-one was demolished at 4 mM in MCF-7 cells and significantly inhibited at 8 mM in MDA-MB-231 cells. A: MCF-7, B: MDA-MB231. Asterisk (*) represents p-value ($P<0.05$) compared to ESE-one treated cells.

Trolox, a peroxyl radical inhibitor, was used to determine if the antiproliferative effects induced by ESE-one are dependent on production of peroxyl radical. Co-exposure to trolox and ESE-one resulted in 56% (10 µM), 64% (20 µM), 75% (40 µM) and 72% (80 µM) cell growth respectively compared to cells exposed to ESE-one only (60%) in MCF-7 cells (figure 3.6 A). Thus, trolox significantly opposed the antiproliferative effect of ESE-one at in a dose-dependent manner at 40 µM and 80 µM. In MDA-MB-231 cells, trolox exposure restored cell growth to 75% (10 µM), 80% (20 µM), 73% (40 µM) and 84% (80 µM) respectively compared to ESE-one only exposed cells (69%) (figure 3.6 B). A significant effect was observed at the highest trolox concentration in MDA-MB-231 cells. Trolox demonstrated significant effects in inhibiting the antiproliferative activity induced by ESE-one in both cell lines suggesting that peroxyl radical partially plays a role in the antiproliferative effect induced by ESE-one in tumourigenic cell lines.

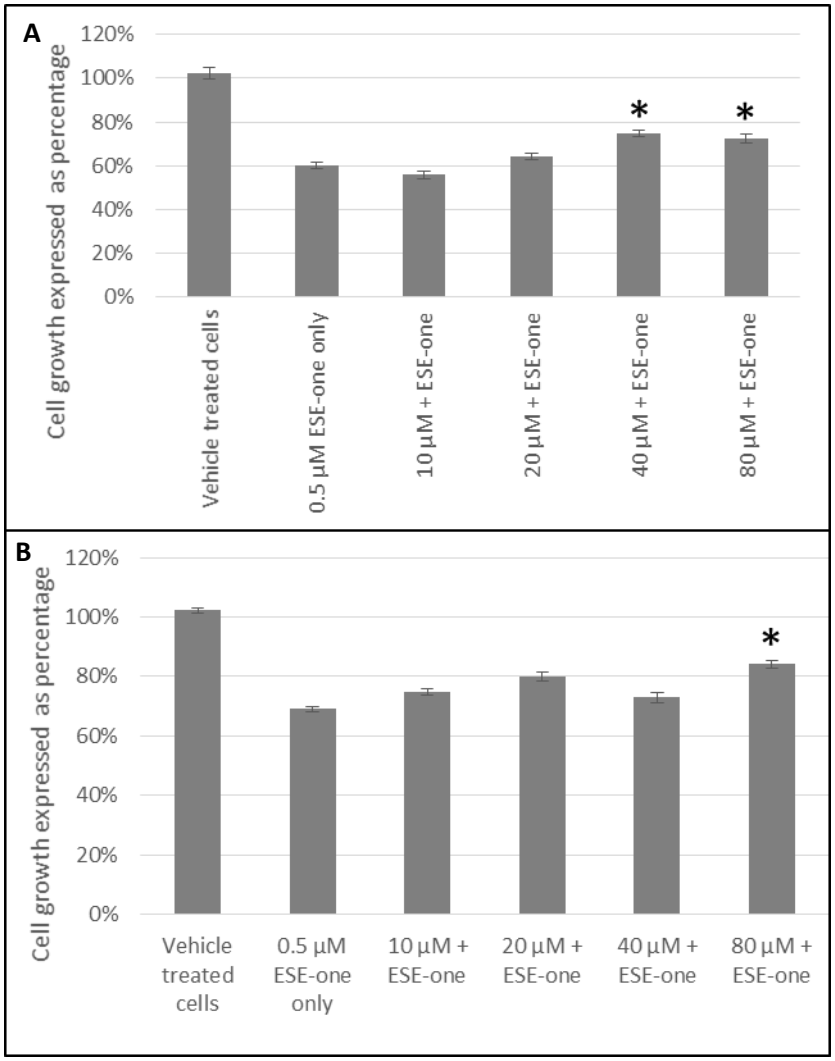


Figure 3.6: Cell growth inhibition graphs demonstrating MCF-7- and MDA-MB-231 cells exposed to ESE-one in combination with trolox (peroxyl radical inhibitor). Trolox exposure to MCF-7 and MDA-MB-231 cells partially opposed the antiproliferative effect of ESE-one in both cell lines. The antiproliferative effect of ESE-one was significantly countered at 40 µM and 80 µM in MCF-7 cells and 80 µM in MDA-MB-231 cells. A: MCF-7, B: MDA-MB231. Asterisk (*) represents p-value ($P<0.05$) compared to ESE-one treated cells.

Mannitol, a hydroxyl radical inhibitor, was used in combination with ESE-one (0.5 µM) in order to determine if ESE-one exerted antiproliferative activity dependent on the hydroxyl radical. Mannitol co-exposure with ESE-one resulted in 67% (20 mM) and 66% (40 mM – 100 mM) cell growth in MCF-7 cell lines (figure 3.7 A) compared to ESE-one only exposed cells which exhibited 60% cell growth. In MDA-MB-231 cells, mannitol exposure resulted in 81% (20 mM), 79 (40 mM), 82% (80 mM) and 84% (100 mM) cell growth compared to cells exposed to ESE-one only (74%) (figure

3.7 B). These results demonstrated that mannitol exerted no significant effect on the growth inhibitory effect of ESE-one in both MCF-7- and MDA-MB-231 cells. This suggests that hydroxyl radical does not play a role in the growth inhibitory pathway induced by ESE-one.

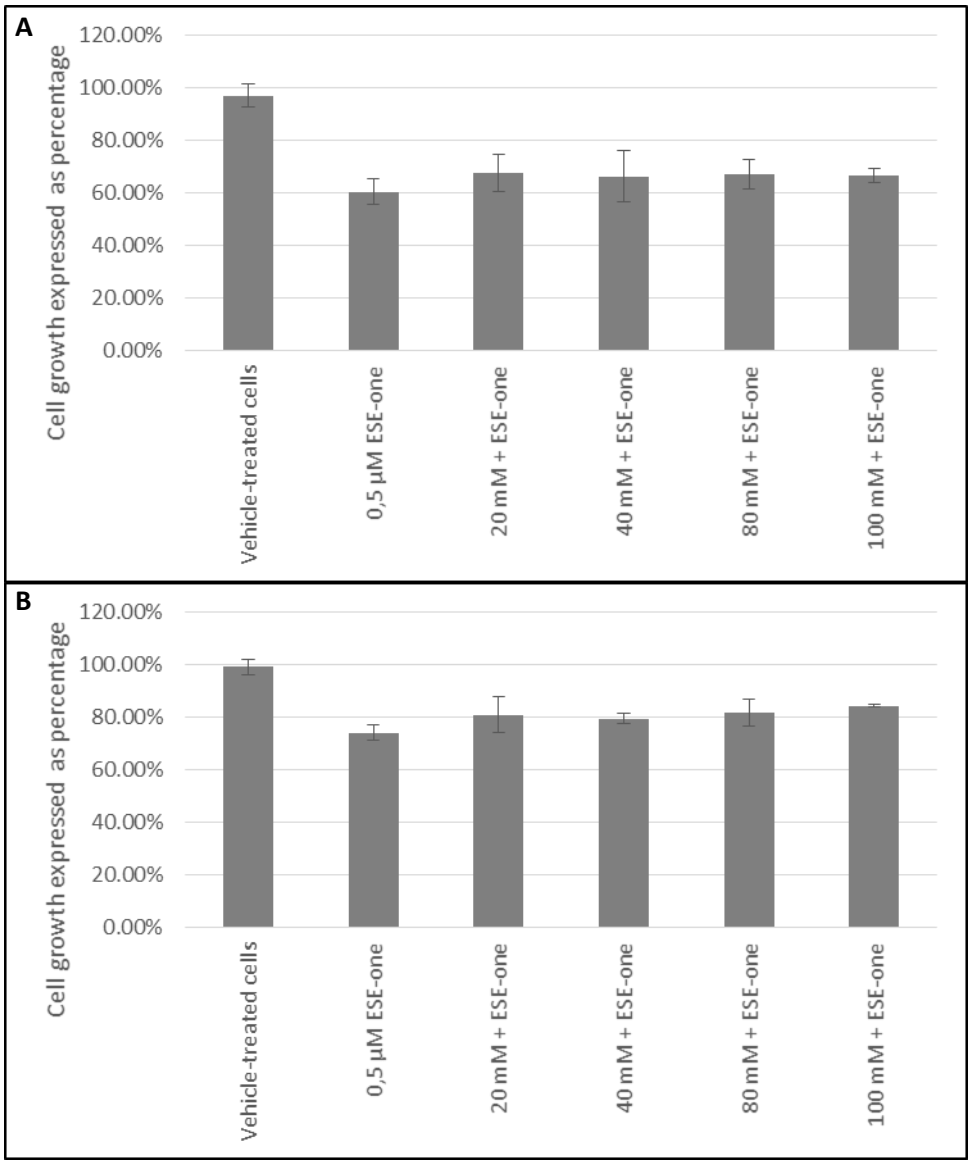


Figure 3.7: Cell growth inhibition graphs of MCF-7 and MDA-MB-231 cells exposed to ESE-one in combination with mannitol (hydroxyl radical inhibitor). Mannitol exposure to MCF-7 and MDA-MB-231 cells did not significantly oppose the antiproliferative effect of ESE-one in both cell lines. A: MCF-7, B: MDA-MB231.

Cells were exposed to ESE-one in the presence and absence of sodium azide (1mM to 10 mM), an inhibitor of singlet oxygen, to determine if the antiproliferative activity exerted by ESE-one is dependent on singlet oxygen. Co-exposure to sodium azide

resulted in 67% (1 mM), 61% (2 mM), 55% (4 mM), 59% (8 mM) and 61 % (10 mM) cell growth compared to 60% cell growth induced by ESE-one exposure in MCF-7 cells (figure 3.8 A). In MDA-MB-231 cells, sodium azide exposure demonstrated a 63% (1 mM), 66% (2 mM), 67% (4 mM), 58% (8 mM) and 62% (10 mM) cell growth compared to 70% growth induced by ESE-one only exposure (figure 3.8 B). Thus, no significant differences were observed between ESE-one only exposed cells and cells exposed to ESE-one and sodium azide in either cell line suggesting that singlet oxygen does not play a role in the growth inhibitory pathway exerted by ESE-one.

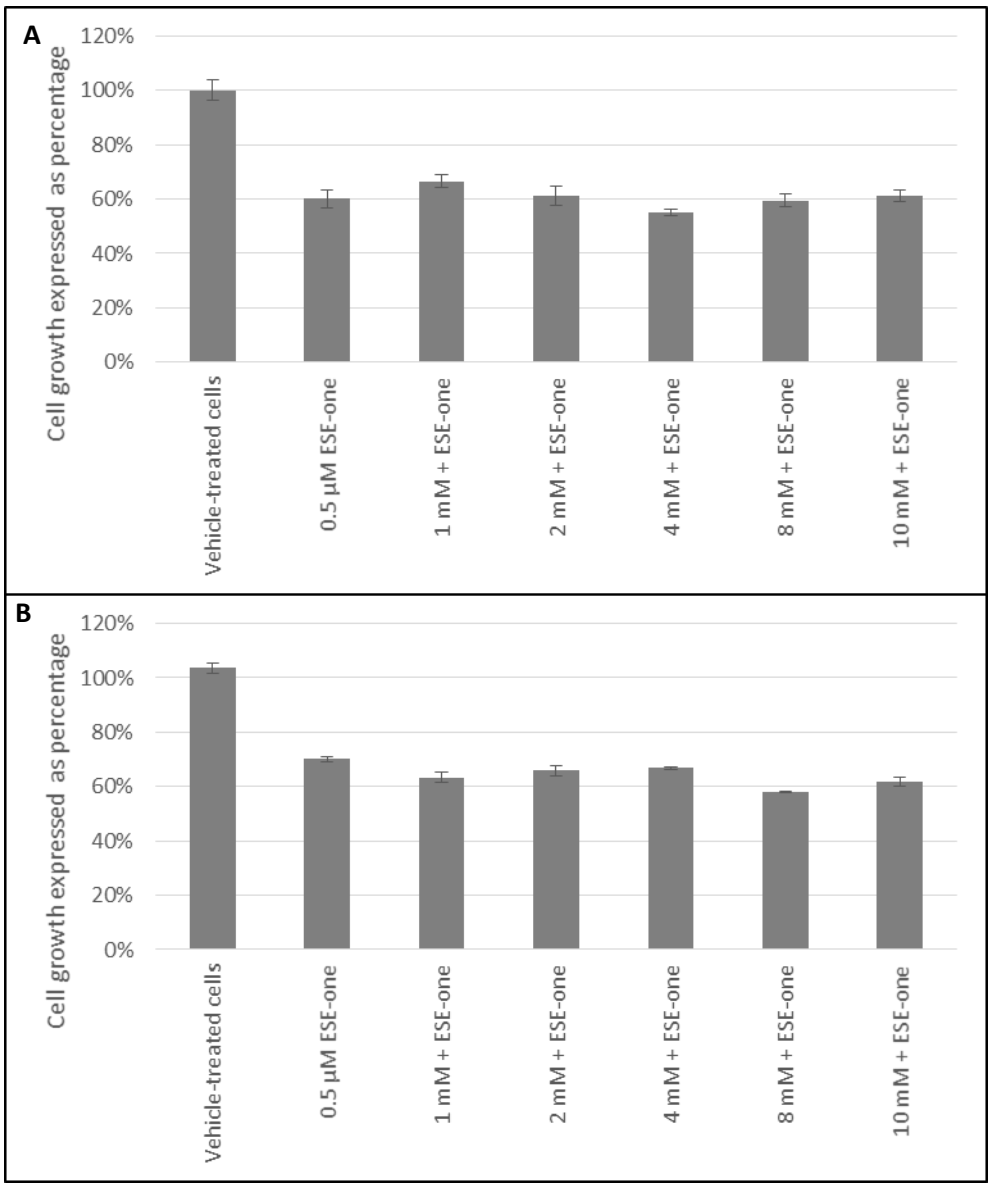


Figure 3.8: Cell growth inhibition graphs of MCF-7 and MDA-MB-231 cells exposed to ESE-one in combination with sodium azide (oxygen singlet inhibitor). Sodium azide exposure to

MCF-7 and MDA-MB-231 cells did not oppose the antiproliferative effect of ESE-one in both cell lines. A: MCF-7, B: MDA-MB231.

Carboxy-PTIO, a nitric oxide inhibitor, was used in combination with ESE-one (0.5 µM) in order to determine if ESE-one exerted antiproliferative activity dependent on nitric oxide. Co-exposure to carboxy-PTIO resulted in 64% (10 µM), 67% (20 µM), 60% (40 and 80 µM) and 58% (100 µM) cell growth respectively compared to ESE-one only exposed cells which resulted in 60% cell growth in MCF-7 cells (figure 3.9 A). In MDA-MB-231 cells, carboxy-PTIO exposure resulted in 64% (10 µM), 57% (20 µM), 49% (40 µM), 51% (80 µM) and 42% (100 µM) cell growth respectively compared to ESE-one only exposed cells which demonstrated a 70% cell growth (figure 3.9 B). The results thus indicated that carboxy-PTIO has no significant effect on the antiproliferative activity exerted by ESE-one in either cell line suggesting that cell growth inhibition is not dependent on nitric oxide.

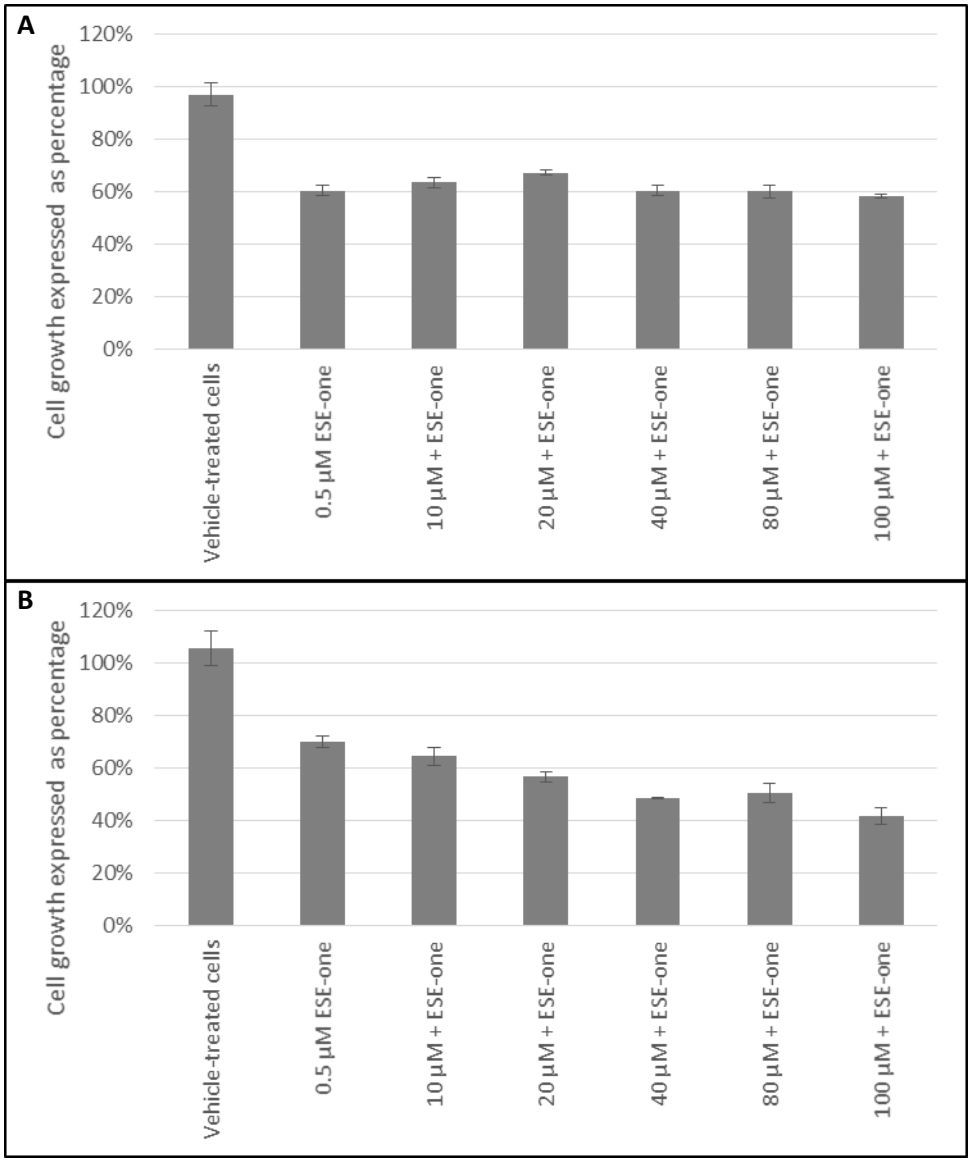


Figure 3.9: Cell growth inhibition graphs of MCF-7 and MDA-MB-231 cells exposed to ESE-one in combination with carboxy-PTIO (nitric oxide inhibitor). Carboxy-PTIO exposure to MCF-7 and MDA-MB-231 cells did not oppose the antiproliferative effect of ESE-one in both cell lines. A: MCF-7, B: MDA-MB231.

Only three ROS inhibitors had a significant inhibitory effect on the antiproliferative activity of ESE one; namely tiron, DMTU and trolox. Hence, subsequent experiments that investigated cell morphology, antioxidant activity, cell cycle progression, cell death and mitochondrial membrane potential were done exposing cells to ESE-one in the presence and absence of tiron (5 mM), DMTU (8 mM) and trolox (80 µM). These scavengers and doses were selected based on the above-mentioned crystal

violet studies that demonstrated that the scavengers inhibited the antiproliferative activity optimally at these doses.

### 3.1.4 Cell morphology

3.1.4.1 Light microscopy

For morphology studies, cells were exposed to 0.5 µM ESE-one in the absence and presence of tiron (5 mM), DMTU (8 mM) and trolox (80 µM) for 24 hours since the proliferation studies showed partial or complete inhibition of the antiproliferative activity exerted by ESE-one by the three aforementioned ROS inhibitors. Thereafter, light microscopy images were captured to assess the change in cell morphology when exposed to the ESE-one in comparison with cells exposed to both ESE-one and ROS inhibitors (tiron, DMTU and trolox) (figure 3.10- figure 3.13).

ESE-one exposure further resulted in decreased cell density, shrunken cells, blebbing and appearance of apoptotic bodies in both MCF-7- and MDA-MB-231 cells. Exposure to only ESE-one resulted in 40% rounded cells and 20% abnormal cells (cells that are elongated and/or shrunken or demonstrating blebbing/apoptotic bodies) respectively in MCF-7 cells (figure 3.10 E and table 3.3) whereas MDA-MB-231 cells demonstrated 29% rounded and 30% abnormal cells (figure 3.10 F and table 3.4).

Combination exposure with tiron and ESE-one resulted in 12% rounded cells and 7% abnormal cells in MCF-7 cells, respectively (figure 3.10 C and table 3.3) and only 10% rounded cells and 6% abnormal cells in MDA-MB-231 cells, respectively (figure 3.11 D and figure table 3.4). DMTU co-exposure resulted in an appearance of rounded cells (33% and 20%) and abnormal cell morphology (15% and 6%) in MCF-7- (figure 3.12 C and table 3.3) and MDA-MB-231 (figure 3.12 D and table 3.4) cells, respectively. Trolox co-exposure with ESE-one also demonstrated fewer rounded cells compared to ESE-one only exposure at 25% and 17% rounded cells in MCF-7- (figure 3.13 C and table 3.3) and MDA-MB-231 cells (figure 3.13 D and table 3.4), respectively. Trolox co-exposure also resulted in less abnormal cells in MCF-7 (15%) and MDA-MB-231 (7%) cells compared to ESE-one only exposed cells.

Morphology studies suggest that all three ROS inhibitors oppose the effects of ESE-one in MCF-7 (table 3.3) and MDA-MB-231 (table 3.4) cells. This is observed in the cell morphology micrographs where ESE-one only exposed cells have significantly low cell density, increased cell rounding, shrunken cells and apoptotic bodies whereas these effects are at a lesser extent in tiron-, DMTU- and trolox co-exposure in both cell lines. Tiron had the most prominent inhibitory effect on the activity exerted by ESE-one compared to trolox and DMTU as the co-exposure demonstrated less cell rounding and more normal cells (81% and 86%) compared to ESE-one alone suggesting that tiron exposure can potentially rescue the cells from the antiproliferative and antimitotic effect of ESE-one in both MCF-7 and MDA-MB-231 cells. This suggests that superoxide anion, hydrogen peroxide and peroxyl radical play a role in the antimitotic effects exerted by ESE-one however, superoxide anion to a greater extent.

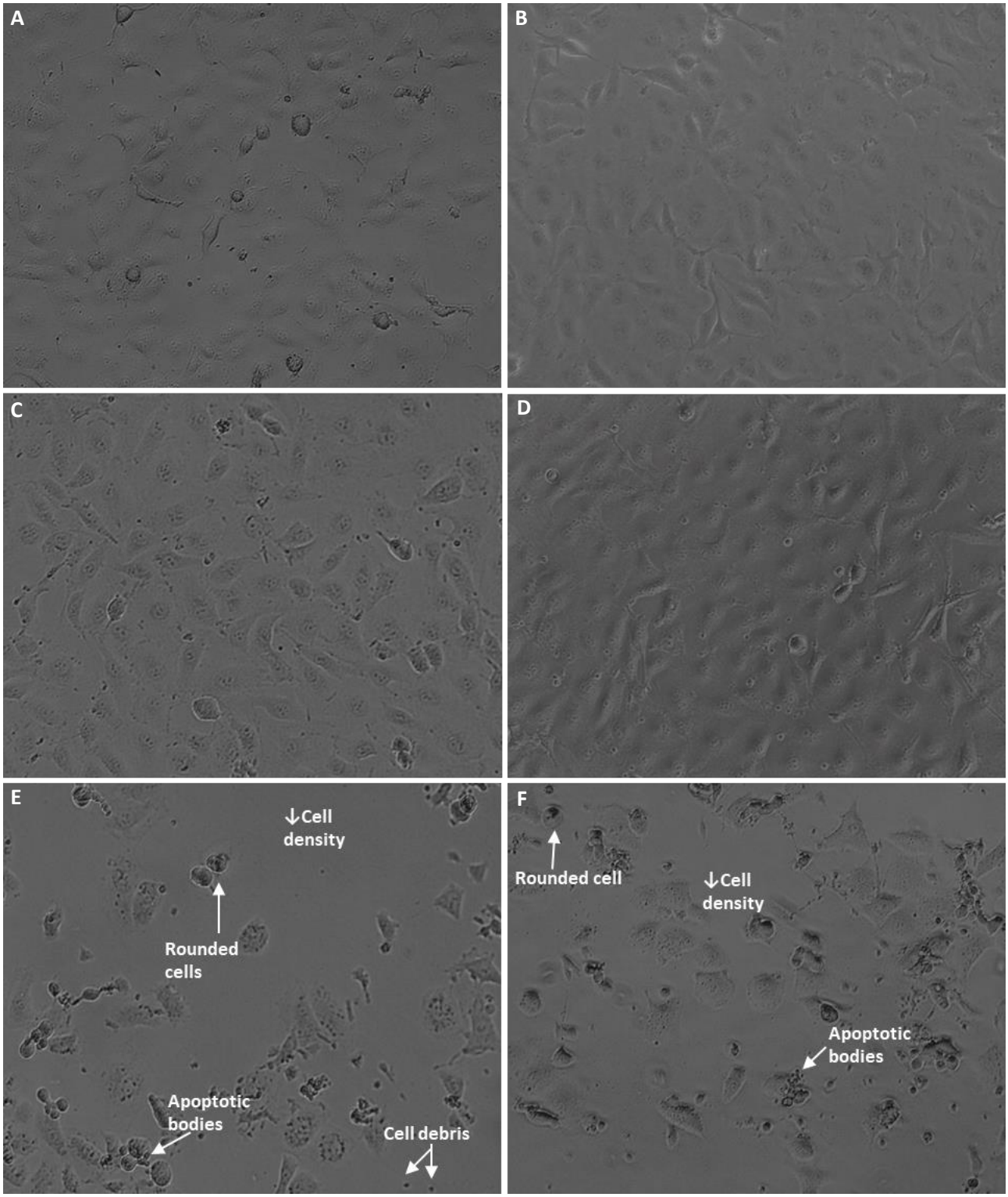


Figure 3.10: Light micrographs of MCF-7- and MDA-MB-231 cells propagated in growth medium, vehicle treated and ESE-one exposed. ESE-one exposed cells resulted in low cell density, rounded cells and an appearance of apoptotic bodies compared to negative control

cells in both MCF-7- and MDA-MB-231 cells. A: MCF-7 cells propagated in growth medium, B: MDA-MB-231 cells propagated in growth medium, C: MCF-7 vehicle treated cells, D: MDA-MB-231 vehicle treated cells, E: MCF-7 cells exposed to 0.5 µM ESE-one, F: MDA-MB-231 cells exposed to 0.5 µM ESE-one.

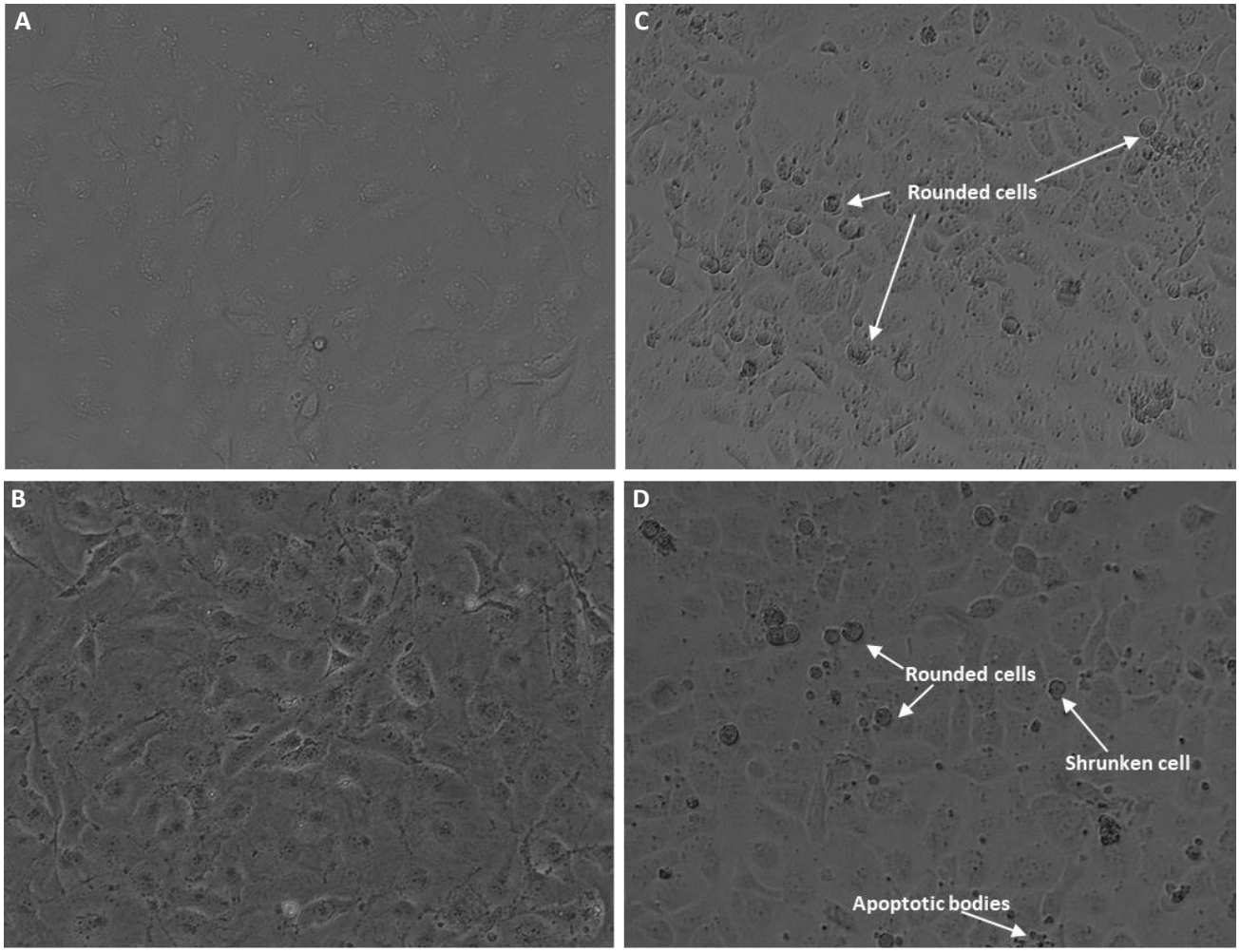


Figure 3.11: Light micrographs of MCF-7- and MDA-MB-231 cells exposed to tiron alone, and tiron in combination with ESE-one. Tiron co-exposure with ESE-one resulted in rounded cells and apoptotic bodies in both MCF-7- and MDA-MB-231 cell lines compared to cells exposed to tiron only. However, there was a decrease in rounded cells in the tiron co-exposed cells compared to ESE-one only exposed cells. A: MCF-7 cells exposed to 5 mM tiron, B: MDA-MB-231 cells exposed to 5 mM tiron, C: MCF-7 cells exposed to tiron and ESE-one, D: MDA-MB-231 cells exposed to tiron and ESE-one.

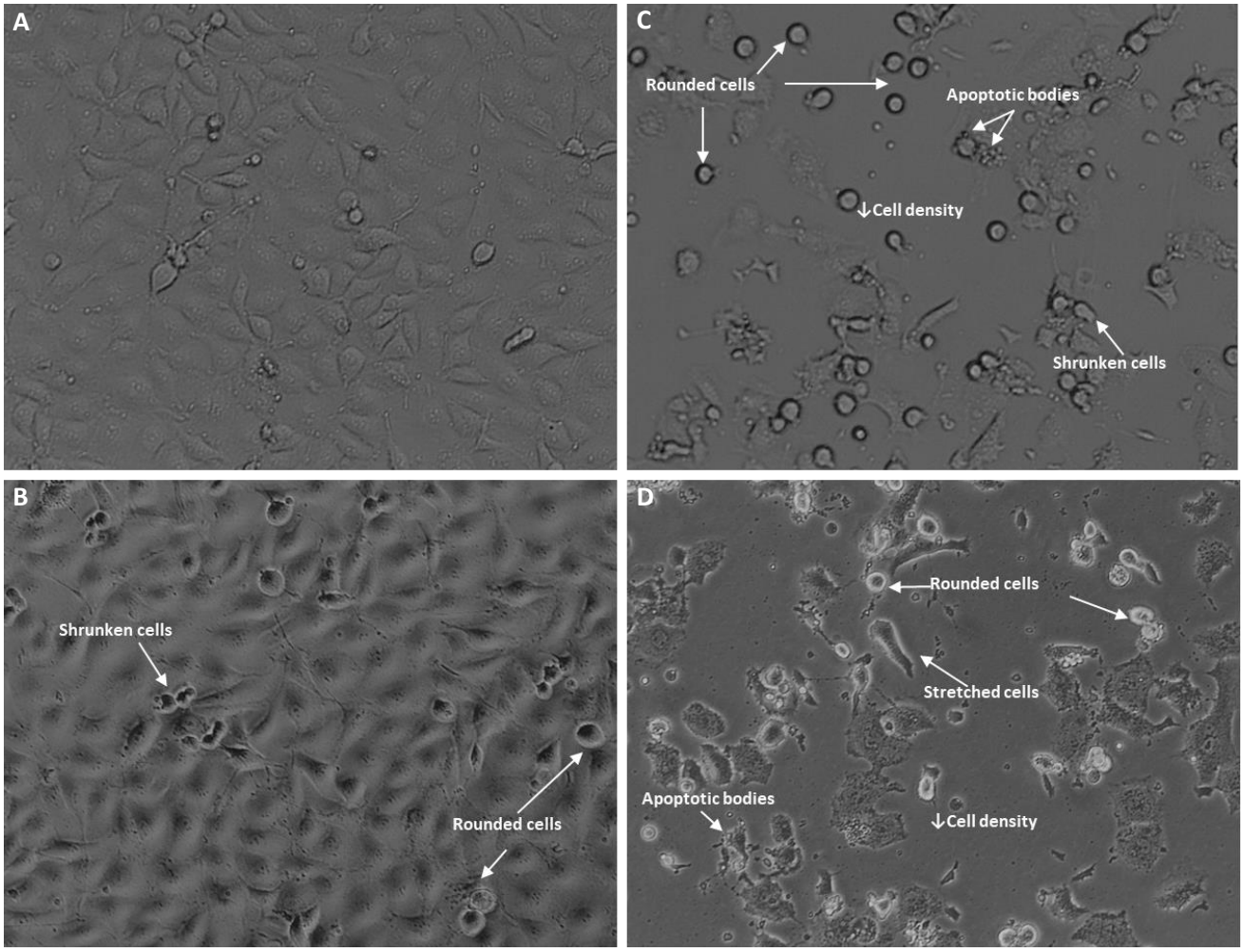


Figure 3.12: Light micrographs of MCF-7- and MDA-MB-231 cells exposed to DMTU alone, and DMTU in combination with ESE-one. DMTU co-exposure with ESE-one resulted in rounded cells, shrunken cells, stretched cells and apoptotic bodies in both MCF-7- and MDA-MB-231 cell lines compared to cells exposed to DMTU only. However, there was a decrease in rounded cells in the DMTU co-exposed cells compared to ESE-one only exposed cells. A: MCF-7 cells exposed to 8 mM DMTU, B: MDA-MB-231 cells exposed to 8 mM DMTU, C: MCF-7 cells exposed to DMTU and ESE-one, D: MDA-MB-231 cells exposed to DMTU and ESE-one.

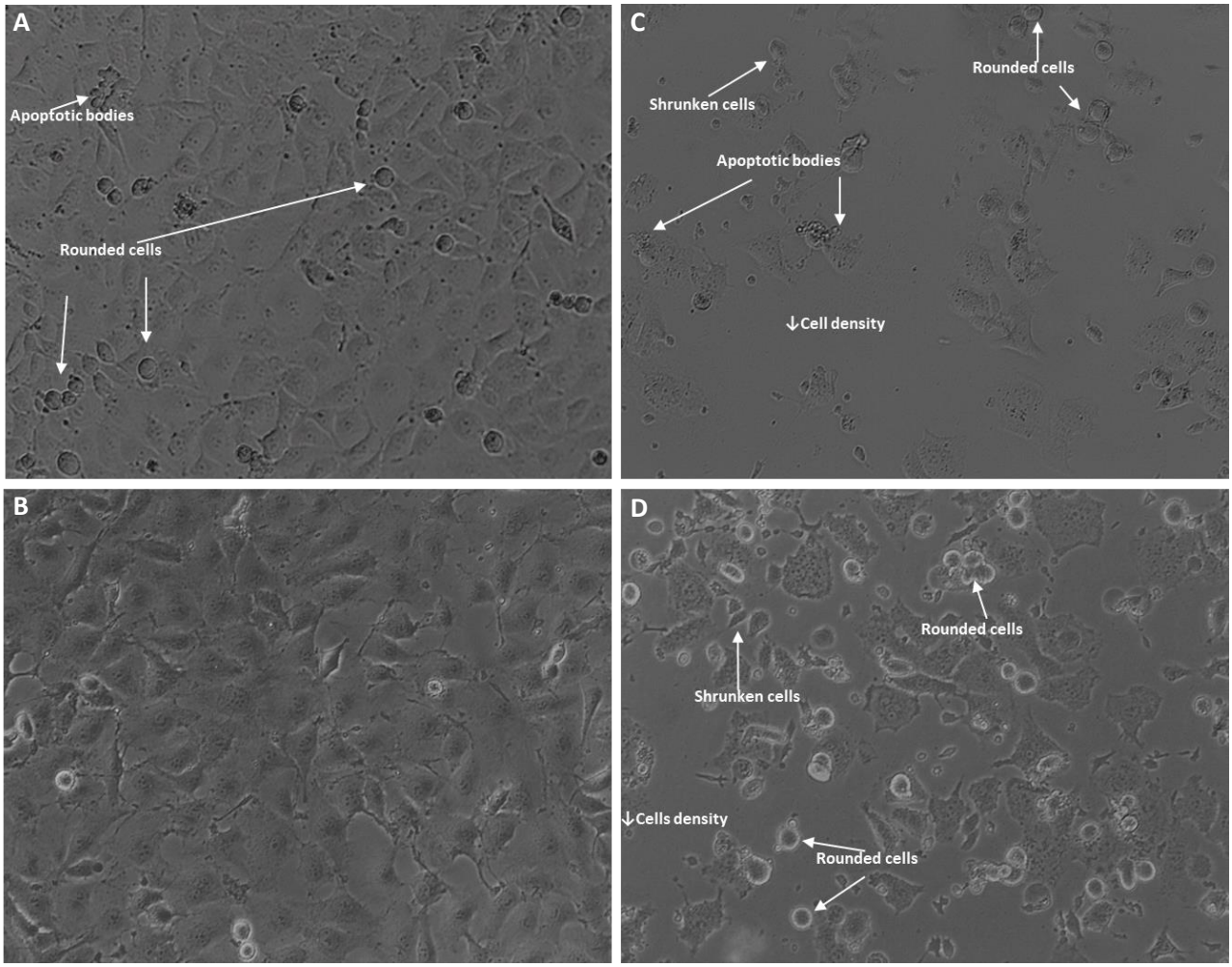


Figure 3.13: Light micrographs of MCF-7- and MDA-MB-231 cells exposed to trolox alone, and trolox in combination with ESE-one. Trolox co-exposure with ESE-one resulted in rounded cells, shrunken cells, stretched cells and apoptotic bodies in both MCF-7 and MDA-MB-231 cell lines compared to cells exposed to trolox only. However, there was a decrease in rounded cells in the trolox co-exposed cells compared to ESE-one only exposed cells. A: MCF-7 cells exposed to 80 µM trolox, B: MDA-MB-231 cells exposed to 80 µM trolox, C: MCF-7 cells exposed to trolox and ESE-one, D: MDA-MB-231 cells exposed to trolox and ESE-one.

Table 3.3 Percentage of MCF-7 cells in different morphological states as determined by means of light microscopy. An asterisk (*) indicates p-value (*P*<0.05) compared to ESE-one treated cells.

| **MCF-7** | | | |
|---|---|---|---|
| | **Normal cells** | **Rounded cells** | **Abnormal cells** |
| **Cells propagated in growth medium** | 92.0 ± 1.0 | 7.0 ± 1.0 | 1.0 ± 1.0 |
| **Vehicle treated cells** | 91.0 ± 2.6 | 6.0 ± 2.5 | 3.3 ± 1.5 |
| **ESE-one only** | 39.7 ± 3.2 | 40.7 ± 3.1 | 19.7 ± 1.5 |
| **Tiron - ESE-one** | 93.3 ± 1.2 | 3.0 ± 1.0 | 3.7 ± 1.5 |
| **Tiron + ESE-one** | 81.0 ± 4.4* | 12.0 ± 2.6* | 7.0 ± 2.0* |
| **Trolox - ESE-one** | 85.3 ± 3.2 | 7.7 ± 4.0 | 7.0 ± 2.0 |
| **Trolox + ESE-one** | 59.3 ± 3.5* | 25.3 ± 3.5* | 15.3 ± 3.5* |
| **DMTU - ESE-one** | 71.7 ± 1.5 | 18.0 ± 2.0 | 10.3 ± 1.5 |
| **DMTU + ESE-one** | 51.7 ± 4.2* | 33.3 ± 4.5* | 15.0 ± 3.0* |

Table 3.4 Percentage of MDA-MB-231 cells in different morphological states as determined by means of light microscopy. An asterisk (*) indicates p-value (*P*<0.05) compared to ESE-one treated cells.

| **MDA-MB-231** | | | |
|---|---|---|---|
| | **Normal cells** | **Rounded cells** | **Abnormal cells** |
| **Cells propagated in growth medium** | 96.7 ± 1.5 | 2.3 ± 1.5 | 1.0 ± 0.0 |
| **Vehicle treated cells** | 94.0 ± 1.0 | 4.3 ± 1.2 | 1.7 ± 0.6 |
| **ESE-one only** | 41.7 ± 2.5 | 28.7 ± 1.5 | 29.7 ± 2.3 |
| **Tiron - ESE-one** | 95.0 ± 2.0 | 1.3 ± 0.6 | 3.7 ± 1.5 |
| **Tiron + ESE-one** | 86.2 ± 2.0* | 8.7 ± 3.1* | 5.7 ± 1.5* |
| **Trolox - ESE-one** | 88.7 ± 2.1 | 9.7 ± 2.5 | 3.7 ± 0.6 |
| **Trolox + ESE-one** | 76.0 ± 4.6* | 17.0 ± 2.6* | 7.0 ± 2.0* |
| **DMTU - ESE-one** | 9.0 ± 3.0 | 7.0 ± 2.6 | 3.0 ± 1.1 |
| **DMTU + ESE-one** | 74.0 ± 4.6* | 19.7 ± 4.5* | 6.3 ± 0.6* |

### 3.1.5 Cell cycle progression

PI, permeabilization using triton X-100 and ethanol fixation was used in order to investigate the effects of ESE-one on cell cycle progression studies in the presence or absence of tiron, DMTU and trolox. Cells were exposed to ESE-one in the presence or absence of ROS inhibitors for 24 hours (figure 3.14, table 3.5 and table 3.6). ESE-one exposure induced an accumulation of cells in $G_2$/M phase (48% and 59%) and a 16% and 25% increase of cells occupying the sub-$G_1$ phase in MCF-7- (figure 3.14 C) and MDA-MB-231 cells (figure 3.14 F), respectively. Tiron co-exposure resulted in a decrease in the percentage of cells occupying the sub-$G_1$ phase to 14% and 15%, and 17% and 42% $G_2$/M phase in MCF-7 (figure 3.14 J) and MDA-MB-231 (figure 3.14 P) cell lines. Furthermore, trolox co-exposure with ESE-one resulted in 24% and 28% of cells occupying the sub-$G_1$ phase, and 24% and 43% percentage of cells occupying the $G_2$/M phase in MCF-7- (figure 3.14 K) and MDA-MB-231 (figure 3.14 Q) cells, respectively. Co-exposure of DMTU with ESE-one demonstrated 11% and 16% percentage of cells occupying the sub-$G_1$ phase, with 49% and 57% in the $G_2$/M phase in MCF-7 (figure 3.14 L) and MDA-MB-231 (figure 3.14 R) cells, respectively. There was a significant decrease of cells in the $G_2$/M phase for combination exposure of tiron and trolox in both MCF-7 (table 3.5) and MDA-MB-231 (table 3.6) cells compared to ESE-one only cells, and cells in sub-G1 in MDA-MB-231 due to tiron and DMTU.

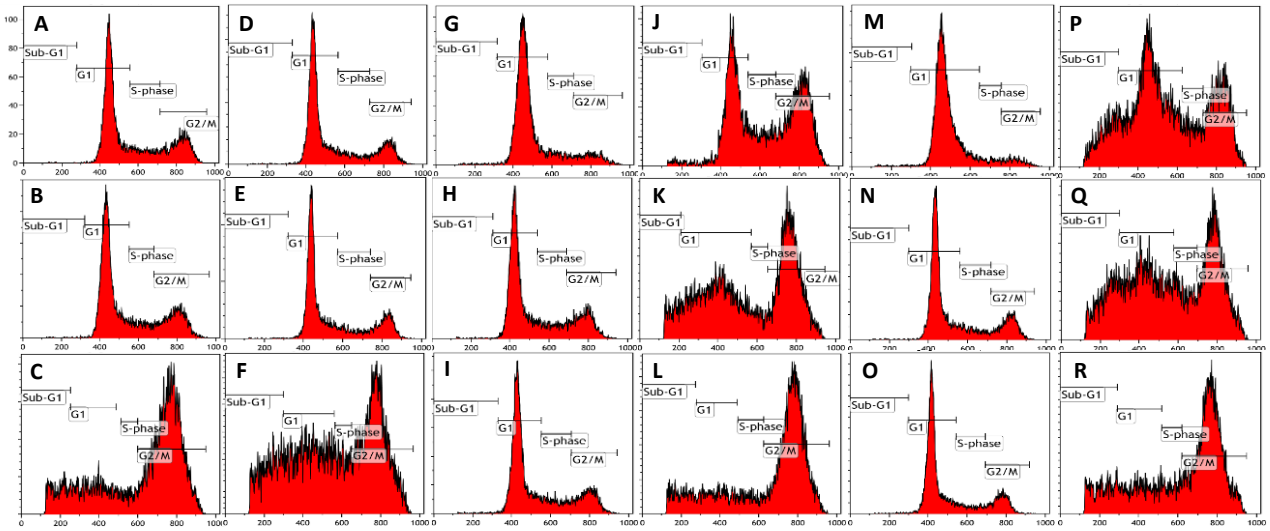


Figure 3.14: Cell cycle progression graphs of MCF-7- and MDA-MB-231 cells exposed to ESE-one in the presence or absence of ROS inhibitors (tiron, trolox and DMTU) for 24 hours. ESE-one exposure resulted in a $G_2$/M block in both MCF-7- and MDA-MB-231 cells. Tiron and DMTU exposure significantly decreased the number of cells blocked in sub-$G_1$ phase in MDA-MB-231 cells and tiron as well as trolox exposure significantly decreased the number of cells blocked in $G_2$/M phase in both MCF-7- and MDA-MB-231 cells. A: MCF-7 cells propagated in growth medium, B: vehicle-treated MCF-7 cells, C: MCF-7 cells exposed to ESE-one only, D: MDA-MB-231 cells propagated in growth medium, E: vehicle-treated MDA-MB-231 cells, F: MDA-MB-231 cells exposed to ESE-one, G: MCF-7 cells exposed to tiron only, H: MCF-7 cells exposed to trolox only, I: MCF-7 cells exposed to DMTU only, J: MCF-7 cells exposed to tiron and ESE-one, K: MCF-7 cells exposed to trolox and ESE-one, L: MCF-7 cells expose to DMTU and ESE-one, M: MDA-MB-231 cells exposed to tiron only, N: MDA-MB-231 cells exposed to trolox only, O: MDA-MB-231 cells exposed to DMTU only, P: MDA-MB-231 cells exposed to tiron and ESE-one, Q: MDA-MB-231 cells exposed to trolox and ESE-one, R: MDA-MB-231 cells exposed to DMTU and ESE-one.

Table 3.5: Percentage of MCF-7 cells occupying each cell cycle phase as determined by means of flow cytometry using PI after 24 hours exposure. An asterisk (*) indicates p-value (*P*<0.05) compared to ESE-one treated cells.

| **MCF-7 24 hours exposure** | | | | |
|---|---|---|---|---|
| | **Sub-$G_1$** | **$G_1$** | **S-phase** | **$G_2$/M** |
| **Cells propagated in growth medium** | 1.82 ± 0.16 | 68.98 ± 0.12 | 11.8 ± 1.79 | 18.19 ± 0.59 |
| **Vehicle treated cells** | 1.68 ± 0.13 | 63.7 ± 2.46 | 11.59 ± 1.71 | 22.59 ± 0.14 |
| **ESE-one only** | 17.23 ± 2.65 | 23.83 ± 0.83 | 11.61 ± 0.96 | 47.82 ± 3.44 |
| **Tiron - ESE-one** | 2.45 ± 0.65 | 74.16 ± 2.83 | 8.62 ± 1.14 | 14.13 ± 1.97 |
| **Tiron + ESE-one** | 13.47 ± 2.5 | 50.52 ± 3.64 | 12.97 ± 3.27 | 16.94 ± 1.13* |
| **Trolox - ESE-one** | 1.52 ± 0.40 | 62.83 ± 1.81 | 11.45 ± 1.23 | 24.44 ± 2.33 |
| **Trolox + ESE-one** | 23.68 ± 3.49 | 31.57 ± 3.30 | 13.13 ± 2.05 | 23.89 ± 3.84* |
| **DMTU - ESE-one** | 3.42 ± 1.02 | 69.09 ± 1.85 | 11.11 ± 1.33 | 17.68 ± 1.24 |
| **DMTU + ESE-one** | 10.65 ± 1.42 | 28.61 ± 1.13 | 12.0 ± 0.69 | 49.11 ± 0.82 |

Table 3.6: Percentage of MDA-MB-231 cells occupying each cell cycle phase as determined by means of flow cytometry using PI after 24 hours exposure. An asterisk (*) indicates p-value (*P*<0.05) compared to ESE-one treated cells.

| **MDA-MB-231 24 hours exposure** | | | | |
|---|---|---|---|---|
| | **Sub-$G_1$** | **$G_1$** | **S-phase** | **$G_2$/M** |
| **Cells propagated in growth medium** | 0.50 ± 0.14 | 67.79 ± 0.23 | 11.45 ± 0.39 | 20.15 ± 0.52 |
| **Vehicle treated cells** | 0.58 ± 0.11 | 68.10 ± 2.14 | 12.71 ± 2.20 | 18.51 ± 1.71 |
| **ESE-one only** | 25.72 ± 1.62 | 7.57 ± 1.33 | 8.18 ± 1.62 | 59.0. ± 4.62 |
| **Tiron - ESE-one** | 3.45 ± 0.88 | 71.57 ± 3.90 | 9.85 ± 1.45 | 13.42 ± 1.80 |
| **Tiron + ESE-one** | 15.21 ± 1.57* | 28.25 ± 2.44 | 17.50 ± 2.19 | 41.99 ± 1.76* |
| **Trolox - ESE-one** | 2.68 ± 0.87 | 71.76 ± 3.95 | 6.67 ± 0.87 | 22.13 ± 1.37 |
| **Trolox + ESE-one** | 27.48 ± 2.56 | 16.95 ± 1.29 | 6.94 ± 1.02 | 42.98 ± 1.69* |
| **DMTU - ESE-one** | 3.07 ± 1.11 | 62.76 ± 2.96 | 11.23 ± 1.05 | 21.60 ± .55 |
| **DMTU + ESE-one** | 15.73 ± 2.18* | 12.26 ± 0.81 | 8.35 ± 0.21 | 56.55 ± 4.21 |

Cell cycle progression was also evaluated after exposure to ESE-one in the presence or absence of ROS inhibitors (tiron, trolox and DMTU) for 48 hours (figure 3.15, table 3.7 and table 3.8). Exposure to ESE-one only resulted in an increase of cells occupying the sub-$G_1$ phase with 65% and 52% in MCF-7- (figure 3.15 C) and MDA-MB-231 (figure 3.15 F) cells, respectively. Tiron co-exposure resulted in 28% and 29% percentage of cells occupying the in sub-$G_1$, and only 24% and 27% cells in the $G_2$/M phase in MCF-7- (figure 3.15 J) and MDA-MB-231 (figure 3.15 P) cells, respectively. Trolox co-exposure with ESE-one resulted in 55% and 40% cells occupying the sub-$G_1$ phase and 14% and 23% cells occupying the $G_2$/M phase in MCF-7- (figure 3.15 K) and MDA-MB-231 (figure 3.15 Q) cells, respectively. DMTU co-exposure resulted in 47% and 32% of cells present in the sub-$G_1$ phase and 12% and 21% of cells occupying the $G_2$/M phase in MCF-7- (figure 3.15 L) and MDA-MB-231 (figure 3.15 R) cells, respectively. Tiron had the most prominent rescue effect in both MCF-7- and MDA-MB-231 cells compared to the effects of exposure to trolox and DMTU in the presence of ESE-one. Tiron, trolox and DMTU significantly decreased the number of cells in sub-$G_1$ and only tiron exposure demonstrated a significant decrease in cells in $G_2$/M phase in MCF-7 cell lines when compared to cells exposed only to ESE-one (table 3.7). In MDA-MB-231 cells, tiron and DMTU significantly decreased the percentage of cells in sub-$G_1$ phase. Furthermore, the percentage of cells in $G_2$/M phase were significantly decreased by tiron, trolox and DMTU (table 3.8).

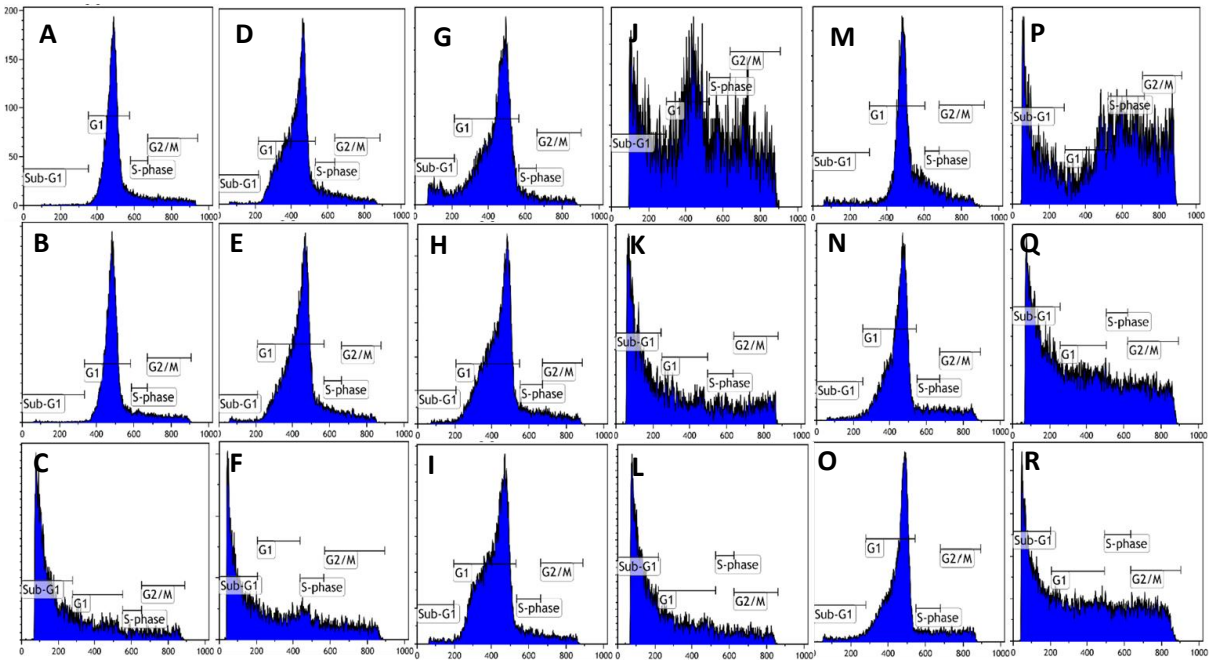


Figure 3.15: Cell cycle progression graphs of MCF-7- and MDA-MB-231 cells exposed to ESE-one in the presence or absence of ROS inhibitors (tiron, trolox and DMTU) for 48 hours. ESE-one exposure resulted in a significant increase in the percentage of cells occupying the sub-$G_1$ phase in both MCF-7- and MDA-MB-231 cells. Tiron, trolox and DMTU exposure significantly decreased the number of cells occupying the sub-$G_1$ phase in MCF-7 cells (table 3.5) and tiron as well as DMTU exposure significantly decreased the number of cell present in the sub-$G_1$ phase in MDA-MB-231 cells (table 3.6). Tiron, trolox and DMTU significantly decreased the number of cells in $G_2$/M phase in MDA-MB-231 cells and only tiron had a significant effect in MCF-7 cells. A: MCF-7 cells propagated in growth medium, B: vehicle-treated MCF-7 cells, C: MCF-7 cells exposed to ESE-one only, D: MDA-MB-231 cells propagated in growth medium, E: vehicle-treated MDA-MB-231 cells, F: MDA-MB-231 cells exposed to ESE-one, G: MCF-7 cells exposed to tiron only, H: MCF-7 cells exposed to trolox only, I: MCF-7 cells exposed to DMTU only, J: MCF-7 cells exposed to tiron and ESE-one, K: MCF-7 cells exposed to trolox and ESE-one, L: MCF-7 cells expose to DMTU and ESE-one, M: MDA-MB-231 cells exposed to tiron only, N: MDA-MB-231 cells exposed to trolox only, O: MDA-MB-231 cells exposed to DMTU only, P: MDA-MB-231 cells exposed to tiron and ESE-one, Q: MDA-MB-231 cells exposed to trolox and ESE-one, R: MDA-MB-231 cells exposed to DMTU and ESE-one.

Table 3.7 Percentage of MCF-7 cells occupying each cell cycle phase as determined by means of flow cytometry using PI after 48 hours exposure. An asterisk (*) indicates p-value (*P*<0.05) compared to ESE-one treated cells.

| **MCF-7 48 hours exposure** | | | | |
|---|---|---|---|---|
| | **Sub-$G_1$** | **$G_1$** | **S-phase** | **$G_2$/M** |
| **Cells propagated in growth medium** | 1.31 ± 0.08 | 83.55 ± 2.14 | 5.68 ± 0.30 | 11.5 ± 1.68 |
| **Vehicle treated cells** | 1.32 ± 0.11 | 84.69 ± 0.82 | 5.55 ± 0.67 | 8.73 ± 0.55 |
| **ESE-one only** | 65.30 ± 0.28 | 22.57 ± 0.86 | 4.18 ± 0.04 | 7.81 ± 0.59 |
| **Tiron - ESE-one** | 8.27 ± 0.11 | 83.77 ± 0.35 | 3.85 ± 0.42 | 3.58 ± 0.45 |
| **Tiron + ESE-one** | 28.27 ± 1.31* | 34.77 ± 1.65 | 12.08 ± 1.27 | 23.52 ± 1.51* |
| **Trolox - ESE-one** | 1.17 ± 0.01 | 67.94 ± 0.00 | 6.14 ± 0.52 | 20.76 ± 0.34 |
| **Trolox + ESE-one** | 54.80 ± 3.69* | 23.03 ± 0.65 | 8.66 ± 0.42 | 14.39 ± 2.48 |
| **DMTU - ESE-one** | 1.77 ± 0.01 | 87.05 ± 0.40 | 7.15 ± 0.52 | 5.47 ± 1.18 |
| **DMTU + ESE-one** | 46.81 ± 0.84* | 24.53 ± 0.98 | 5.63 ± 0.37 | 11.63 ± 1.97 |

Table 3.8: Percentage of MDA-MB-231 cells occupying each cell cycle phase as determined by means of flow cytometry using PI after 48 hours exposure. An asterisk (*) indicates p-value (*P*<0.05) compared to ESE-one treated cells.

| **MDA-MB-231 48 hours exposure** | | | | |
|---|---|---|---|---|
| | **Sub-$G_1$** | **$G_1$** | **S-phase** | **$G_2$/M** |
| **Cells propagated in growth medium** | 0.80 ± 0.16 | 78.09 ± 0.07 | 6.32 ± 0.19 | 13.09 ± 0.75 |
| **Vehicle treated cells** | 1.28 ± 0.28 | 76.34 ± 4.69 | 6.65 ± 2.21 | 11.96 ± 1.3 |
| **ESE-one only** | 52.1 ± 8.36 | 23.82 ± 0.39 | 5.76 ± 1.04 | 11.76 ± 0.67 |
| **Tiron - ESE-one** | 4.12 ± 1.55 | 80.66 ± 4.18 | 4.61 ± 0.87 | 4.55 ± 0.71 |
| **Tiron + ESE-one** | 29.4 ± 2.59* | 48.8 ± 8.24 | 5.92 ± 2.40 | 27.28 ± 5.71* |
| **Trolox - ESE-one** | 2.15 ± 0.69 | 80.71 ± 1.40 | 7.19 ± 1.42 | 10.59 ± 1.42 |
| **Trolox + ESE-one** | 39.51 ± 0.35* | 28.16 ± 0.22 | 10.28 ± 0.35 | 23.56 ± 3.16 |
| **DMTU - ESE-one** | 0.96 ± 0.08 | 79.96 ± 1.10 | 7.39 ± 1.92 | 13.13 ± 1.31 |
| **DMTU + ESE-one** | 32.48 ± 2.09* | 30.86 ± 0.04 | 10.28 ± 2.89 | 20.61 ± 0.16 |

### 3.1.6 Mitochondrial membrane potential

Mitochondrial membrane potential studies were conducted using the MitoProbe™ JC-1 assay kit and flow cytometry in MCF-7- (figure 3.16) and MDA-MB-231 (figure 3.17) cells exposed to ESE-one and the presence or absence of tiron, trolox or DMTU. This was done to assess the depolarization of the mitochondrial membrane potential induced by ESE-one and whether the co-exposure with the ROS inhibitor will counter the effects of ESE-on on the mitochondrial membrane potential. When the mitochondria is intact, the membrane potential is polarized thus the JC-1 dye will fluoresce red due to polarization. Damage to the mitochondria results in depolarization of the membrane potential and this will show green fluorescence of the JC-1 dye (162).

ESE-one only exposure resulted in 15% and 24% depolarization of the mitochondrial membrane in MCF-7- (figure 3.16 C) and MDA-MB-231 (figure 3.17 C) cells respectively, compared to the vehicle treated cells indicating that ESE-one has deleterious effects on the mitochondria. Tiron co-exposure with ESE-one significantly decreased the membrane depolarization to 9% (figure 3.16 F) whereas trolox and DMTU co-exposure with ESE-one triggered an insignificant increase in the depolarization of the membrane potential (19% and 16% respectively) in MCF-7 cells ( figure 3.16 H & J, table 3.9). In MDA-MB-231 cells, tiron (22%) and trolox (29%) co-exposure with ESE-one induced an insignificant decrease in membrane depolarization, respectively (figure 3.17 F & H, table 3.10) whereas DMTU (41%) co-exposure with ESE-one resulted in a significant increase in mitochondrial membrane depolarization (figure 3.17 J, table 3.10). This suggests that superoxide anion might play a role in mitochondrial membrane depolarization in MCF-7 cells as tiron significantly decrease depolarization of the membrane potential in ESE-one exposed cells, demonstrating an opposing effect on ESE-one.

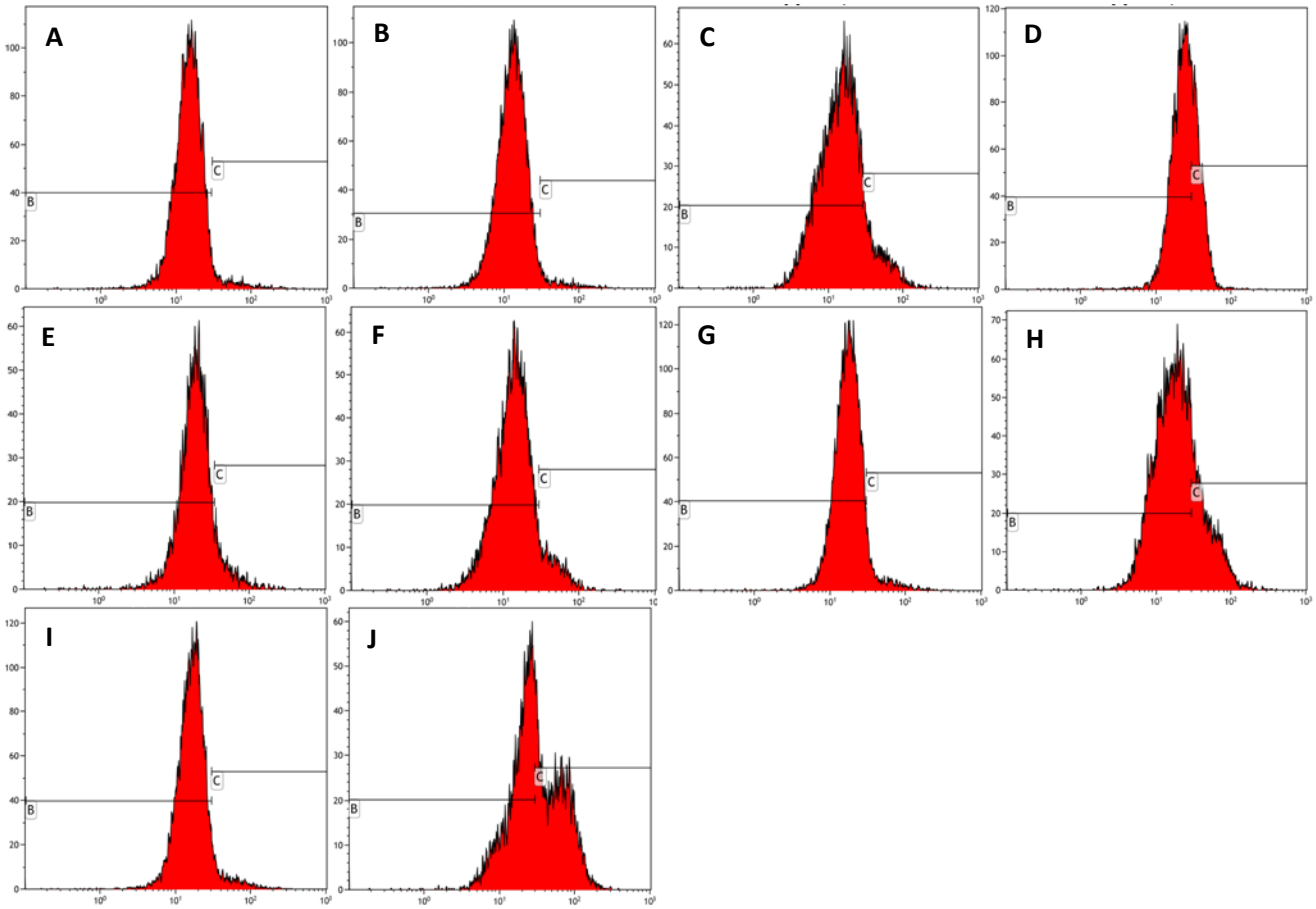


Figure 3.16: Mitochondrial membrane graphs of MCF-7 cells exposed to ESE-one in the presence or absence of ROS inhibitors (tiron, trolox and DMTU). ESE-one only exposure resulted in depolarization of the mitochondrial membrane potential in MCF-7 cells and tiron counted that effect significantly. Trolox and DMTU did not have an opposing effect on the membrane depolarization exerted by ESE-one (B indicates polarized population and C indicated depolarized population). A: Cells propagated in growth medium, B: Vehicle treated cells, C: Cells exposed to ESE-one, D: Cells exposed to CCCP, E: Cells exposed to tiron only, F: Cells exposed to tiron in combination with ESE-one, G: Cells exposed to trolox only, H: Cells exposed to trolox in combination with ESE-one, I: Cells exposed to DMTU only, J: Cells exposed to DMTU in combination with ESE-one.

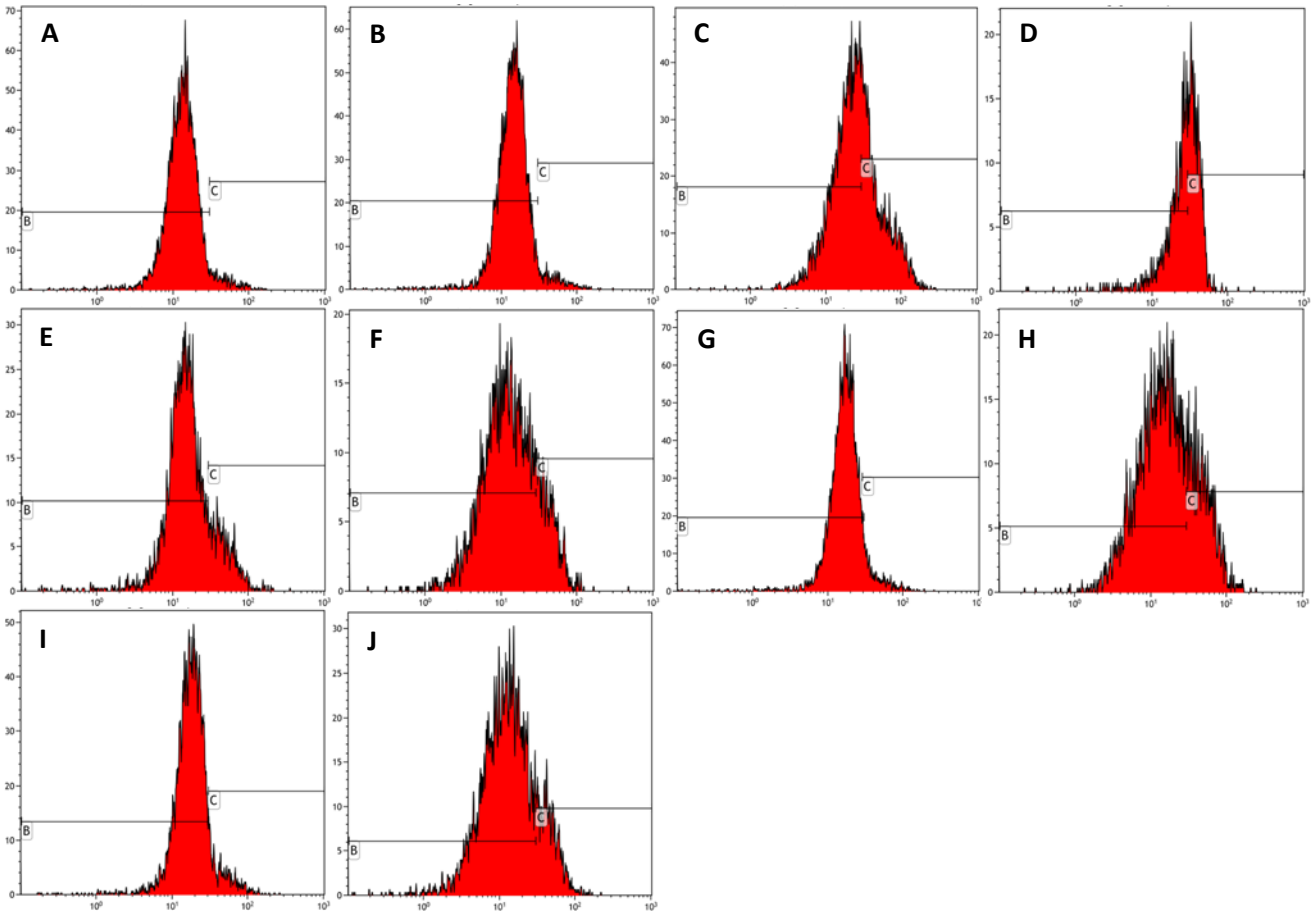


Figure 3.17: Mitochondrial membrane graphs of MDA-MB-231 cells exposed to ESE-one in the presence or absence of ROS inhibitors (tiron, trolox and DMTU). ESE-one only exposure resulted in depolarization of the mitochondrial membrane potential in MDA-MB-231 cells and tiron exposure resulted in an insignificant decrease in membrane depolarization. Trolox and DMTU did not have an opposing effect on the membrane depolarization exerted by ESE-one (B indicates polarized population and C indicated depolarized population). A: Cells propagated in growth medium, B: Vehicle treated cells, C: Cells exposed to ESE-one, D: Cells exposed to CCCP, E: Cells exposed to tiron only, F: Cells exposed to tiron in combination with ESE-one, G: Cells exposed to trolox only, H: Cells exposed to trolox in combination with ESE-one, I: Cells exposed to DMTU only, J: Cells exposed to DMTU in combination with ESE-one.

Table 3.9: Percentage of MCF-7 cells polarity of the mitochondrial membrane potential as determined by means of flow cytometry. An asterisk (*) indicates p-value (*P*<0.05) compared to ESE-one treated cells.

| **MCF-7 cells** | | |
|---|---|---|
| | **Polarized** | **Depolarized** |
| **Cells propagated in growth medium** | 97.2 ± 1.7 | 2.6 ± 1.5 |
| **Vehicle treated cells** | 97.8 ± 1.1 | 2.2 ± 1.1 |
| **ESE-one only** | 85.4 ± 0.2 | 14.6 ± 0.2 |
| **CCCP** | 67.0 ± 1.2* | 33.0 ± 1.2* |
| **Tiron - ESE-one** | 93.7 ± 1.0 | 6.0 ± 1.0 |
| **Tiron + ESE-one** | 90.6 ± 1.0* | 9.3 ± 1.0* |
| **Trolox - ESE-one** | 96.6 ± 1.0 | 3.3 ± 1.0 |
| **Trolox + ESE-one** | 80.7 ± 6.1 | 19.3 ± 6.1 |
| **DMTU - ESE-one** | 97.6 ± 1.2 | 2.4 ± 1.2 |
| **DMTU + ESE-one** | 84.2 ± 4.0 | 15.8 ± 4.1 |

Table 3.10: Percentage of MDA-MB-231 cells polarity of the mitochondrial membrane potential as determined by means of flow cytometry. An asterisk (*) indicates p-value (*P*<0.05) compared to ESE-one treated cells.

| **MDA-MB-231 cells** | | |
|---|---|---|
| | **Polarized** | **Depolarized** |
| **Cells propagated in growth medium** | 96.7 ± 2.3 | 2.9 ± 1.9 |
| **Vehicle treated cells** | 96.0 ± 1.7 | 3.8 ± 1.8 |
| **ESE-one only** | 75.8 ± 8.0 | 24.1 ± 8.1 |
| **CCCP** | 64.4 ± 16.8 | 35.6 ± 16.5 |
| **Tiron - ESE-one** | 97.1 ± 2.4 | 2.8 ± 2.5 |
| **Tiron + ESE-one** | 78.0 ± 3.4 | 21.6 ± 3.9 |
| **Trolox - ESE-one** | 93.7 ± 2.2 | 6.7 ± 3.1 |
| **Trolox + ESE-one** | 71.1 ± 4.5 | 28.8 ± 4.5 |
| **DMTU - ESE-one** | 71.6 ± 3.5 | 8.0 ± 3.2 |
| **DMTU + ESE-one** | 58.5 ± 1.3* | 41.4 ± 1.5 * |

### 3.1.7 Antioxidant activity

3.1.7.1 Superoxide dismutase inhibition

Superoxide dismutase inhibition activity was measured using a superoxide dismutase activity kit with spectrophotometry on MCF-7- and MDA-MB-231 cells exposed to ESE-one in the presence or absence of ROS inhibitors. ESE-one only exposure demonstrated a 97% inhibition rate in MCF-7 cells and tiron co-exposure resulted in 110%, trolox co-exposure resulted in 104% and DMTU co-exposure resulted in 103% SOD inhibition (figure 3.18 A). This suggests that tiron, trolox and DMTU co-exposure with ESE-one causes an increase in SOD inhibition however, these are insignificant. Cells exposed to tiron only demonstrated a significant decrease in SOD inhibition compared to vehicle-treated cells. In MDA-MB-231 cells, ESE-one exposure resulted in 89% SOD inhibition whereas combination exposure with tiron, trolox and DMTU resulted in 85%, 104% and 78% SOD inhibition respectively (figure 3.18 B). These results demonstrate that DMTU has the best inhibitory effect on SOD compared to tiron and trolox.

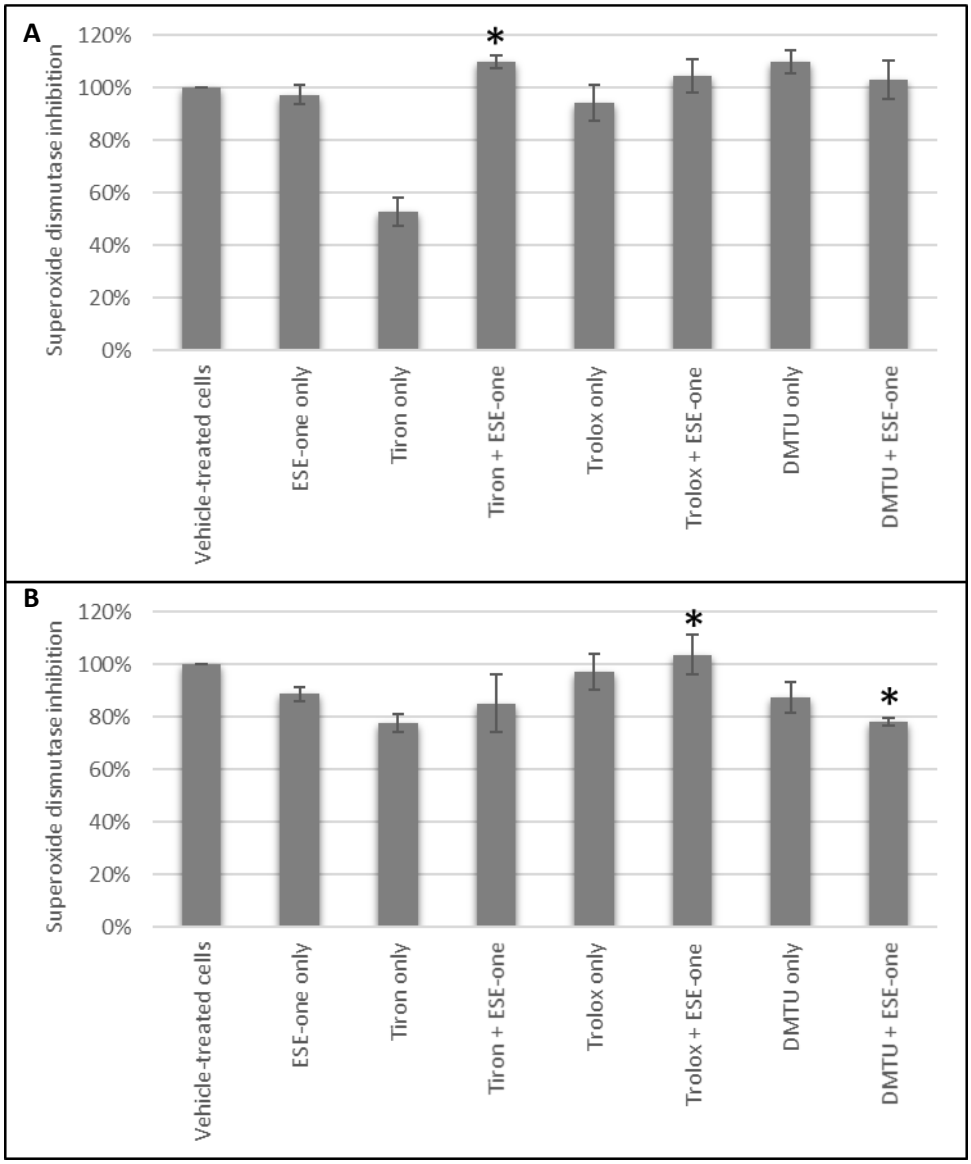


Figure 3.18: SOD inhibition graphs of MCF-7- (A) and MDA-MB-231 (B) cells exposed to ESE-one in the presence or absence of ROS inhibitors (tiron, trolox and DMTU). Tiron, trolox and DMTU co-exposure with ESE-one resulted in an increased SOD inhibition percentage compared to ESE-one only exposure in MCF-7 cells suggesting that superoxide anion, peroxyl radical and hydrogen peroxide so not play a role in the inhibition of SOD. In MDA-MB-231, DMTU demonstrated a decrease in SOD inhibition percentage suggesting that hydrogen peroxide affects the superoxide anion activity. A: MCF-7, B: MDA-MB-231. An asterisk (*) indicates p-value ($P<0.05$) compared to ESE-one treated cells.

3.1.7.2 Catalase activity

Enzyme linked immunosorbent assay (ELISA) was used to study the catalase activity in cells exposed to ESE-one in the presence or absence of ROS inhibitors. Exposure to only ESE-one decreased catalase protein to 87% in MCF-7 cells compared to cells propagated in complete growth medium. However, co-exposure with ESE-one and tiron and DMTU increased catalase concentration significantly to 113% and 144% when compared to ESE-one only exposed cells (figure 3.19 A). Trolox, however, demonstrated a significant decrease in catalase protein concentration. These results demonstrate a significant increase due to tiron and DMTU exposure (combined with ESE-one) suggesting that superoxide anion and hydrogen peroxide pathway is utilized by ESE-one. In MDA-MB-231 cells, ESE-one exposure resulted in decreased catalase protein to 74% compared to cells propagated in complete growth medium. However, co-exposure with ESE-one and tiron and trolox increased catalase concentration significantly to 91 and 90 respectively (figure 3.19 B) however, DMTU had an insignificant increase in catalase protein concentration (88%).

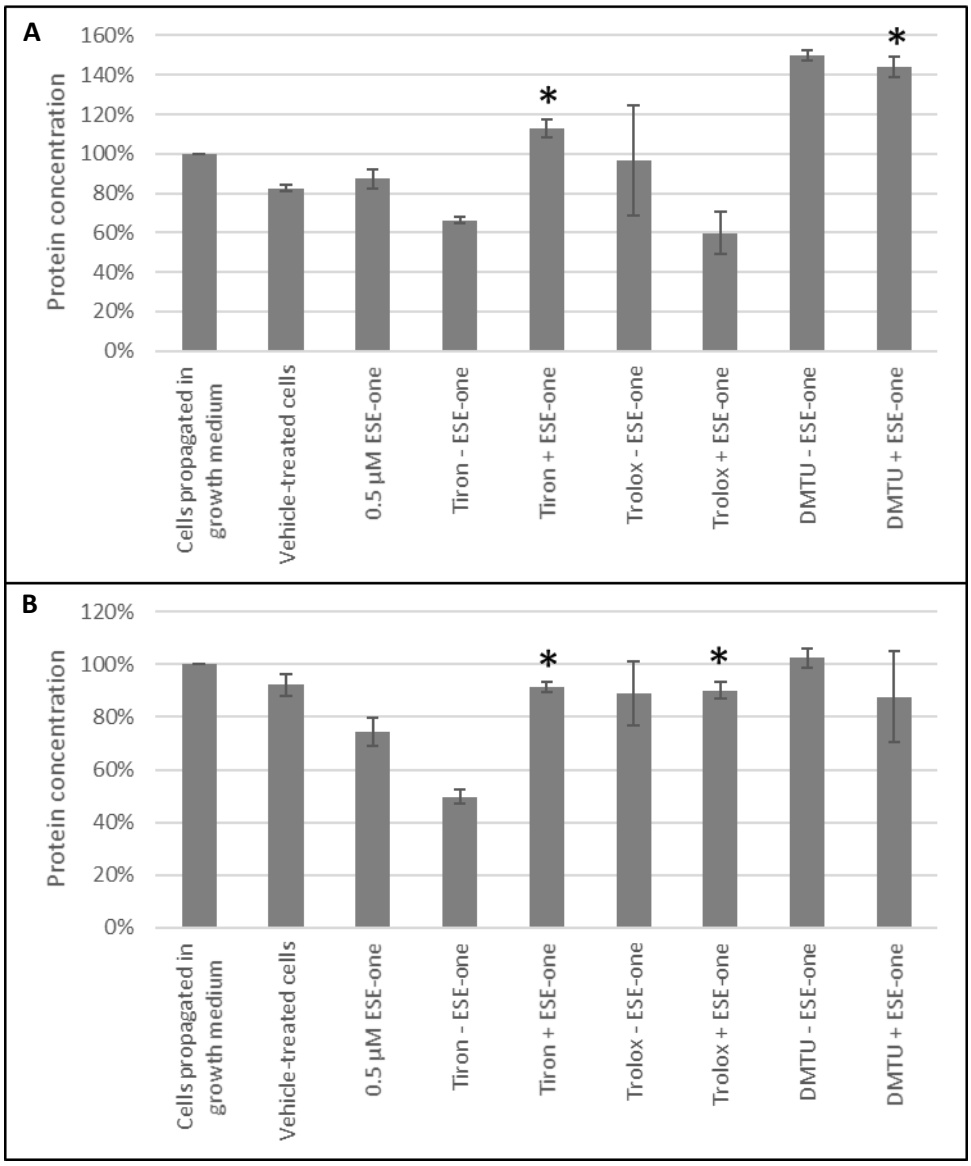


Figure 3.19: Catalase activity graphs of MCF-7 and MDA-MB-231 cells exposed to ESE-one in the presence or absence of ROS inhibitors (tiron, trolox and DMTU). Tiron and DMTU co-exposure with ESE-one increased the catalase protein concentration significantly in MCF-7 cells- and in MDA-MB-231 cells, tiron and trolox induced a significant increase in catalase protein concentration. A: MCF-7, B: MDA-MB-231. An asterisk (*) indicates p-value ($P<0.05$) compared to ESE-one treated cells.

## Chapter 4

### 4.1 Discussion

2ME is an antimitotic-, antiangiogenic- and pro-apoptotic estradiol metabolite which exhibits anticancer effects *in vitro* and *in vivo;* however, it was found that 2ME possesses low bioavailability (116, 121). This subsequently led to the *in silico*-design of 2ME derivatives with a sulphamate moiety including ESE-15-ol, ESE-one and ESE-ol. Sulphamoylated estradiol analogues have been shown to induce apoptosis and cell cycle arrest in tumourigenic cells. The additional sulphamoyl group plays a role in the induction of the aforementioned effects since these anticancer effects were not observed in the non-sulphamoylated 2ME estradiol derivatives (163). Sulphamoylated compounds are reported to induce antiproliferative-, antimitotic- and apoptotic effects via ROS production hence the current study being to investigate the specific ROS species requires for apoptotic activity induced by sulphamoylated estradiol analogues in tumourigenic breast cell lines. A study of this nature has not been reported on yet.

Elevated ROS are associated with various malignancies including cancer and various ROS including hydrogen peroxide and superoxide anions are cytotoxic (164, 165). ROS was reported to induce apoptotic- and autophagic cell death in MCF-7- and MB-MDA--231 breast cancer cell lines which was attenuated by NAC indicating the role of antioxidants in oxidative stress (166). Fluorescent microscopy studies by means of DCFDA and DHE indicated that sulphamoylated compounds induce a higher fluorescent intensity compared to non-sulphamoylated compounds, this was observed when ESE-15-ol, ESE-one and ESE-ol induced a greater fluorescent intensity compared to their non-sulphamoylated counterparts (EE-15-ol, EE-one and 2E-diol) in MCF-7- and MDA-MB-231 cells. However, this effect was observed more prominently in MCF-7 cells and to a lesser extent in MDA-MB-231 cells. The high green- and red fluorescent intensity observed in cells exposed to sulphamoylated compounds compared to cells exposed to the non-sulphamoylated counterparts suggests that the sulphamoylated compounds induced hydrogen peroxide and superoxide anion production (167). It was previously reported that 2-methoxyestradiol-bis-sulphamate (2MEBM), another sulphamoylated estradiol

compound, induced ROS (hydrogen peroxide and superoxide anion) production in MCF-7 cells which is similar to data obtained in the current study using other *in silico*-designed estradiol sulphamoylated compounds (116). Due to the cytotoxic effects of high ROS, proliferation studies were conducted to assess the role of ROS in the antiproliferative effects of sulphamoylated estradiol compounds.

Cell proliferation studies demonstrated a statistically significant decrease in cell proliferation after exposure to the sulphamoylated compounds compared to exposure to the non-sulphamoylated compounds which promoted cell growth. This effect was more prominent in MCF-7 cells indicating that the ER positive adenocarcinoma cells are more sensitive to the antiproliferative effects exerted by sulphamoylated compounds compared to ER negative adenocarcinoma cells (MDA-MB-231). Thus, decreased proliferation correlated with increased hydrogen peroxide production- and superoxide production after exposure to the sulphamoylated compounds. This effect was confirmed by literature where a sulphamoylated compound, ESE-ol (also known as C16), significantly inhibited cell growth in MCF-7- and MDA-MB-231 breast tumourigenic cells after 24 hours exposure at a nanomolar concentration (200 nM) (117). Furthermore, antiproliferative effects of sulphamoylated 2ME analogues (EMBS, ESE-16 and ESE-15-one) on the triple negative breast cancer cell line (MDA-MB-231) and cervical cancer cell lines (HeLa) were reported previously which supports the results observed in the current study (121). Spectrophotometry data confirmed the fluorescent microscopy results indicating that ROS are responsible for the antiproliferative effects of sulphamoylated estradiol compounds. ESE-one was thus chosen as a representative of the sulphamoylated compounds and subsequent experiments were conducted with ESE-one as it exhibited optimal phenomena.

Due to previous studies that demonstrated that sulphamoylated compounds induce antiproliferative effects via ROS production (126), ROS scavengers were utilized to identify the different ROS involved in the antiproliferative activity exerted by sulphamoylated compounds such as ESE-one. Three out of six scavengers (tiron,

trolox, DMTU) had a rescue effect in the antiproliferative action induced by ESE-one. Tiron scavenges superoxide anion whereas trolox scavenges peroxyl radical and DMTU scavenges hydrogen peroxide. The cell proliferation results suggest that superoxide anion, peroxyl radical and hydrogen peroxide are involved in the cell death effect induced by ESE-one in breast tumourigenic cell lines as tiron, trolox and DMTU had an opposing effect on ESE-one in both cell lines. Homobrassinin, an anticancer indole phytoalexin compound, induced intracellular ROS production in human colorectal cancer cells (Caco2) which was associated with apoptosis (also observed in decreased cell viability) however, trolox significantly decreased the ROS intensity  the effect was best observed after 24 hours exposure (168). Furthermore, a bacterial cyclic lipopeptide with anticancer properties (surfactin) induced apoptotic cell death in MCF-7 cells via ROS production which was inhibited by NAC and catalase (169). This is similar to the data obtained from the current study where co-exposure with ROS inhibitors opposed the antiproliferative effect of ESE-one. The effect of ROS scavengers on the antiproliferative effect of sulphamoylated estradiol compounds has not been reported on yet.

Antiproliferative- and antimitotic effects of a compound can also be evaluated morphologically where the morphology of the cell is assessed microscopically to identify the changes induced by the compound of interest, in this case, ESE-one. The current study demonstrated that ESE-one exposure resulted in decreased cell density, shrunken cells, blebbing and appearance of apoptotic bodies. Other sulphamoylated estradiol compounds like ESE-ol and EMBS, are reported to possess antimitotic effects which are evident in the exposed cells experiencing a metaphase arrest manifested in rounded cells (117, 170). It was reported that another sulphamoylated compound, ESE-16 (also known as C19), induced cell rounding, apoptotic bodies and decreased cell density in MCF-7 cells at 0.18 µM (171). Previous studies also demonstrated that another sulphamoylated estradiol analogue (ESE-ol) induced cell rounding, loss of cell density and apoptotic characteristics which was observed in MCF-7- and MDA-MB-231 cells (117). Similar observations were also made in MCF-7 cells exposed to 2-methoxyoestradiol-bis-sulphamate (sulphamoylated compound) for 24 hours indicating the cell rounding

effects of sulphamoylated estadiol compounds (172). However, the current study also demonstrated light microscopy indicated that the cell rounding effect induced by ESE-one was partially reversed by tiron, trolox and DMTU as cell co-exposed with ESE-one and the three ROS inhibitors demonstrated fewer rounded cells and more normal cells. This effect was observed in both MCF-7 and MDA-MB-231 cells however, the effect was more prominently observed in the in MCF-7 cells. Tiron opposed ESE-one's antimitotic effect to a greater extent suggesting that ESE-one induces cell rounding and metaphase block via the superoxide pathway. Co-exposure with ROS inhibitors depicted the specific ROS involved in the cell rounding effect of ESE-one, this combination has not been reported on to date. An arrest of cells in metaphase suggests that there is a yield in the mitosis phase of the cell cycle which was induced by ESE-one exposure.

This was confirmed by cell cycle progression studies which indicated an accumulation of cells in $G_2$/M phase in both MCF-7- and MDA-MB-231 cells after exposure to ESE-one for 24 hours which was opposed by tiron and trolox, However, exposure to ESE-one for 48 hours resulted in a significant increase in cells occupying the sub-$G_1$ phase which is indicative of cell death. This increase in the sub-$G_1$ phase after exposure to ESE-one was inhibited by tiron, trolox and DMTU after 48 hours in both MCF-7- and MDA-MB-231 cells. These effects were more prominent in ER positive breast adenocarcinoma epithelial MCF-7 cells compared to the ER negative breast adenocarcinoma epithelial MDA-MB-231 cells. This indicates that superoxide anion, peroxyl radical and hydrogen peroxide play a role in the cell cycle disruption induced by ESE-one resulting in cell death (evident in accumulation of cells in sub-$G_1$). Raobaikady *et al*. (2005) reported that sulphamoylated estradiol analogues (2-ethyloestradiol-3,17-*O*,*O*-*bis*-sulphamate, 2-ethyloestradiol-3-*O*-sulphamate, 2-methoxyoestrone-3-*O*-sulphamate and 2-methoxyoestrone-3-*O*-O-bis-sulphamate) induced a $G_2$/M block in MDA-MB-231 cells (173). Previous studies by Hye-Kyung *et al*. (2012) using diallyl trisulfide, an antitumourigenic garlic extract, demonstrated a ROS-dependent cell death in MCF-7 breast cancer cells and an accumulation of cells in sub-$G_1$ which is indicates cell death (174). The specific ROS involved are not known, making the current study the

first to report on the specific ROS in ROS-dependent cell death. ROS scavengers were utilized to identify the specific ROS playing a role in the antitumourigenic properties of ESE-one.

SOD and catalase are well known ROS inhibitors which inhibit superoxide anion and hydrogen peroxide, respectively (175, 176). The SOD inhibition rate was not distinctly affected by ESE-one and combination exposure with the ROS inhibitors. However, ESE-one combination exposure with tiron and combination exposure with DMTU increased the catalase protein concentration in MCF-7 cells indicating that tiron and DMTU play a role in hydrogen peroxide inhibition. Tiron and trolox had a similar effect in MDA-MB-231 cells. An increase in catalase protein concentration indicated a decline in the hydrogen peroxide concentration suggesting that superoxide anion and peroxyl radical upstream of hydrogen peroxide push the reaction forward thus promotion the conversion of hydrogen peroxide to water and oxygen by catalase. ROS are involved in the intrinsic pathway of apoptosis which involves mitochondrial permeabilization resulting in cytochrome *c* release (177, 178). This process is inhibited by antioxidants including catalase which oxidise the ROS. Mitochondrial SOD and catalase is regulated by protein kinase B (Akt)/Forkhead box (Foxo) transcription factor pathway however, FoxO3a specifically regulates catalase. FoxO3a is regulated by Akt signaling pathway; this signaling pathway is said to supress catalase expression in cancer cells (179). The catalase results suggest that ESE-one may induce ROS-dependence cell death via the Akt signaling pathway because catalase protein was suppressed in ESE-one only treated cells which was recovered by co-treatment with tiron, trolox and DMTU. ROS are generated by the mitochondria and elevated ROS can be cytotoxic but the mitochondrial antioxidants (SOD and catalase) eliminate the ROS to maintain homeostasis thus it is important to assess the mitochondrial membrane potential (180-182).

Mitochondrial integrity is an factor important in apoptosis signaling, a drop in the mitochondrial membrane potential is indicative of apoptosis (113). Elevated ROS cause disruptions in the mitochondria which results in opening of the mitochondrial

channel and ultimately, a drop of mitochondrial membrane potential (183, 184). A study by Visagie *et al*. (2017) demonstrated the anticancer effects induced by EMBS (sulphamoylated compound) including mitochondrial membrane damage in MDA-MB-231 cells which were inhibited by NAC, these new findings suggested that sulphamoylated estradiol analogues induce mitochondrial damage via ROS (126). ESE-one exposure induced mitochondrial depolarization in MCF-7- and MDA-MB-231 cells which was rescued by tiron in MCF-7 cells and DMTU in MDA-MB-231 cells. This suggests that superoxide anion and hydrogen peroxide play a role in the depolarization of the mitochondrial membrane induced by ESE-one.

This *in vitro* study demonstrated that ESE-one is an antiproliferative-, antimitotic- and apoptotic compound in breast tumourigenic cells (MCF-7 and MDA-MB-231) which operates via ROS production. Suggesting that superoxide anion, peroxyl radical and hydrogen peroxide are the specific ROS utilized in the cell death mechanism induced by ESE-one. The proposed mechanism is that ESE-one induces ROS production which causes cell cycle arrest and depolarization of the mitochondrial membrane resulting in further production of ROS, and ultimately apoptosis (figure 4.1). This was demonstrated in the sub-$G_1$ block and mitochondrial membrane depolarization which was rescued by tiron, trolox and DMTU.

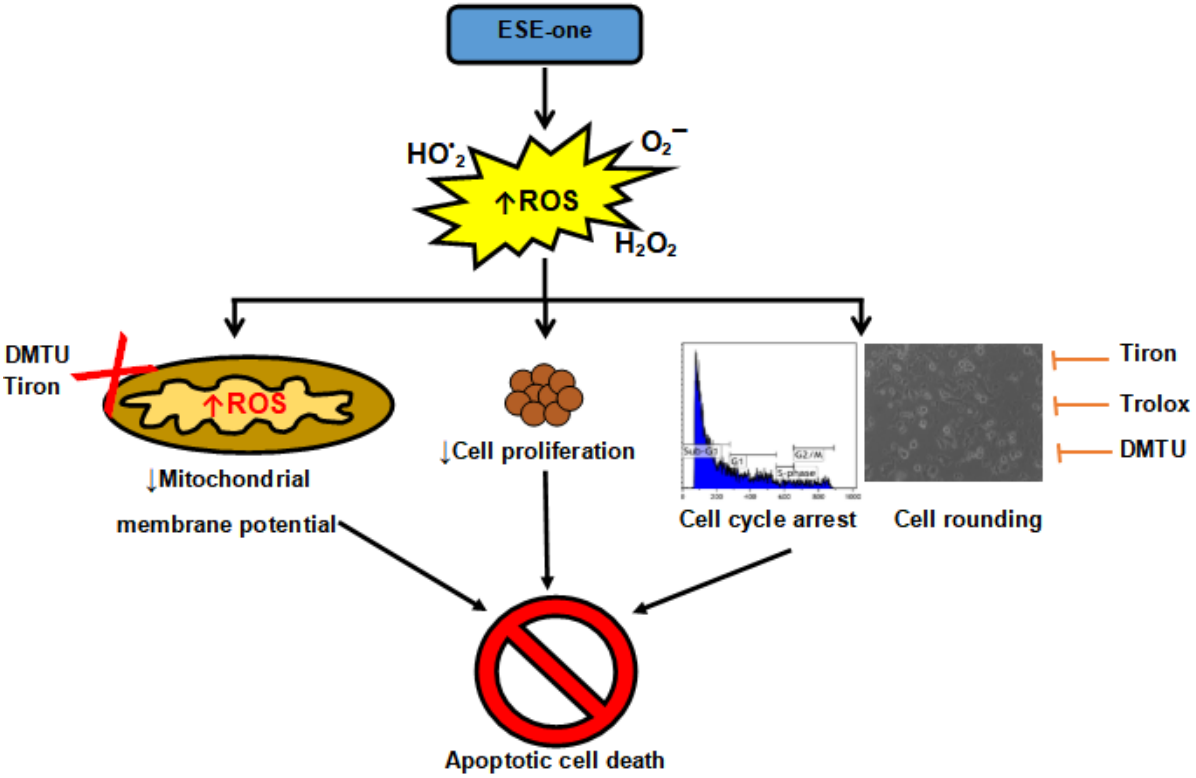


Figure 4.1: Proposed mechanism utilized by ESE-one to induce cell death. The proposed mechanism in which sulphamoylated compounds induce cell death is by the elevation of ROS (superoxide anion, hydrogen peroxide and peroxyl radical) which causes depolarization of the mitochondrial membrane potential, decreased cell proliferation, cell cycle arrest and cell rounding culminating in apoptosis.

## Chapter 5

### 5.1 Conclusion

The main aim of this *in vitro* study was to investigate the role of ROS in apoptosis induced by sulphamoylated estradiol analogue in breast cell lines on proliferation, ROS production, morphology, cell cycle progression, antioxidant activity and mitochondrial membrane potential. Data from the current study showed that ESE-one induced ROS production, rounded cells and apoptotic bodies, inhibition of cell growth, sub-$G_1$ block and depolarization the mitochondrial membrane potential in breast tumourigenic cell lines. These effects can be inhibited by ROS (tiron, trolox and DMTU) inhibitors indicating that superoxide anion-, peroxyl radical- and hydrogen peroxide are essential for the pathways induced by ESE-one. Thus, exposure to ESE-one reduced cell growth, cell rounding, mitochondrial membrane depolarisation, cell cycle abnormalities and cell death that are dependent on the production of superoxide anion-, peroxyl radical- and hydrogen peroxide that are induced by ESE-one

This study involving various ROS inhibitors to identify the specific ROS involved in the cell death effect of sulphamoylated estradiol analogue is the first to be reported on. Thus, can contribute to future mechanistic studies aimed at targeting specific ROS to inhibit cell death in breast tumourigenic cells. This will contribute to the improvement of current therapy targeting ROS-induced pathways in cancer.

**References**

1. Nalini M, Oranuba E, Poustchi H, Sepanlou SG, Pourshams A, Khoshnia M, et al. Causes of premature death and their associated risk factors in the Golestan Cohort Study, Iran. BMJ Open. 2018;8(7):e021479.

2. Feng Y, Spezia M, Huang S, Yuan C, Zeng Z, Zhang L, et al. Breast cancer development and progression: Risk factors, cancer stem cells, signaling pathways, genomics, and molecular pathogenesis. Genes & diseases. 2018;5(2):77-106.

3. Bray F, Ferlay J, Soerjomataram I, Siegel RL, Torre LA, Jemal A. Global cancer statistics 2018: GLOBOCAN estimates of incidence and mortality worldwide for 36 cancers in 185 countries. CA Cancer J Clin. 2018;68(6):394-424.

4. Zheng B, Yoon SW, Lam SS. Breast cancer diagnosis based on feature extraction using a hybrid of K-means and support vector machine algorithms. Expert Syst Appl. 2014;41(4):1476-1482.

5. Siegel RL, Miller KD, Jemal A. Cancer statistics, 2019. CA Cancer J Clin. 2019;69(1):7-34.

6. Made F, Wilson K, Jina R, Tlotleng N, Jack S, Ntlebi V, et al. Distribution of cancer mortality rates by province in South Africa. Cancer Epidemiol. 2017;51:56-61.

7. Jemal A, Bray F, Forman D, O'brien M, Ferlay J, Center M, et al. Cancer burden in Africa and opportunities for prevention. Cancer. 2012;118(18):4372-4384.

8. Bhardwaj A, Tiwari A. Breast cancer diagnosis using genetically optimized neural network model. Expert Syst Appl. 2015;42(10):4611-4620.

9. Weigelt B, Reis-Filho JS. Histological and molecular types of breast cancer: is there a unifying taxonomy? Nat Rev Clin Oncol. 2009;6(12):718-730.

10. Weigelt B, Horlings H, Kreike B, Hayes M, Hauptmann M, Wessels L, et al. Refinement of breast cancer classification by molecular characterization of histological special types. J Pathol. 2008;216(2):141-150.

11. Adélaïde J, Finetti P, Bekhouche I, Repellini L, Geneix J, Sircoulomb F, et al. Integrated profiling of basal and luminal breast cancers. Cancer Res. 2007;67(24):11565-11575.

12. Tarcic O, Granit RZ, Pateras IS, Masury H, Maly B, Zwang Y, et al. RNF20 and histone H2B ubiquitylation exert opposing effects in Basal-Like versus luminal breast cancer. Cell Death Differ. 2017;24(4):694-704.

13. Krstic M, Macmillan CD, Leong HS, Clifford AG, Souter LH, Dales DW, et al. The transcriptional regulator TBX3 promotes progression from non-invasive to invasive breast cancer. BMC Cancer. 2016;16(1):671.
14. Wellings S, Jensen HM. On the origin and progression of ductal carcinoma in the human breast. J Natl Cancer Inst. 1973;50(5):1111-1118.
15. Obenauf AC, Massagué J. Surviving at a distance: organ-specific metastasis. Trends in cancer. 2015;1(1):76-91.
16. Scully OJ, Bay B-H, Yip G, Yu Y. Breast cancer metastasis. Cancer Genom Proteom. 2012;9(5):311-320.
17. Cheung KJ, Ewald AJ. A collective route to metastasis: Seeding by tumor cell clusters. Science. 2016;352(6282):167-769.
18. Chambers AF, Groom AC, MacDonald IC. Metastasis: dissemination and growth of cancer cells in metastatic sites. Nat Rev Cancer. 2002;2(8):563-572.
19. Goss PE, Chambers AF. Does tumour dormancy offer a therapeutic target? Nat Rev Cancer. 2010;10(12):871-888.
20. Sosa MS, Bragado P, Aguirre-Ghiso JA. Mechanisms of disseminated cancer cell dormancy: an awakening field. Nat Rev Cancer. 2014;14(9):611-622.
21. Prat A, Adamo B, Cheang MC, Anders CK, Carey LA, Perou CM. Molecular characterization of basal-like and non-basal-like triple-negative breast cancer. The oncologist. 2013;18(2):123-133.
22. Prat A, Perou CM. Deconstructing the molecular portraits of breast cancer. Mol Oncol. 2011;5(1):5-23.
23. Rouzier R, Perou CM, Symmans WF, Ibrahim N, Cristofanilli M, Anderson K, et al. Breast cancer molecular subtypes respond differently to preoperative chemotherapy. Clin Cancer Res. 2005;11(16):5678-5685.
24. Li LT, Jiang G, Chen Q, Zheng JN. Ki67 is a promising molecular target in the diagnosis of cancer. Mol Med Rep. 2015;11(3):1566-1572.
25. Cheang MC, Chia SK, Voduc D, Gao D, Leung S, Snider J, et al. Ki67 index, HER2 status, and prognosis of patients with luminal B breast cancer. JNCI: J Nat Cancer Inst. 2009;101(10):736-750.
26. Inwald E, Klinkhammer-Schalke M, Hofstädter F, Zeman F, Koller M, Gerstenhauer M, et al. Ki-67 is a prognostic parameter in breast cancer patients:

results of a large population-based cohort of a cancer registry. Breast Cancer Res Treat. 2013;139(2):539-552.

27. Yerushalmi R, Woods R, Ravdin PM, Hayes MM, Gelmon KA. Ki67 in breast cancer: prognostic and predictive potential. Lancet Oncol. 2010;11(2):174-183.

28. Li H, Han X, Liu Y, Liu G, Dong G. Ki67 as a predictor of poor prognosis in patients with triple‐negative breast cancer. Oncol Lett. 2015;9(1):149-152.

29. Shokouh TZ, Ezatollah A, Barand P. Interrelationships between Ki67, HER2/neu, p53, ER, and PR status and their associations with tumor grade and lymph node involvement in breast carcinoma subtypes: retrospective-observational analytical study. Medicine. 2015;94(32):e1359.

30. Kelsey JL, Gammon MD, John EM. Reproductive factors and breast cancer. Epidemiol Rev. 1993;15(1):36-47.

31. Bray F, McCarron P, Parkin DM. The changing global patterns of female breast cancer incidence and mortality. Breast Cancer Res. 2004;6(6):229-239.

32. Brewer HR, Jones ME, Schoemaker MJ, Ashworth A, Swerdlow AJ. Family history and risk of breast cancer: an analysis accounting for family structure. Breast Cancer Res Treat. 2017;165(1):193-200.

33. Andrade JE, Ju YH, Baker C, Doerge DR, Helferich WG. Long-term exposure to dietary sources of genistein induces estrogen-independence in the human breast cancer (MCF-7) xenograft model. Mol Nutr Food Res. 2015;59(3):413-423.

34. Gil EMC. Targeting the PI3K/AKT/mTOR pathway in estrogen receptor-positive breast cancer. Cancer Treat Rev. 2014;40(7):862-871.

35. Sampson JN, Falk RT, Schairer C, Moore SC, Fuhrman BJ, Dallal CM, et al. Association of estrogen metabolism with breast cancer risk in different cohorts of postmenopausal women. Cancer Res. 2017;77(4):918-925.

36. Brown SB, Hankinson SE. Endogenous estrogens and the risk of breast, endometrial, and ovarian cancers. Steroids. 2015;99:8-10.

37. Carraro DM, Folgueira MAAK, Lisboa BCG, Olivieri EHR, Krepischi ACV, de Carvalho AF, et al. Comprehensive analysis of BRCA1, BRCA2 and TP53 germline mutation and tumor characterization: a portrait of early-onset breast cancer in Brazil. PLoS One. 2013;8(3):e57581.

38. Aparicio T, Baer R, Gautier J. DNA double-strand break repair pathway choice and cancer. DNA repair. 2014;19:169-175.

39. Robson M, Im S-A, Senkus E, Xu B, Domchek SM, Masuda N, et al. Olaparib for metastatic breast cancer in patients with a germline BRCA mutation. New Engl J Med. 2017;377(6):523-533.

40. Miller KD, Siegel RL, Lin CC, Mariotto AB, Kramer JL, Rowland JH, et al. Cancer treatment and survivorship statistics, 2016. CA: Cancer J Clin. 2016;66(4):271-289.

41. DeSantis CE, Lin CC, Mariotto AB, Siegel RL, Stein KD, Kramer JL, et al. Cancer treatment and survivorship statistics, 2014. CA: Cancer J Clin. 2014;64(4):252-271.

42. Pusztai L, Karn T, Safonov A, Abu-Khalaf MM, Bianchini G. New strategies in breast cancer: immunotherapy. Clin Cancer Res. 2016;22(9):2105-2110.

43. Gu Z, Gao D, Al-Zubaydi F, Li S, Singh Y, Rivera K, et al. The effect of size and polymer architecture of doxorubicin–poly (ethylene) glycol conjugate nanocarriers on breast duct retention, potency and toxicity. Eur J Pharm Sci. 2018;121:118-125.

44. N'da D. Synthesis of methotrexate and Ferrocene conjugates as potential anticancer agents: PhD Dissertation.(School of Chemistry, Cambridge, 2004); 2004.

45. Kennecke H, Yerushalmi R, Woods R, Cheang MCU, Voduc D, Speers CH, et al. Metastatic behavior of breast cancer subtypes. J Clinical Oncol. 2010;28(20):3271-3277.

46. Shapiro CL, Recht A. Side effects of adjuvant treatment of breast cancer. New Engl J Med. 2001;344(26):1997-2008.

47. Baskar R, Lee KA, Yeo R, Yeoh K-W. Cancer and radiation therapy: current advances and future directions. Int J Med Sci. 2012;9(3):193-199.

48. Collignon J, Lousberg L, Schroeder H, Jerusalem G. Triple-negative breast cancer: treatment challenges and solutions. Breast Cancer: Targets and Therapy. 2016;8:93-107.

49. Asselain B, Barlow W, Bartlett J, Bergh J, Bergsten-Nordström E, Bliss J, et al. Long-term outcomes for neoadjuvant versus adjuvant chemotherapy in early breast cancer: meta-analysis of individual patient data from ten randomised trials. Lancet Oncol. 2018;19(1):27-39.

50. Huang C-Y, Ju D-T, Chang C-F, Reddy PM, Velmurugan BK. A review on the effects of current chemotherapy drugs and natural agents in treating non–small cell lung cancer. Biomedicine. 2017;7(4):12-23.

51. Vermorken JB, Mesia R, Rivera F, Remenar E, Kawecki A, Rottey S, et al. Platinum-based chemotherapy plus cetuximab in head and neck cancer. New Engl J Med. 2008;359(11):1116-1127.

52. Pardoll DM. The blockade of immune checkpoints in cancer immunotherapy. Nat Rev Cancer. 2012;12(4):252-264.

53. Schumacher TN, Schreiber RD. Neoantigens in cancer immunotherapy. Science. 2015;348(6230):69-74.

54. Emens LA. Breast cancer immunobiology driving immunotherapy: vaccines and immune checkpoint blockade. Expert Rev Anticancer Ther. 2012;12(12):1597-1611.

55. Vonderheide RH, Domchek SM, Clark AS. Immunotherapy for breast cancer: what are we missing? Clin Cancer Res. 2017;23(11):2640-2646.

56. Group EBCTC. Aromatase inhibitors versus tamoxifen in early breast cancer: patient-level meta-analysis of the randomised trials. The Lancet. 2015;386(10001):1341-1352.

57. Xue X, Yang YA, Zhang A, Fong K, Kim J, Song B, et al. LncRNA HOTAIR enhances ER signaling and confers tamoxifen resistance in breast cancer. Oncogene. 2016;35(21):2746-2755.

58. Smith IE, Dowsett M, Ebbs SR, Dixon JM, Skene A, Blohmer J, et al. Neoadjuvant treatment of postmenopausal breast cancer with anastrozole, tamoxifen, or both in combination: the Immediate Preoperative Anastrozole, Tamoxifen, or Combined with Tamoxifen (IMPACT) multicenter double-blind randomized trial. J Clin Oncol. 2005;23(22):5108-5116.

59. André F, O'Regan R, Ozguroglu M, Toi M, Xu B, Jerusalem G, et al. Everolimus for women with trastuzumab-resistant, HER2-positive, advanced breast cancer (BOLERO-3): a randomised, double-blind, placebo-controlled phase 3 trial. Lancet Oncol. 2014;15(6):580-591.

60. Hartwell LH, Kastan MB. Cell cycle control and cancer. Science. 1994;266(5192):1821-1828.

61. Vermeulen K, Van Bockstaele DR, Berneman ZN. The cell cycle: a review of regulation, deregulation and therapeutic targets in cancer. Cell proliferation. 2003;36(3):131-149.
62. Otto T, Sicinski P. Cell cycle proteins as promising targets in cancer therapy. Nat Rev Cancer. 2017;17(2):93-115.
63. O'Leary B, Finn RS, Turner NC. Treating cancer with selective CDK4/6 inhibitors. Nat Rev Clin Oncol. 2016;13(7):417-430.
64. Davis PK, Ho A, Dowdy SF. Biological methods for cell-cycle synchronization of mammalian cells. Biotechniques. 2001;30(6):1322-1331.
65. Saqcena M, Menon D, Patel D, Mukhopadhyay S, Chow V, Foster DA. Amino acids and mTOR mediate distinct metabolic checkpoints in mammalian G1 cell cycle. PloS one. 2013;8(8):e74157.
66. Bertoli C, Skotheim JM, De Bruin RA. Control of cell cycle transcription during G1 and S phases. Nat Rev Mol Cell Bio. 2013;14(8):518-528.
67. Rieder CL, Cole RW. Entry into mitosis in vertebrate somatic cells is guarded by a chromosome damage checkpoint that reverses the cell cycle when triggered during early but not late prophase. J Cell Bio. 1998;142(4):1013-1022.
68. Medema R, Macůrek L. Checkpoint control and cancer. Oncogene. 2012;31(21):2601-2613.
69. Langerak P, Russell P. Regulatory networks integrating cell cycle control with DNA damage checkpoints and double-strand break repair. Phil Trans R Soc B. 2011;366(1584):3562-3571.
70. Anders L, Ke N, Hydbring P, Choi YJ, Widlund HR, Chick JM, et al. A systematic screen for CDK4/6 substrates links FOXM1 phosphorylation to senescence suppression in cancer cells. Cancer cell. 2011;20(5):620-634.
71. Murray AW. Recycling the cell cycle: cyclins revisited. Cell. 2004;116(2):221-234.
72. Lim S, Kaldis P. Cdks, cyclins and CKIs: roles beyond cell cycle regulation. Development. 2013;140(15):3079-3093.
73. Abou-Ghali M, Stiban J. Regulation of ceramide channel formation and disassembly: Insights on the initiation of apoptosis. Saudi J Biol Sci. 2015;22(6):760-772.

74. Guo Y, Stacey DW, Hitomi M. Post-transcriptional regulation of cyclin D1 expression during G2 phase. Oncogene. 2002;21(49):7545-7556.
75. Zarkowska T, Mittnacht S. Differential phosphorylation of the retinoblastoma protein by G1/S cyclin-dependent kinases. J Biol Chem. 1997;272(19):12738-12746.
76. Sherr CJ, Roberts JM. CDK inhibitors: positive and negative regulators of G1-phase progression. Gene Dev. 1999;13(12):1501-1512.
77. Keenan SM, Lents NH, Baldassare JJ. Expression of cyclin E renders cyclin D-CDK4 dispensable for inactivation of the retinoblastoma tumor suppressor protein, activation of E2F, and G1-S phase progression. J Biol Chem. 2004;279(7):5387-5396.
78. Whittaker AJ, Royzman I, Orr-Weaver TL. Drosophila double parked: a conserved, essential replication protein that colocalizes with the origin recognition complex and links DNA replication with mitosis and the down-regulation of S phase transcripts. Gene Dev. 2000;14(14):1765-1776.
79. Méndez J, Zou-Yang XH, Kim S-Y, Hidaka M, Tansey WP, Stillman B. Human origin recognition complex large subunit is degraded by ubiquitin-mediated proteolysis after initiation of DNA replication. Mol cell. 2002;9(3):481-491.
80. Lei M, Tye BK. Initiating DNA synthesis: from recruiting to activating the MCM complex. J Cell Sci. 2001;114(8):1447-1454.
81. Borlado LR, Méndez J. CDC6: from DNA replication to cell cycle checkpoints and oncogenesis. Carcinogenesis. 2007;29(2):237-243.
82. Tada S. Cdt1 and geminin: role during cell cycle progression and DNA damage in higher eukaryotes. Front Biosci. 2007;12(1):1629-1641.
83. Wang Z, Fan M, Candas D, Zhang T-Q, Qin L, Eldridge A, et al. Cyclin B1/Cdk1 coordinates mitochondrial respiration for cell-cycle G2/M progression. Dev Cell. 2014;29(2):217-232.
84. Shaltiel IA, Krenning L, Bruinsma W, Medema RH. The same, only different–DNA damage checkpoints and their reversal throughout the cell cycle. J Cell Sci. 2015;128(4):607-620.
85. Delia D, Fontanella E, Ferrario C, Chessa L, Mizutani S. DNA damage-induced cell-cycle phase regulation of p53 and p21 waf1 in normal and ATM-defective cells. Oncogene. 2003;22(49):7866-7869.

86. Ishikawa K, Ishii H, Saito T. DNA damage-dependent cell cycle checkpoints and genomic stability. DNA Cell Biol. 2006;25(7):406-411.

87. Molnar C, Gair J. Concepts of Biology: 1st Canadian Edition. 2015.

88. Mazia D. The cell cycle. Sci Am. 1974;230(1):54-68.

89. Mailand N, Podtelejnikov AV, Groth A, Mann M, Bartek J, Lukas J. Regulation of G2/M events by Cdc25A through phosphorylation-dependent modulation of its stability. EMBO J. 2002;21(21):5911-5920.

90. Yu H. Regulation of APC–Cdc20 by the spindle checkpoint. Curr Opin Cell Biol. 2002;14(6):706-714.

91. Novák B, Sible JC, Tyson JJ. Checkpoints in the cell cycle. e LS. 2001.

92. Jia L, Kim S, Yu H. Tracking spindle checkpoint signals from kinetochores to APC/C. Trends in Biochem Sci. 2013;38(6):302-311.

93. Manchado E, Guillamot M, Malumbres M. Killing cells by targeting mitosis. Cell Death Differ. 2012;19(3):369-377.

94. Visconti R, Della Monica R, Grieco D. Cell cycle checkpoint in cancer: a therapeutically targetable double-edged sword. J Exp Clin Cancer Res. 2016;35(1):153-160.

95. Chaabane W, User SD, El-Gazzah M, Jaksik R, Sajjadi E, Rzeszowska-Wolny J, et al. Autophagy, apoptosis, mitoptosis and necrosis: interdependence between those pathways and effects on cancer. Arch Immunol Ther Exp. 2013;61(1):43-58.

96. Koopman G, Reutelingsperger C, Kuijten G, Keehnen R, Pals S, Van Oers M. Annexin V for flow cytometric detection of phosphatidylserine expression on B cells undergoing apoptosis. Blood. 1994;84(5):1415-1420.

97. Van Engeland M, Nieland LJ, Ramaekers FC, Schutte B, Reutelingsperger CP. Annexin V-affinity assay: a review on an apoptosis detection system based on phosphatidylserine exposure. Cytometry. 1998;31(1):1-9.

98. Segawa K, Nagata S. An apoptotic ‘eat me’ signal: Phosphatidylserine exposure. Trends Cell Biol. 2015;25(11):639-650.

99. Yang ST, Huang AC, Tang NY, Liu HC, Liao CL, Ji BC, et al. Bisdemethoxycurcumin-induced S phase arrest through the inhibition of cyclin A and E and induction of apoptosis via endoplasmic reticulum stress and

mitochondria-dependent pathways in human lung cancer NCI H 460 cells. Environ Toxicol. 2016;31(12):1899-1908.
100. Liu H, Baliga R. Endoplasmic reticulum stress–associated caspase 12 mediates cisplatin-induced LLC-PK1 cell apoptosis. J Am Soc Nephrol. 2005;16(7):1985-1992.
101. Lorenzo HK, Susin SA, Penninger J, Kroemer G. Apoptosis inducing factor (AIF): a phylogenetically old, caspase-independent effector of cell death. Cell Death Differ. 1999;6(6):516-524.
102. Ouyang L, Shi Z, Zhao S, Wang FT, Zhou TT, Liu B, et al. Programmed cell death pathways in cancer: a review of apoptosis, autophagy and programmed necrosis. Cell proliferation. 2012;45(6):487-498.
103. Ashkenazi A. Targeting the extrinsic apoptosis pathway in cancer. Cytokine Growth Factor Rev. 2008;19(3-4):325-331.
104. Park M-R, Kim S-G, Cho I-A, Oh D, Kang K-R, Lee S-Y, et al. Licochalcone-A induces intrinsic and extrinsic apoptosis via ERK1/2 and p38 phosphorylation-mediated TRAIL expression in head and neck squamous carcinoma FaDu cells. Food Chem Toxicol. 2015;77:34-43.
105. Fulda S, Debatin K-M. Extrinsic versus intrinsic apoptosis pathways in anticancer chemotherapy. Oncogene. 2006;25(34):4798-4811.
106. Circu ML, Aw TY. Reactive oxygen species, cellular redox systems, and apoptosis. Free Radic Biol Med. 2010;48(6):749-762.
107. Dong F, Pirbhai M, Xiao Y, Zhong Y, Wu Y, Zhong G. Degradation of the proapoptotic proteins Bik, Puma, and Bim with Bcl-2 domain 3 homology in Chlamydia trachomatis-infected cells. Infect Immun. 2005;73(3):1861-1864.
108. Du H, Wolf J, Schafer B, Moldoveanu T, Chipuk JE, Kuwana T. BH3 domains other than Bim and Bid can directly activate Bax/Bak. J Biol Chem. 2011;286(1):491-501.
109. Kantari C, Walczak H. Caspase-8 and bid: caught in the act between death receptors and mitochondria. BBA-Mol Cell Res. 2011;1813(4):558-563.
110. Deng Y, Lin Y, Wu X. TRAIL-induced apoptosis requires Bax-dependent mitochondrial release of Smac/DIABLO. Genes Dev. 2002;16(1):33-45.
111. Kandasamy K, Srinivasula SM, Alnemri ES, Thompson CB, Korsmeyer SJ, Bryant JL, et al. Involvement of proapoptotic molecules Bax and Bak in tumor

necrosis factor-related apoptosis-inducing ligand (TRAIL)-induced mitochondrial disruption and apoptosis: differential regulation of cytochrome c and Smac/DIABLO release. Cancer Res. 2003;63(7):1712-1721.

112. Westphal D, Dewson G, Czabotar PE, Kluck RM. Molecular biology of Bax and Bak activation and action. BBA-Mol Cell Res. 2011;1813(4):521-531.

113. Kim K-Y, Yu S-N, Lee S-Y, Chun S-S, Choi Y-L, Park Y-M, et al. Salinomycin-induced apoptosis of human prostate cancer cells due to accumulated reactive oxygen species and mitochondrial membrane depolarization. Biochem Bioph Res Com. 2011;413(1):80-86.

114. Gogvadze V, Orrenius S, Zhivotovsky B. Multiple pathways of cytochrome c release from mitochondria in apoptosis. BBA-Bioenergetics. 2006;1757(5-6):639-647.

115. Ott M, Robertson JD, Gogvadze V, Zhivotovsky B, Orrenius S. Cytochrome c release from mitochondria proceeds by a two-step process. P Natl Acad Sci USA. 2002;99(3):1259-1263.

116. Visagie MH, Joubert AM. In vitro effects of 2-methoxyestradiol-bis-sulphamate on reactive oxygen species and possible apoptosis induction in a breast adenocarcinoma cell line. Cancer Cell Int. 2011;11(1):43-49.

117. Visagie M, Mqoco T, Joubert A. Sulphamoylated estradiol analogue induces antiproliferative activity and apoptosis in breast cell lines. Cell Mol Biol Lett. 2012;17(4):549-559.

118. Visagie MH, St BA, Birkholtz L-M, Joubert AM. Effects of a 17-beta estradiol analogue on gene expression and morphology in a breast epithelial adenocarcinoma cell line: A potential antiproliferative agent. Biomed Res. 2013;24(4):525-530.

119. Stander XX, Stander BA, Joubert AM. In vitro effects of an in silico-modelled 17β-estradiol derivative in combination with dichloroacetic acid on MCF-7 and MCF-12A cells. Cell Proliferation. 2011;44(6):567-581.

120. Pastorekova S, Ratcliffe PJ, Pastorek J. Molecular mechanisms of carbonic anhydrase IX-mediated pH regulation under hypoxia. BJU Int. 2008;101(s4):8-15.

121. Visagie M, Theron A, Mqoco T, Vieira W, Prudent R, Martinez A, et al. Sulphamoylated 2-methoxyestradiol analogues induce apoptosis in adenocarcinoma cell lines. PLoS One. 2013;8(9):e71935.

122. Stander A, Joubert F, Joubert A. Docking, synthesis, and in vitro evaluation of antimitotic estrone analogs. Chem Biol Drug Des. 2011;77(3):173-81.
123. Visagie MH, Birkholtz LM, Joubert AM. 17-beta-estradiol analog inhibits cell proliferation by induction of apoptosis in breast cell lines. Microsc Res Techniq. 2014;77(3):236-242.
124. Wolmarans E, Mqoco TV, Stander A, Nkandeu SD, Sippel K, McKenna R, et al. Novel estradiol analogue induces apoptosis and autophagy in esophageal carcinoma cells. Cell Mol Biol Lett. 2014;19(1):98-115.
125. Visagie MH, Birkholtz L-M, Joubert AM. A 2-methoxyestradiol bis-sulphamoylated derivative induces apoptosis in breast cell lines. Cell Biosci. 2015;5(1):19-33.
126. Visagie MH, van den Bout I, Joubert AM. A bis-sulphamoylated estradiol derivative induces ROS-dependent cell cycle abnormalities and subsequent apoptosis. PLoS One. 2017;12(4):e0176006.
127. Liou G-Y, Storz P. Detecting reactive oxygen species by immunohistochemistry. Stress Responses: Methods and Protocols. 2015:97-104.
128. Zorov DB, Juhaszova M, Sollott SJ. Mitochondrial reactive oxygen species (ROS) and ROS-induced ROS release. Physiol Rev. 2014;94(3):909-950.
129. Sullivan LB, Chandel NS. Mitochondrial reactive oxygen species and cancer. Cancer Metab. 2014;2(1):17-29.
130. Simon H-U, Haj-Yehia A, Levi-Schaffer F. Role of reactive oxygen species (ROS) in apoptosis induction. Apoptosis. 2000;5(5):415-418.
131. Poljsak B, Šuput D, Milisav I. Achieving the balance between ROS and antioxidants: when to use the synthetic antioxidants. Oxid Med Cell Longev. 2013;2013:1-11.
132. Glasauer A, Chandel NS. Targeting antioxidants for cancer therapy. Biochem Pharm. 2014;92(1):90-101.
133. Diebold L, Chandel NS. Mitochondrial ROS regulation of proliferating cells. Free Radic Biol Med. 2016;100:86-93.
134. Prasad S, Gupta SC, Tyagi AK. Reactive oxygen species (ROS) and cancer: Role of antioxidative nutraceuticals. Cancer Lett. 2017;387:95-105.
135. Gupta SC, Hevia D, Patchva S, Park B, Koh W, Aggarwal BB. Upsides and downsides of reactive oxygen species for cancer: the roles of reactive oxygen

species in tumorigenesis, prevention, and therapy. Antiox Red Sig. 2012;16(11):1295-1322.
136. Schumacker PT. Reactive oxygen species in cancer: a dance with the devil. Cancer Cell. 2015;27(2):156-157.
137. Lebelo MT, Joubert AM, Visagie MH. Warburg effect and its role in tumourigenesis. Arch Pharm Res.1-15.
138. Pisano M, Arru C, Serra M, Galleri G, Sanna D, Garribba E, et al. Antiproliferative activity of vanadium compounds: effects on the major malignant melanoma molecular pathways. Metallomics. 2019;11(10):1687-1699.
139. Marchi S, Giorgi C, Suski JM, Agnoletto C, Bononi A, Bonora M, et al. Mitochondria-ros crosstalk in the control of cell death and aging. J Sig Trans. 2012;2012.
140. Ly JD, Grubb DR, Lawen A. The mitochondrial membrane potential (Δψ m) in apoptosis; an update. Apoptosis. 2003;8(2):115-128.
141. Li PF, Dietz R, von Harsdorf R. p53 regulates mitochondrial membrane potential through reactive oxygen species and induces cytochrome c-independent apoptosis blocked by Bcl-2. EMBO J. 1999;18(21):6027-6036.
142. Redza-Dutordoir M, Averill-Bates DA. Activation of apoptosis signalling pathways by reactive oxygen species. BBA-Mol Cell Res. 2016;1863(12):2977-2992.
143. Holliday DL, Speirs V. Choosing the right cell line for breast cancer research. Breast cancer Res. 2011;13(4):215-221.
144. Stander BA, Marais S, Vorster CJJ, Joubert AM. In vitro effects of 2-methoxyestradiol on morphology, cell cycle progression, cell death and gene expression changes in the tumorigenic MCF-7 breast epithelial cell line. J Steroid Biochem Mol Biol. 2010;119(3):149-160.
145. Myhre O, Andersen JM, Aarnes H, Fonnum F. Evaluation of the probes 2′, 7′-dichlorofluorescin diacetate, luminol, and lucigenin as indicators of reactive species formation. Biochem Pharm. 2003;65(10):1575-1582.
146. Zhao H, Kalivendi S, Zhang H, Joseph J, Nithipatikom K, Vásquez-Vivar J, et al. Superoxide reacts with hydroethidine but forms a fluorescent product that is distinctly different from ethidium: potential implications in intracellular fluorescence detection of superoxide. Free Rad Biol Med. 2003;34(11):1359-1368.

147. Marais S, Mqoco TV, Stander A, Van Papendorp DH, Joubert AM. The in vitro effects of a sulphamoylated derivative of 2-methoxyestradiol on cell number, morphology and alpha-Tubulin disruption in cervical adenocarcinoma (HeLa) cells. 2012;23(3):357-362.

148. Franco R, Panayiotidis MI, Cidlowski JA. Glutathione depletion is necessary for apoptosis in cells independent of reactive oxygen species formation. Journal of Biol Chem. 2007;282(42):30452-30465.

149. Bhowmick R, Girotti AW. Cytoprotective induction of nitric oxide synthase in a cellular model of 5-aminolevulinic acid-based photodynamic therapy. Free Radic Biol Med. 2010;48(10):1296-1301.

150. Drummen GP, Makkinje M, Verkleij AJ, den Kamp JAO, Post JA. Attenuation of lipid peroxidation by antioxidants in rat-1 fibroblasts: comparison of the lipid peroxidation reporter molecules cis-parinaric acid and C11-BODIPY 581/591 in a biological setting. BBA-Mol Cell Biol Lipids. 2004;1636(2):136-150.

151. Nicolescu AC, Li Q, Brown L, Thatcher GR. Nitroxidation, nitration, and oxidation of a BODIPY fluorophore by RNOS and ROS. Nitric Oxide. 2006;15(2):163-176.

152. Moisenovich MM, Ol'shevskaya VA, Rokitskaya TI, Ramonova AA, Nikitina RG, Savchenko AN, et al. Novel photosensitizers trigger rapid death of malignant human cells and rodent tumor transplants via lipid photodamage and membrane permeabilization. PLoS One. 2010;5(9):e12717.

153. Bleeke T, Zhang H, Madamanchi N, Patterson C, Faber JE. Catecholamine-induced vascular wall growth is dependent on generation of reactive oxygen species. Circ Res. 2004;94(1):37-45.

154. Gauuan PJF, Trova MP, Gregor-Boros L, Bocckino SB, Crapo JD, Day BJ. Superoxide dismutase mimetics: synthesis and structure–activity relationship study of MnTBAP analogues. Bioorg Med Chem. 2002;10(9):3013-3021.

155. Visagie MH, Joubert AM. In vitro effects of 2-methoxyestradiol-bis-sulphamate on reactive oxygen species and possible apoptosis induction in a breast adenocarcinoma cell line. Cancer Cell Int. 2011;11(1):43-49.

156. Moos PJ, Chung K, Woessner D, Honeggar M, Cutler NS, Veranth JM. ZnO particulate matter requires cell contact for toxicity in human colon cancer cells. Chem Res Toxicol. 2010;23(4):733-739.

157. Honeggar M, Beck R, Moos PJ. Thioredoxin reductase 1 ablation sensitizes colon cancer cells to methylseleninate-mediated cytotoxicity. Toxicol App Pharm. 2009;241(3):348-355.

158. NavaneethaKrishnan S, Rosales JL, Lee K-Y. Loss of Cdk5 in breast cancer cells promotes ROS-mediated cell death through dysregulation of the mitochondrial permeability transition pore. Oncogene. 2018;37(13):1788-1804.

159. Brand MD. Mitochondrial generation of superoxide and hydrogen peroxide as the source of mitochondrial redox signaling. Free Rad Biol Med. 2016;100:14-31.

160. Carocho M, Ferreira IC. A review on antioxidants, prooxidants and related controversy: natural and synthetic compounds, screening and analysis methodologies and future perspectives. Food Chem Toxicol. 2013;51:15-25.

161. Vega-Avila E, Pugsley MK, editors. An overview of colorimetric assay methods used to assess survival or proliferation of mammalian cells. Proc West Pharm Soc; 2011;54:10-14.

162. Hasinoff BB, Schnabl KL, Marusak RA, Patel D, Huebner E. Dexrazoxane (ICRF-187) protects cardiac myocytes against doxorubicin by preventing damage to mitochondria. Cardiovasc Toxicol. 2003;3(2):89-99.

163. Botes M, Jurgens T, Riahi Z, Visagie M, van Vuuren RJ, Joubert AM, et al. A novel non-sulphamoylated 2-methoxyestradiol derivative causes detachment of breast cancer cells by rapid disassembly of focal adhesions. Cancer Cell Int. 2018;18(1):188-200.

164. Waris G, Ahsan H. Reactive oxygen species: role in the development of cancer and various chronic conditions. J Carcinogenesis. 2006;5:14-21.

165. Zhang M, Harashima N, Moritani T, Huang W, Harada M. The roles of ROS and caspases in TRAIL-induced apoptosis and necroptosis in human pancreatic cancer cells. PLoS One. 2015;10(5):e0127386.

166. Chang C-T, Korivi M, Huang H-C, Thiyagarajan V, Lin K-Y, Huang P-J, et al. Inhibition of ROS production, autophagy or apoptosis signaling reversed the anticancer properties of Antrodia salmonea in triple-negative breast cancer (MDA-MB-231) cells. Food Chem Toxicol. 2017;103:1-17.

167. Gille J, Joenje H. Cell culture models for oxidative stress: superoxide and hydrogen peroxide versus normobaric hyperoxia. Mutation Research/DNAging. 1992;275(3-6):405-414.

168. Kello M, Drutovic D, Chripkova M, Pilatova M, Budovska M, Kulikova L, et al. ROS-dependent antiproliferative effect of brassinin derivative homobrassinin in human colorectal cancer Caco2 cells. Molecules. 2014;19(8):10877-10897.
169. Cao X-h, Wang A-h, Wang C-l, Mao D-z, Lu M-f, Cui Y-q, et al. Surfactin induces apoptosis in human breast cancer MCF-7 cells through a ROS/JNK-mediated mitochondrial/caspase pathway. Chem Biol Interact. 2010;183(3):357-362.
170. Mqoco TV, Marais S, Joubert AM. Influence of estradiol analogue on cell growth, morphology and death in esophageal carcinoma cells. Biocell. 2010;34:113-120.
171. Nkandeu DS, Mqoco TV, Visagie MH, Stander BA, Wolmarans E, Cronje MJ, et al. In vitro changes in mitochondrial potential, aggresome formation and caspase activity by a novel 17-β-estradiol analogue in breast adenocarcinoma cells. Cell Biochem Funct. 2013;31(7):566-574.
172. Raobaikady B, Purohit A, Chander SK, Woo LL, Leese MP, Potter BV, et al. Inhibition of MCF-7 breast cancer cell proliferation and in vivo steroid sulphatase activity by 2-methoxyoestradiol-bis-sulphamate. J Steroid Biochem Mol Biol. 2003;84(2-3):351-358.
173. Raobaikady B, Reed MJ, Leese MP, Potter BV, Purohit A. Inhibition of MDA-MB-231 cell cycle progression and cell proliferation by C-2-substituted oestradiol mono-and bis-3-O-sulphamates. Int J Cancer. 2005;117(1):150-159.
174. Na H-K, Kim E-H, Choi M-A, Park J-M, Kim D-H, Surh Y-J. Diallyl trisulfide induces apoptosis in human breast cancer cells through ROS-mediated activation of JNK and AP-1. Biochem Pharmacol. 2012;84(10):1241-1250.
175. Afonso V, Champy R, Mitrovic D, Collin P, Lomri A. Reactive oxygen species and superoxide dismutases: role in joint diseases. Joint Bone Spine. 2007;74(4):324-329.
176. Matés JM, Sánchez-Jiménez FM. Role of reactive oxygen species in apoptosis: implications for cancer therapy. Int J Biochem Cell Biol. 2000;32(2):157-170.
177. Lee HH, Park C, Jeong J-W, Kim MJ, Seo MJ, Kang BW, et al. Apoptosis induction of human prostate carcinoma cells by cordycepin through reactive oxygen species‐mediated mitochondrial death pathway. Int J Oncol. 2013;42(3):1036-1044.

178. Chen T, Wong Y-S. Selenocystine induces caspase-independent apoptosis in MCF-7 human breast carcinoma cells with involvement of p53 phosphorylation and reactive oxygen species generation. Int J Biochem Cell Biol. 2009;41(3):666-676.
179. Glorieux C, Auquier J, Dejeans N, Sid B, Demoulin J-B, Bertrand L, et al. Catalase expression in MCF-7 breast cancer cells is mainly controlled by PI3K/Akt/mTor signaling pathway. Biochem Pharm. 2014;89(2):217-223.
180. Li Z-y, Yang Y, Ming M, Liu B. Mitochondrial ROS generation for regulation of autophagic pathways in cancer. Biochem Biophys Res Com. 2011;414(1):5-8.
181. Laurent A, Nicco C, Chéreau C, Goulvestre C, Alexandre J, Alves A, et al. Controlling tumor growth by modulating endogenous production of reactive oxygen species. Cancer Res. 2005;65(3):948-956.
182. Pelicano H, Carney D, Huang P. ROS stress in cancer cells and therapeutic implications. Drug Resist Updates. 2004;7(2):97-110.
183. Bonnet S, Archer SL, Allalunis-Turner J, Haromy A, Beaulieu C, Thompson R, et al. A mitochondria-K+ channel axis is suppressed in cancer and its normalization promotes apoptosis and inhibits cancer growth. Cancer Cell. 2007;11(1):37-51.
184. Zhu YY, Huang HY, Wu YL. Anticancer and apoptotic activities of oleanolic acid are mediated through cell cycle arrest and disruption of mitochondrial membrane potential in HepG2 human hepatocellular carcinoma cells. Mol Med Reports. 2015;12(4):5012-5018.

**Appendix A: Ethical approval certificate**

UNIVERSITEIT VAN PRETORIA
UNIVERSITY OF PRETORIA
YUNIBESITHI YA PRETORIA

Faculty of Health Sciences

The Research Ethics Committee, Faculty Health Sciences, University of Pretoria complies with ICH-GCP guidelines and has US Federal wide Assurance.

- FWA 00002567, Approved dd 22 May 2002 and Expires 03/20/2022.
- IRB 0000 2235 IORG0001762 Approved dd 22/04/2014 and Expires 03/14/2020.

6 November 2019

**Approval Certificate**
**Annual Renewal**

**Ethics Reference No.: 14/2018**
**Title: Investigating the role of oxidative stress in apoptosis induced by a sulphamoylated estradiol analogue in breast cell lines.**

Dear Miss MT Lebelo

The **Annual Renewal** as supported by documents received between 2019-10-02 and 2019-11-06 for your research, was approved by the Faculty of Health Sciences Research Ethics Committee on its quorate meeting of 2019-11-06.

Please note the following about your ethics approval:

- Renewal of ethics approval is valid for 1 year, subsequent annual renewal will become due on 2020-11-06.
- Please remember to use your protocol number (14/2018 ) on any documents or correspondence with the Research Ethics Committee regarding your research.
- Please note that the Research Ethics Committee may ask further questions, seek additional information, require further modification, monitor the conduct of your research, or suspend or withdraw ethics approval.

**Ethics approval is subject to the following:**

- The ethics approval is conditional on the research being conducted as stipulated by the details of all documents submitted to the Committee. In the event that a further need arises to change who the investigators are, the methods or any other aspect, such changes must be submitted as an Amendment for approval by the Committee.

We wish you the best with your research.

**Yours sincerely**

**Dr R Sommers**
MBChB MMed (Int) MPharmMed PhD
**Deputy Chairperson** of the Faculty of Health Sciences Research Ethics Committee, University of Pretoria

*The Faculty of Health Sciences Research Ethics Committee complies with the SA National Act 61 of 2003 as it pertains to health research and the United States Code of Federal Regulations Title 45 and 46. This committee abides by the ethical norms and principles for research, established by the Declaration of Helsinki, the South African Medical Research Council Guidelines as well as the Guidelines for Ethical Research: Principles Structures and Processes, Second Edition 2015 (Department of Health)*

Research Ethics Committee
Room 4-60, Level 4, Tswelopele Building
University of Pretoria, Private Bag x323
Gezina 0031, South Africa
Tel +27 (0)12 356 3084
Email: deepeka.behari@up.ac.za
www.up.ac.za

Fakulteit Gesondheidswetenskappe
Lefapha la Disaense tša Maphelo